BORON/CALCIUM IN PLANKTONIC FORAMINIFERA: PROXY DEVELOPMENT AND APPLICATION TO THE PALEOCENE-EOCENE BOUNDARY

By

TALI LEA BABILA

A Dissertation submitted to the

Graduate School-New Brunswick

Rutgers, The State University of New Jersey

In partial fulfillment of the requirements

For the degree of

Doctor of Philosophy

Graduate Program in Oceanography

Written under the direction of

Yair Rosenthal

And approved by

_____

_____

_____

_____

New Brunswick, New Jersey

JANUARY, 2014

ABSTRACT OF THE DISSERTATION

BORON IN PLANKTONIC FORAMINIFERA: PROXY DEVELOPMENT AND APPLICATION TO THE PALEOCENE-EOCENE BOUNDARY

Tali L.Babila

Dissertation Director:

Yair Rosenthal

Climate transitions on recent and geologic timescales are linked to perturbations in atmospheric carbon dioxide concentrations (pCO_2). Records of ocean carbonate chemistry allow us to investigate the role of CO_2 during past climate events but are limited by the availability of paleo-proxies. This thesis presents the development and calibration of Boron/Calcium (B/Ca) in planktonic foraminifera as a proxy for surface ocean carbonate chemistry from sediment traps and modern surface sediments. The B/Ca proxy is then used to reconstruct surface ocean acidification across the Paleocene-Eocene boundary (~55.8 Myr).

Observations of B/Ca in the surface dwelling planktonic foraminifer *Globigerinoides ruber* white from the Oceanic Flux Program (OFP) sediment trap time-series located near Bermuda are used to suggest that the photosynthetic activity of symbiotic algae within the living foraminifer modify the internal pH relative to the ambient seawater, thereby influencing the B/Ca recorded in the calcitic test (Chapter Two). I hypothesize that the apparent covariance between *G. ruber* B/Ca and the temperature at the OFP site is due to the seasonal change in incident light affecting the symbiont activity, which can increase the internal pH during calcification from seawater by ~0.2-0.3 units.

Measurements of B/Ca and $\delta^{11}B$ in different species of planktonic foraminifera from globally distributed core-top sediments reveal that symbiotic foraminifera are offset from the theoretically predicted equilibrium with seawater (Chapter Three). I find no significant temperature effect on B/Ca and the departure from equilibrium for symbiont-bearing species is attributed to biological effects. I provide empirical calibrations for thermocline and deep-dwelling planktonic foraminifera as being primarily controlled by seawater $\left[B(OH)_4^- / HCO_3^-\right]$.

Paired isotopic ($\delta^{13}C$, $\delta^{18}O$) and elemental (Mg/Ca, B/Ca) measurements are applied to reconstruct the relative timing and magnitude of environmental changes across the Paleocene-Eocene boundary, occurring ~55.8 Myr using sections from ODP Leg 174AX sites at Bass River and Ancora. Reconstructions of ocean temperature (Mg/Ca) and carbonate chemistry ($\delta^{13}C$ and B/Ca) from planktonic foraminifera document an abrupt and significant decrease in B/Ca ratios, coincident with $\delta^{13}C$ records and the concomitant ~6-8°C warming. The synchronous changes in all three proxies do not support the occurrence of significant precursor warming or carbon release argued elsewhere.

Acknowledgements

I want to thank my advisor Yair Rosenthal. To express my gratitude for his mentorship, guidance and willingness to go above and beyond to teach me valuable lessons about trace metal geochemistry, academia and life. I am incredibly grateful for his continued support which was instrumental in my ability to navigate and grow both professionally and personally throughout my time at Rutgers. For reminding me of the importance of taking the time to step back and see the larger picture, the forest (world) from the trees (boron in foraminifera). תודה רבה

I would like to acknowledge my committee members, Jim Wright, Ken Miller and Bärbel Hönisch for their scientific advice and support during my PhD. Jim and Ken you always made me feel welcome and part of the EPS department. Jim, I am thankful that you opened your office door to invite me for coffee to talk about everything from stable isotopes to life. Ken I am grateful for the opportunity to get muddy in the Pine Barrens and appreciative for exposing this Californian to the wonders and possibilities of New Jersey geology. I want to recognize Dr. Olsson for taking the time to teach me about planktonic foraminifera which provided the foundation for my research. Marie Pierre-Aubry, thank you for your insight, support and enthusiasm which continues to motivate me in my career. Rob Sherrell I am grateful for the opportunity to go out to sea and your valuable training on the basics of geochemistry. Thank you to Maureen Conte and Chen-Feng You for providing their lab facility, training and scientific expertise that was vital to this dissertation.

I would also like to thank my fellow Scarlet Knights Ali, Stella, Maria, Kat, Audrey, Julie, Sindia, Eleni, Carrie, Michele and Denner for their support during the hard

times, rejoice during the celebrations and most importantly their friendship. I want to thank Katie, Sofie, Joelle, Amira and Gretchen for their constant encouragement that kept me motivated through grad school. A special thanks to Noelle who has been my biggest cheerleader since the UMiami days and whom I feel incredibly lucky to have as a best friend. I want to express my gratitude to my family especially my Mom for being the rock in my life and giving me the strength to achieve my aspiration of becoming an Oceanographer.

I want to recognize my high school teachers for encouraging me to pursue my scientific interests and being the catalyst that transformed my excitement for Marine Science into a career path.

This dissertation research was supported by the Joanna M. Resig Foraminiferal Research Fellowship, Schlanger Ocean Drilling Fellowship, National Science Foundation, The Manasquan River Marlin and Tuna Club, The International Women's Fisheries Association, American Chemical Society and the Institute of Marine and Coastal Sciences.

Table of Contents

List of Tables

List of illustrations

1.0 Chapter One

1.1 Thesis Introduction

Atmospheric greenhouse gas concentrations are an integral component in mediating global climate. Carbon dioxide (pCO_2) concentrations are proposed to drive variations in global temperature on recent and throughout geologic history (*Mann et al.*, 1998; *Royer et al.*, 2004). Proxies of past atmospheric pCO_2 provide the opportunity to investigate the relationship between the carbon cycle and climate. For example, ice core records document significant variations in pCO_2 and are associated with the growth and decay of continental ice sheets throughout the Quaternary (*Petit et al.*, 1999). Marine sediment cores allow paleoceanographers to document the evolution of deep ocean temperatures over the Cenozoic, past 65 million years (*Cramer et al.*, 2011; *Lear et al.*, 2000; *Miller et al.*, 1987; *Pagani et al.*, 2005; *Pearson et al.*, 2000; *Zachos et al.*, 2005). However, to evaluate the role of atmospheric pCO_2 beyond instrumental and ice core archives proxies for oceanic carbonate chemistry are needed.

Boron to calcium (B/Ca) in fossil planktonic foraminifera were used to estimate past surface ocean carbonate chemistry and ultimately atmospheric pCO_2 (*Foster*, 2008; *Tripati et al.*, 2009; *Yu et al.*, 2007b; *Yu et al.*, 2013). An ideal geochemical proxy should depend strictly on a single environmental variable (i.e. pH) but a growing body of evidence suggests most proxies currently used in paleoceaography are affected by multiple variables. Observations from culture, modern sediments, down-core records indicate variable patterns of B/Ca in planktonic foraminifera, suggesting uncertainty regarding the environmental variable(s) influencing boron incorporation into their calcitic tests (*Allen et al.*, 2012; *Allen et al.*, 2011; *Foster*, 2008; *Yu et al.*, 2007b). In Chapter two

of this thesis I evaluate the relative effects of temperature, carbonate chemistry and light intensity on *Globigernoides ruber*, commonly used planktonic foraminifer in paleoceanographic studies from Bermuda Oceanic flux program (OFP). In Chapter three, I provide the first rigorous assessment of B/Ca in multiple planktonic foraminifera in recent core top sediments.

A major advantage of trace elemental work in foraminifera is the ability for simultaneous data collection with the potential to evaluate phase relationships between paleo records. For example, paired analysis of B/Ca and Magnesium/Calcium (Mg/Ca), an independent paleothermometer would allow determination of both oceanic carbonate chemistry and temperature. In Chapter four, I combine B/Ca and Mg/Ca to evaluate the temporal relationship between surface ocean temperature, carbonate chemistry and in relation to the carbon released during the PETM.

Rising atmospheric carbon dioxide (pCO_2) concentrations are contributing to an acidification of the oceans (*Feely et al.*, 2004; *Sabine et al.*, 2004). Instrumental records currently document a decrease of 0.05 pH units since the 1980s (*Bates et al.*, 2012) and model based projections estimate a 0.07 pH units by 2300 (*Caldeira et al.*, 2003). Recent trends of declining surface ocean pH coincide with a lowering of the carbonate saturation state, proposed to adversely influence the ability of marine organisms to produce tests or skeletons from calcium carbonate ($CaCO_3$) (*Hoegh-Guldberg et al.*, 2007; *Orr et al.*, 2005). As carbon emissions are projected to continue, concerns are mounting over the potential impacts of a persistent acidification conditions on marine ecosystems. Similar events from the geologic record may provide insight on the biotic responses to acidification. Considered one of the best and most recent geologic analogs is the

Paleocene-Eocene thermal maximum (PETM), occurring ~55.8 Myr (*Hönisch et al.*, 2012). To achieve this goal, a proxy for surface ocean carbonate chemistry (paleo-*acidimetry)* is required. This B/Ca records from mixed-layer and thermocline dwelling foraminifera at the PETM reveal a significant anomaly, estimated as a pH change of ~0.2-0.3. The drop in B/Ca closely tracks the negative CIE providing the first evidence of surface ocean carbonate chemistry decline at the PETM.

1.2 References

Allen, K.A., Hönisch, B., Eggins, S.M., and Rosenthal, Y. (2012), Environmental controls on B/Ca in calcite tests of the tropical planktic foraminifer species Globigerinoides ruber and Globigerinoides sacculifer, *Earth and Planetary Science Letters*, *351–352*(0), 270-280.

Allen, K.A., et al. (2011), Controls on boron incorporation in cultured tests of the planktic foraminifer Orbulina universa, *Earth and Planetary Science Letters*, *309*(3–4), 291-301.

Bates, N.R., et al. (2012), Detecting anthropogenic carbon dioxide uptake and ocean acidification in the North Atlantic Ocean, *Biogeosciences*, *9*(7), 2509–2522.

Caldeira, K., and Wickett, M.E. (2003), Oceanography: Anthropogenic carbon and ocean pH, *Nature*, *425*(6956), 365-365.

Cramer, B.S., Miller, K.G., Barrett, P.J., and Wright, J.D. (2011), Late Cretaceous–Neogene trends in deep ocean temperature and continental ice volume: Reconciling records of benthic foraminiferal geochemistry (δ18O and Mg/Ca) with sea level history, *Journal of Geophysical Research: Oceans*, *116*(C12), C12023.

Feely, R.A., et al. (2004), Impact of Anthropogenic CO2 on the CaCO3 System in the Oceans, *Science*, *305*(5682), 362-366.

Foster, G.L. (2008), Seawater pH, pCO2 and [CO2-3] variations in the Caribbean Sea over the last 130 kyr: A boron isotope and B/Ca study of planktic foraminifera, *Earth and Planetary Science Letters*, *271*(1-4), 254-266.

Hoegh-Guldberg, O., et al. (2007), Coral Reefs Under Rapid Climate Change and Ocean Acidification, *Science*, *318*(5857), 1737-1742.

Hönisch, B., et al. (2012), The Geological Record of Ocean Acidification, *Science*, *335*(6072), 1058-1063.

Lear, C.H., Elderfield, H., and Wilson, P.A. (2000), Cenozoic Deep-Sea Temperatures and Global Ice Volumes from Mg/Ca in Benthic Foraminiferal Calcite, *Science*, *287*(5451), 269-272.

Mann, M.E., Bradley, R.S., and Hughes, M.K. (1998), Global-scale temperature patterns and climate forcing over the past six centuries, *Nature*, *392*(6678), 779-787.

Miller, K.G., Janecek, T.R., Katz, M.E., and Keil, D.J. (1987), Abyssal Circulation and Benthic Foraminiferal Changes Near the Paleocene/Eocene Boundary, *Paleoceanography*, *2*(6), 741-761.

Orr, J.C., et al. (2005), Anthropogenic ocean acidification over the twenty-first century and its impact on calcifying organisms, *Nature*, *437*, 681-683.

Pagani, M., et al. (2005), Marked Decline in Atmospheric Carbon Dioxide Concentrations During the Paleogene, *Science*, *309*(5734), 600-603.

Pearson, P.N., and Palmer, M.R. (2000), Atmospheric carbon dioxide concentrations over the past 60 million years, *Nature*, *406*(6797), 695-699.

Petit, J.R., et al. (1999), Climate and atmospheric history of the past 420,000 years from the Vostok ice core, Antarctica, *Nature*, *399*, 429-436.

Royer, D.L., et al. (2004), CO2 as a primary driver of Phanerozoic climate, *GSA Today*, *14*(3), 4-10.

Sabine, C.L., et al. (2004), The Oceanic Sink for Anthropogenic CO2, *Science*, *305*(5682), 367-371.

Tripati, A.K., Roberts, C.D., and Eagle, R.A. (2009), Coupling of CO2 and Ice Sheet Stability Over Major Climate Transitions of the Last 20 Million Years *Science*, *326*(5958), 1394-1397.

Yu, J., Elderfield, H., and Hönisch, B. (2007), B/Ca in planktonic foraminifera as a proxy for surface seawater pH, *Paleoceanography*, *22*(2), PA2202.

Yu, J., Thornalley, D.J.R., Rae, J.W.B., and McCave, N.I. (2013), Calibration and application of B/Ca, Cd/Ca, and δ11B in Neogloboquadrina pachyderma (sinistral) to constrain CO2 uptake in the subpolar North Atlantic during the last deglaciation, *Paleoceanography*, *28*(2), 237-252.

Zachos, J.C., et al. (2005), Rapid Acidification of the Ocean During the Paleocene-Eocene Thermal Maximum, *Science*, *308*(5728), 1611-1615.

2.0 Chapter Two

Evaluation of the biogeochemical controls on B/Ca of *Globigerinoides ruber* white from the Oceanic Flux Program, Bermuda

Babila, Tali L.[a], Rosenthal, Yair[ab] and Maureen H. Conte[c]

[a] Institute of Marine and Coastal Sciences, Rutgers, State University of New Jersey, 71 Dudley Road, New Brunswick, New Jersey 08901, USA

[b] Department of Earth and Planetary Sciences, Rutgers, State University of New Jersey, 610 Taylor Road, Piscataway, New Jersey 08854, USA

[c] Bermuda Institute of Ocean Sciences, Ferry Reach, St Georges, Bermuda and Ecosystems Center, Marine Biological Laboratory, Woods Hole, Massachusetts 02543, USA

*Submitted to Earth and Planetary Science Letters

2.1 Abstract

Boron to calcium (B/Ca) ratios in planktonic foraminifera is suggested to be a proxy for the surface oceanic carbonate system. The reliability of the proxy has been questioned due to conflicting reports from culture and sediment calibrations on the influence of temperature on B/Ca. To assess this issue, B/Ca and Mg/Ca ratios and $\delta^{18}O$ were measured in tests of the symbiont-bearing surface dwelling planktonic foraminifer *Globigerinoides ruber* white collected by the Oceanic Flux Program (OFP) time series sediment traps, located approximately 75 km SE of Bermuda. B/Ca ratios in the 300-400μm size fraction of *G. ruber* were approximately 10-20 % higher than that in the 200-300μm size fraction. In contrast, Mg/Ca ratios and $\delta^{18}O$ values do not exhibit any relationship to test size, which indicates that the size effect observed for B/Ca is not due to differences in depth habitat but to vital effects. Seasonal variation in the B/Ca ratio was similar in both size fractions and ranged by ~20-30 μmol/mol. This range is larger than that predicted by seasonal variations in seawater $[B(OH)_4^-/HCO_3^-]$, the proposed boron species incorporated into planktonic foraminiferal calcite, and indicates that B/Ca in *G.ruber* is influenced by an additional variable(s). The seasonal cycle of B/Ca in *G. ruber* white was more strongly correlated with light intensity than with temperature. Both observations suggest that the presence of symbionts in *G.ruber* and seasonal variability in their photosynthetic activity act to modify the internal pH during calcification, by up to ~0.2 units relative to ambient seawater.

2.2 Introduction

Boron isotopes ($\delta^{11}B$) and more recently Boron to calcium ratios (B/Ca) of planktonic foraminifera are used in paleoceanography to reconstruct oceanic carbonate

system parameters in the geologic record (*Foster*, 2008; *Hönisch et al.*, 2009; *Pearson et al.*, 2000; *Spivack et al.*, 1993; *Tripati et al.*, 2009). Seawater boron species exist predominantly as boric acid $B(OH)_3$ and borate $B(OH)_4^-$ and their relative concentrations and isotope composition depend on pH. Analysis of modern marine carbonates yields isotopic values consistent with the isotopic composition of $B(OH)_4^-$ in seawater suggesting that $B(OH)_4^-$ is apparently the dominant species incorporated into biogenic calcium carbonate ($CaCO_3$) minerals (*Hemming and Hanson* 1992). However, spectroscopic evidence for the presence of tetrahedral and trigonal coordinated boron in various marine carbonates led *Klochko et al.*, (2009) to suggest that in addition to $B(OH)_4^-$, $B(OH)_3$ may also be incorporated during crystal growth. Based on B/Ca results of *O.universa* the amount of boric acid incorporation into foraminiferal calcite is likely small (*Allen et al.*, 2011). Therefore, in this study we assume the borate is the primary species controlling boron incorporation into carbonate minerals.

Selective incorporation of seawater $B(OH)_4^-$ into the calcite lattice was first proposed by *Hemming and Hanson 1992* as:

$$CaCO_3 + B(OH)_4^- \leftrightarrow Ca(HBO)_3 + HCO_3^- + H_2O \quad (1)$$

Assuming within crystal substitution of the two species, the apparent partition coefficient, K_D between the incorporated seawater boron species and the $CaCO_3$ foraminifera test can be described by:

$$K_D \approx [B/Ca_{CaCO_3}]/[B(OH)_4^-/HCO_3^-]_{seawater} \quad (2)$$

Based on the hypothetical mechanism for boron incorporation proposed by *Hemming and Hanson* 1992, as modified by *Yu et al.,* 2007, the B/Ca ratio in planktonic foraminifera is controlled by variations in $[B(OH)_4^-/HCO_3^-]_{sw}$. This theoretical basis for boron incorporation in planktonic foraminifera is supported by empirically derived relationships observed in culture experiments of *G.ruber*, *G.sacculifer* and *O.universa* (*Allen et al.*, 2012; *Allen et al.*, 2011). A corollary of the above geochemical B-incorporation model, is that B/Ca ratios should increase with $[B(OH)_4^-/HCO_3^-]_{sw}$.

Results from core-top, sediment trap and down-core calibration studies have indicated, however, that K_D is not a constant (*Foster*, 2008; *Hendry et al.*, 2009; *Ni et al.*, 2007; *Tripati et al.*, 2009; *Yu et al.*, 2007b). To explain the non-equilibrium behavior of B/Ca, *Yu et al.,* (2007) proposed that K_D is influenced by calcification temperature. However, contrary to *Yu et al.,* (2007), *Foster* (2008) observed in their survey of core tops a negative relationship between K_D and temperature, despite the lack of covariance between temperature and B/Ca ratios, and proposed that K_D is controlled by seawater $[CO_3^{2-}]$ ion rather than temperature. Consistently, culture studies (*Allen et al.*, 2012; *Allen et al.*, 2011) also failed to find a discernible relationship between B/Ca and temperature, thereby supporting the argument that the carbonate system is the likely principal control mediating boron incorporation in planktonic foraminifera, as observed for benthic foraminifera (*Brown et al.*, 2011; *Rae et al.*, 2011; *Yu et al.*, 2007a). *Allen and Hönisch* (2012) furthermore questioned whether a K_D derived relationship to the carbonate system should be used as a calibration approach, arguing that interpretation of K_D strictly in terms of pH is complicated by the fact that $[B(OH)_4^-/HCO_3^-]_{sw}$ also depends upon the

ambient temperature. This calls into question the down core calibrations used in *Yu et al.*, (2007) and *Tripati et al*., (2009) to derive a K_D-temperature relationship.

Sediment trap studies provide the opportunity to determine the response of foraminifera to environmental parameters under true oceanic conditions that cannot be replicated in cultures. Various environmental parameters may vary simultaneously but diagenesis can be excluded from the evaluation. In this regard sediment trap studies bridge a connection between culture and core top studies. In this study we evaluate the effects of temperature, light and carbonate chemistry on B/Ca ratios in the planktonic foraminifer *G.ruber* white, commonly used in paleoceanographic studies using samples collected by the Bermuda Oceanic Flux Program (OFP) sediment trap time-series between 1993 and 1996.

2.3 Study Site

The Bermuda Time Series site is located in the oligotrophic northern Sargasso Sea. The physical setting and biogeochemistry of the area has been summarized (*Steinberg et al.*, 1996 and references therein). Seasonal variation of sea surface temperature (SST) ranges by ~8-10 °C with maximum temperatures of ~29 °C from July-September and minimum values of ~19 °C from January-March (Figure 2.1). During the interval studied here (1993-1996), surface water pCO_2 ranged seasonally by ~80-100 µatm with maximum values during the late summer of 390-400 µatm and minimum values of 310-320 µatm during the winter (*Bates et al.*, 1996; *Bates et al.*, 1998). Alkalinity and salinity variations are minor (15 µmol/kg, 0.3 respectively) in the seasonal cycle and are mainly controlled by changes in evaporation/precipitation. Seawater pCO_2 and therefore pH are driven mainly by changes in temperature, physical mixing processes

and gas exchange, with minor contributions from biological production (*Bates et al.*, 1996; *Bates et al.*, 1998). During the winter months when the mixed layer is deep (Jan-Apr) pCO_2 is undersaturated (seasonal minimum; relatively constant within the upper 50m) and the site is a CO_2 sink (*Bates*, 2007; *Bates et al.*, 1996). Transitioning from winter to spring (Mar-Apr) the mixed layer shoals and nutrients are mixed upward supporting the spring bloom (*Bates et al.*, 1998). During the summertime (Jun-Sept) thermal stratification is intensified; pCO_2 is supersaturated (seasonal maximum; gradient is established) and the site is a CO_2 source to the atmosphere (*Bates*, 2007; *Bates et al.*, 1996; *Bates et al.*, 1998).

Globigerinoides ruber (D'Orbigny, 1839) is a spinose, symbiont -bearing (dinoflagellates) planktonic foraminifer abundant in surface waters of the tropical-subtropical oceans (*Bé et al.*, 1971). The presence of photosynthetic symbionts means that the depth habitat is restricted to the photic zone spanning a temperature range of 18-28 ºC in the Sargasso Sea based on its $\delta^{18}O$ composition from plankton tows and sediment traps (*Anand et al.*, 2003; *Deuser et al.*, 1981; *Erez et al.*, 1981; *Williams et al.*, 1981). In the Sargasso Sea flux variations indicate maximum abundance of *G. ruber* white during the summer months possibly related to the intensity of primary production, however, the species is present throughout the year and for this reason is assumed to largely reflect annual conditions (*Deuser*, 1987; *Deuser et al.*, 1981).

2.4 Materials and Methods

2.4.1 OFP Sediment Traps

The Oceanic Flux Program (OFP) mooring site is located at 31°50′N, 64°10′W in 4500m water depth approximately 75 km southeast of Bermuda. The sediment-trap mooring and collection protocols are described in *Conte* et al. (2001). McLane Parflux sediment traps (0.5 m^2 surface area; McLane Labs, Falmouth, MA, USA) are positioned at 500, 1500 and 3200 m depths and are programmed at about a two week sampling resolution. Sample cups are filled with high purity seawater brine (40 ppt) that is prepared by freezing Sargasso Sea deep water (3000m depth). The trap cup brine is poisoned with ultra-high purity $HgCl_2$ (200 mg/L) to arrest biological degradation during sample collection.

OFP sample processing and analyses are described in (*Conte et al.*, 2001), (*Huang et al.*, 2009) and (*Shatova et al.*, 2012). The >1 mm-sized material (which interferes with quantitative splitting) is removed by gentle sieving prior to sample splitting and transferred to a pre-weighed Petri dish for swimmer removal and photography. The remaining <1 mm material is split into 10 subsamples using a McLane rotary sample splitter (McLane Labs, Falmouth, MA, USA). Four subsamples are removed for trace elemental and organic studies. The remaining subsamples (60%) are recombined and size fractionated into 500–1000, 125–500 and <125 μm size fractions.

2.4.2 Hydrographic and Environmental Datasets

Data on situ temperature, salinity, dissolved inorganic carbon (DIC) and alkalinity for the time period covering the trap collections for the presumed depth range of *G.ruber* (0-60m) was obtained from the BATS database and from N. Bates (unpublished database). Seawater pH and [CO_3^{2-}] are calculated using the CO_2sys.xls (*Pelletier et al.*, 2007) program and constants K_1, K_2 from (*Mehrbach et al.*, 1973) refit by (*Dickson et al.*, 1987). Total seawater boron concentrations were calculated from the globally defined relationship of *Lee et al.*, (2010), where [B] = 432.6 µmol/kg x (S/35). Light intensities at 20 m, the approximate calcification depth of *G.ruber* were compiled from hourly measurements collected on the Bermuda Testbed Mooring (31°41.77′N, 64°10.52′W, located near the OFP and BATS sites (courtesy of Tommy D. Dickey, UCSB).

2.4.4 Foraminifera Sample Preparation

Foraminifera were picked from the 125-500µm size fraction of each trap sample. Biweekly samples were combined when sufficient material was not available. Individuals were measured using an ocular micrometer and separated into two sample sizes: 200-300 and 300-400µm. Both fractions were analyzed for trace metals and stable isotopes. Samples for trace metal analysis include 20-30 individuals yielding approximately 150-200µg of $CaCO_3$ material.

Foraminifera tests were gently crushed between two glass plates to open the chambers and facilitate the chemical cleaning procedure and then transferred into acid-leached centrifuge vials. Crushed samples were chemically cleaned following the Mg-cleaning protocol (*Barker et al.*, 2003). All reagents and acids were prepared using Milli-

Q water and passed through a boron Q-gard purification filter to obtain low boron water. Samples were cleaned to remove adhering clays by rinsing with Milli-Q water and glass distilled methanol. The reductive cleaning step, conducted to remove metal oxides which can accumulate during post-deposition processes, was omitted as in previous sediment trap protocols (*Anand et al.*, 2003; *Pak et al.*, 2004). The omission of the reductive step from the cleaning is not expected to bias the B/Ca ratio as boron is relatively homogenous within the test and is unaffected by cleaning procedures (*Yu et al.*, 2007c). An extended oxidizing step was conducted to remove organic matter, using a 0.1 M NaOH and 1 % hydrogen peroxide solution and repeated (x2) for a total duration of 1 hour (*Anand et al.*, 2003; *Pak et al.*, 2004). A final dilute acid (0.001 N HNO3) leach was done before completely dissolving samples using 100 μL 0.065 N (OPTIMA®) HNO_3. Samples were diluted with ~100-200 μL (depending on the sample size) of 0.5 N (OPTIMA®) HNO_3 to a final volume of ~300-400 μL. [Ca] concentrations in sample solutions were typically maintained in the range of 1.5 to 4 mmol/L to minimize matrix effects on Mg/Ca and B/Ca (*Rosenthal et al.*, 1999).

2.4.4 Elemental and Isotope Analysis

Trace element measurements (Li, B, Mg, Sr and Ca) were carried out at the Institute of Marine and Coastal Sciences at Rutgers University using a Thermo Finnigan Element XR Sector Field Inductively Coupled Plasma Mass Spectrometer (SF-ICP-MS) operated in low resolution ($m/\Delta m$ =300) following a modified protocol of (*Rosenthal et al.*, 1999). Several modifications to the *Rosenthal et al.*, (1999) method were included to reduce the instrumental boron memory effect, which is caused by the tendency of boric acid to volatilize and form droplets that accumulate in the spray chamber during the

course of an analytical run (*Al-Ammar et al.*, 2000). To reduce the boron memory effect and improve washout efficiency anhydrous ammonia gas was injected (into a high purity quartz cyclonic spray chamber (Elemental Scientific, ESI), raising the pH of the injected sample (>9.14) converting boric acid to ammonium borate which solubilizes and is removed during rinsing (*Al-Ammar et al.*, 2000). Typical B blank levels are ~0.15 ppb (<2 % of [B] of foraminifera samples) and remain stable (±1 %) throughout an analytical run.

Elemental ratios were monitored and corrected for matrix effects for each analytical run by analyzing a suite of solutions prepared by diluting our spiked gravimetric standard (SGS) to varying [Ca] concentrations (1.5 mmol/L to 8 mmol/L) (*Rosenthal et al.*, 1999). Typical matrix corrections were <1 % for Mg/Ca and <5% for B/Ca. Analytical precision of B/Ca = 115.43 μmol/mol was ± 3.3 % (RSD) and for Mg/Ca = 3.32 mmol/mol ± 0.41 % (RSD) based on repeated analysis of laboratory consistency standards throughout the length of the study (Figure 2.2).

For stable isotope analysis, 3-5 individual *G. ruber* tests from 200-300 and 300-400 μm size fractions were measured using an Optima mass spectrometer at the Department of Earth and Planetary Sciences, Rutgers University. Measurements are reported in PDB with precision values of ±0.08 ‰ $\delta^{13}C$ and ±0.05 ‰ $\delta^{18}O$ for NBS19 standard throughout the analysis of this study.

2.5 Results

2.5.1 Seasonal Cycles of B/Ca, Mg/Ca and $\delta^{18}O$

Seasonal variations in B/Ca, Mg/Ca, $\delta^{18}O$ and $\delta^{13}C$ in the planktonic foraminifer *G. ruber* white are shown in Figure 2.3 (Appendix 1.1 and 1.2). Mg/Ca and $\delta^{18}O$ seasonal variations are in phase in both size fractions. No offset in either Mg/Ca or $\delta^{18}O$ values are observed between the two size fractions (200-300 and 300-400 μm). Mg/Ca and $\delta^{18}O$ exhibit small interannual variability. Average Mg/Ca ratios are highest (5.31-4.45 mmol/mol) during July-October and lowest during February-April (3.54-4.12 mmol/mol) (Figure 2.3). $\delta^{13}C$ in both size fractions also varies seasonally, with the lowest $\delta^{13}C$ values observed from January-May (-0.5-0 ‰) and highest values from June until December (0-0.5 ‰) (Figure 2.4). $\delta^{13}C$ values in the 300-400 μm size fraction are higher by ~0.5 ‰ than in the 200-300 μm size fraction (Figure 2.4).

As observed for $\delta^{13}C$, B/Ca ratios also are higher in the 300-400 μm size fraction as compared with the 200-300 μm size fraction, with a relatively constant offset of ~15-20 μmol/mol. B/Ca ratios also vary seasonally. B/Ca ratios are maximal during June-October (114.99-136.67 μmol/mol in the 200-300μm size fraction and 121.26-138.34 μmol/mol in the 300-400 μm size fraction). B/Ca ratios are minimal during January-March (95.30-100.66 μmol/mol in the 200-300 μm size fraction and 97.16-111.02 μmol/mol in the 300-400 μm size fraction).

2.5.2 Estimation of Calcification Depth

Calcification depths were estimated by comparing the measured foraminiferal $\delta^{18}O_c$ of calcite to the predicted $\delta^{18}O_c$ values, assuming equilibrium with seawater over the depth range of 0-50 m. The $\delta^{18}O$ of seawater ($\delta^{18}O_{sw}$) at Bermuda Atlantic Times Series (BATS) was derived from the $\delta^{18}O_{sw}$-salinity relationship compiled from measurements from 0-50 m over the subtropical-tropical Atlantic available through the NASA global seawater database (*Arbuszewski et al.*, 2010; *Schmidt et al.*, 1999). The $\delta^{18}O_{sw}$ was converted from SMOW to Peedee Belemnite (PDB) scale by subtracting 0.27 ‰. The predicted $\delta^{18}O_c$ was calculated using the low light paleo temperature equation for symbiont bearing *O. universa* (*Bemis et al.*, 1998) and $\delta^{18}O_{sw}$.

$\delta^{18}O_c$ values of *G. ruber* for the two size fractions (200-300 and 300-400 μm) analyzed are consistent with the predicted $\delta^{18}O_c$ ranging from 20 to 40 m indicating calcification within the mixed-layer (Figure 2.5). A significant exception is observed from January to April 1995, with deviation from isotopic equilibrium by <0.30 ‰. Assuming that *G. ruber* at OFP calcifies mainly within 20-40 m depth range the $\delta^{18}O_c$-derived calcification temperature estimates agree with the monthly hydrographic temperatures within ±1.74 °C (1σ) (Figure 2.6). Calcification depths estimated from $\delta^{18}O$ are in agreement with those based on Mg/Ca (*Anand et al.*, 2003). Here we chose to use the $\delta^{18}O_c$-derived calcification temperature to be comparable with previous studies.

2.6 Discussion

2.6.1 Depth Habitat

Measured $\delta^{18}O_c$ values of *G. ruber* for both size fractions are similar and consistent with calcification within the mixed-layer. While occasional discrepancies of $\delta^{18}O_c$ of 0-1.0 ‰ from isotopic equilibrium with seawater were measured, as previously observed in the OFP sediment traps (*Anand et al.*, 2003; *Deuser*, 1987), these were generally restricted to winter months when the foraminiferal flux is low (*Deuser*, 1987; *Deuser et al.*, 1981). Therefore, we estimate that an offset of 0.1 ‰ from January-April would not significantly contribute (<0.03 ‰) to the averaged signal preserved in core top sediments.

There are several possible reasons for the offsets in $\delta^{18}O_c$ from that predicted by the surface $\delta^{18}O_{sw}$-salinity relationship. One possible explanation for these offsets may be sampling resolution (i.e. bimonthly versus biweekly) or passage of episodic warm eddies through the region (*McGillicuddy et al.*, 1999) resulting in localized temperature excursions that are not captured by averaged monthly hydrographic measurements. However, the greater hydrographic and sediment trap temporal resolution used in this study would reduce error in the predicted $\delta^{18}O_c$ values and hence apparent isotopic offsets in the data. Secondly, there may be errors associated with the choice of paleotemperature equation and/or the seasonally variable surface $\delta^{18}O_{sw}$-salinity relationship in this location. In this study we used the paleo temperature equation for symbiont-bearing planktonic foraminifer *O. universa* (*Bemis et al.*, 1998) and the $\delta^{18}O_{sw}$-salinity relationship of (*Arbuszewski et al.*, 2010). This equation gives the best agreement

between the predicted $\delta^{18}O_c$ and foraminiferal calcite with a discrepancy of ~0.10-0.20 ‰ at 40 m water depth from August-December (Figure 2.5).

2.6.2 Carbonate system controls on B/Ca

Contemporaneous seawater measurements from BATS allow us to evaluate the carbonate and boron system parameters (pH, CO_3^{2-}, BOH_4^-) that are proposed to influence B/Ca in planktonic foraminifera (*Allen et al.*, 2012; *Allen et al.*, 2011; *Foster*, 2008; *Yu et al.*, 2007b). Dissolved inorganic carbon (DIC) varies seasonally by ~20-30 μmol/kg (and pH by ~0.15 pH) largely due to the 8-10 °C seasonal temperature change. Therefore, if pH is the main control on boron incorporation in planktonic foraminiferal calcite, B/Ca ratios would be highest in the winter (high pH values) and lowest in the summer (low pH) (Fig. 1b).

Alternatively, B/Ca ratios may be controlled by the $[B(OH)_4^-/HCO_3^-]_{sw}$ ratio (*Allen et al.*, 2012) which is not strictly a function of pH but also depends on the seawater temperature (Figure 2.7). At OFP, pH is mainly controlled by temperature through the equilibrium coefficients K_B, K_1 and K_2. Seasonal temperature and pH changes at OFP yield only a small change in $[B(OH)_4^-/HCO_3^-]_{sw}$ (<0.004), which would result in a seasonal change of only ~3-5 μmol/mol in the B/Ca ratio based upon the study of (*Allen et al.*, 2012). However, the observed seasonal change in B/Ca (~20-30 μmol/kg) is nearly an order of magnitude higher, which indicates that in addition to ambient $[B(OH)_4^-/HCO_3^-]_{sw}$ another parameter(s) is influencing B/Ca.

2.6.4 Salinity and temperature influences on B/Ca

Culture studies show a small influence of seawater salinity on planktonic foraminiferal B/Ca (*Allen et al.*, 2012; *Allen et al.*, 2011). The salinity effect on B/Ca is predicted to be negligibly over the small (<0.3) seasonal variations in salinity at OFP. As changes in $[B(OH)_4^-/HCO_3^-]_{sw}$ and salinity cannot account for the seasonal B/Ca record, we evaluate a possible direct influence of temperature, or of another variable(s) that covaries with temperature. A direct temperature influence on B/Ca ratios in planktonic foraminifera is currently debated. Thermodynamic influence of boron incorporation is inferred from the general understanding of temperature controlling trace element partitioning in calcite (*Pearson et al.*, 2006) but has not been tested experimentally in inorganic carbonates. Culture studies reveal that B/Ca is not significantly controlled by temperature (*Allen et al.*, 2011). However, in the ocean, many environmental variables covary with temperature, which complicates the interpretation of B/Ca variations to a single variable.

Paired measurements of B/Ca and Mg/Ca on the same samples enables us to evaluate whether there is any temporal offset in their seasonal cycles, as well as changes in B/Ca relative to temperature and incident light (Figure 2.8). The analysis shows that the maximum in the B/Ca ratio (June-July) precedes the maximum in the Mg/Ca ratio (August-September). This timing in B/Ca maximum most closely corresponds to the seasonal cycle in light intensity, whereas the timing of the maximum in the Mg/Ca ratio most closely corresponds to temperature. This suggests that light intensity, possibly through biologically mediated processes, may influence the B/Ca ratio.

2.6.4 Light and temperature related effects

Several studies linked the modification of pH within the calcifying fluid to the presence of symbionts (photosynthetic activity) (*Hönisch et al.*, 2003; *Wolf-Gladrow et al.*, 1999; *Zeebe et al.*, 2003). Microsensor studies of *O. universa* and *G. sacculifer* show that rates of photosynthetic activity and pH within the foraminifer micro environment are positively correlated with light intensity (*Jørgensen et al.*, 1985; *Rink et al.*, 1998). Based on the boron isotope results for *O. universa* grown in culture it was estimated that pH was 0.2 units higher under high light conditions (321±8 μmol photons m^{-2} s^{-1}) than low light conditions (19±2 μmol photons m^{-2} s^{-1}) (*Hönisch et al.*, 2003). Elevated internal pH at constant temperature increases the $[B(OH)_4^-/HCO_3^-]$ ratio of the internal calcifying pool, which in turn leads to higher B/Ca in the test (Figure 2.7 inset). The $\delta^{11}B$ of planktonic foraminifera is also positively offset from seawater $\delta^{11}B$, consistent with the hypothesis that symbiotic activity increases pH (and therefore borate ion) within the calcifying microenvironment (*Foster*, 2008; *Hönisch et al.*, 2003; *Sanyal et al.*, 2001; *Sanyal et al.*, 1996).

While no data currently exists for *G. ruber*, it is reasonable to expect that *G. ruber* is similar to other symbiont-bearing species in its sensitivity to light and that B/Ca ratios will be influenced by the seasonal light cycle. This is supported by the observation that the seasonality in B/Ca most closely tracks light intensity (Figure 2.8). Assuming the seasonal range in B/Ca (~15-20 μmol/mol) is solely due to changes in internal pH due to phtosynthetic activity, this would equate to a microenvironmental pH that is ~0.2-0.3 higher in summer (and lower in winter) from average annual conditions.

Hydrographic pH at OFP changes seasonally by 0.1 units and is mainly controlled by the temperature influence of the equilibrium constants with a minor contribution from changes in DIC. Given that the carbonate system does not significantly influence seasonality in pH, we can assume that seawater pH is approximately constant at OFP (i.e. 8.1 units at 25 m). Using the sensitivity of B/Ca to pH measured in *G. ruber* pink in culture experiments (*Allen et al.*, 2012), we can estimate the offset of foraminiferal internal pH from ambient seawater (Figure 2.9). Based on the offset is +0.2 units in the summer and -0.2 units winter.

The estimated positive pH offset during the summer and negative offset in winter from annual average foraminiferal B/Ca is consistent with seasonally variation in the relative rates of photosynthesis and respiration (P/R). Culture experiments reveal that P/R in *G. ruber* is strongly influenced by both light and temperature (*Lombard et al.*, 2009). The B/Ca ratios of *G. ruber* in the OFP sediment traps similarly indicate a shift in foraminiferal internal pH relative to ambient seawater due to the combined effects of seasonally changing light intensity and temperature on the P/R ratio.

2.6.5 Size-related effects

Test size in planktonic foraminifera is documented to influence trace metal ratios (*Elderfield et al.*, 2002; *Ni et al.*, 2007). Several factors could contribute to the observed relationship between B/Ca and test size in *G. ruber* white at OFP which include depth habitat, microenvironment chemistry and calcification rate. Similar $\delta^{18}O_c$ and Mg/Ca (Figure 2.3) suggest that foraminifera of the two size fractions calcify within a narrow depth range thereby experiencing the same temperature, pH and light conditions (Figure

2.5). It is conceivable that while differences in $\delta^{18}O$/temperature are not observed, changes in seawater pH might account for the difference in B/Ca ratios. The former possibility, however, seems unlikely given the observation that pH and temperature are tightly coupled at Bermuda (Figure 2.1). Furthermore, given the temperature gradient in the mixed layer (Figure 2.1) it is also difficult to invoke sufficient light level variability between the presumed calcification depths of both size fractions without recording a discernible temperature difference.

An alternative hypothesis to be considered is that changes in growth rate of different sized affect the incorporation of trace elements into foraminiferal calcite. *Elderfield et al*., 2002 proposed that the general increase of trace element ratios with test size is due to smaller individuals calcifying faster during early growth as compared to larger individuals. Conversely *Ni et al*., 2007 suggest that larger individuals calcify faster throughout the life cycle compared with smaller individuals. We note that the interpretation of a calcification rate mechanism is speculative and neither of these studies actually tested the calcification rates. At OFP, the offset in B/Ca ratios between the two size fractions of *G. ruber* remains constant throughout the seasonal cycle (Figure 2.3 and 2.4), suggesting that a stable process is at work. Results from inorganic growth experiments suggest that calcification rate and calcite growth may influence boron incorporation (*Ruiz-Agudo et al.*, 2012). This suggests that larger individuals incorporate more boron compared with smaller individuals due to enhanced calcite precipitation. However, if calcification rate alone was responsible for the offset in the B/Ca ratio we would expect that other trace element ratios (Mg/Ca and Sr/Ca) would behave similarly. This is not observed (Figure 2.4), and argues against the calcification rate hypothesis.

Lastly, the size offset observed for B/Ca may be a response to a biological process. As a symbiont-bearing planktonic foraminifer, *G. ruber* is influenced by the symbionts activity, which tends to enhance carbon fixation through photosynthesis and is thought to provide energy for growth (and hence improve calcification) of the foraminifer (*Gastrich et al.*, 1988; *Hemleben et al.*, 1989; *Spero et al.*, 1985). In our samples, larger tests are more positive in $\delta^{13}C$ by a near constant 0.5 ‰ compared with smaller individuals throughout the seasonal cycle (Figure 2.4). This is consistent with observations from core top studies of $\delta^{13}C$ varying with test size in symbiont bearing species (includes *G. ruber* white) (*Elderfield et al.*, 2002; *Ravelo et al.*, 1995). We postulate that larger individuals host more symbionts than smaller individuals leading to higher overall photosynthetic activity and thus any influence of symbionts' photosynthesis on geochemical signals may be amplified in larger foraminifera (*Spero et al.*, 1985).

The B/Ca ratios increase of ~15-20 μmol/mol between the two size fractions (200-300 and 300-400μm) at OFP implies a pH difference of ~0.2-0.3 (*Allen et al.*, 2012). Recent culture and core top results of *G. ruber* also reveal a significant relationship between test size and $\delta^{11}B$ (*Henehan et al.*, 2013), consistent with higher microenvironment-pH in larger versus smaller individuals. We suggest that the elevated pH within the calcifying microenvironment in larger individuals possibly reflects the ability of larger individuals to host more symbionts, which would increase total photosynthetic activity. This hypothesis is consistent with the generally heavier $\delta^{13}C$ values of larger individuals providing evidence of higher rates of photosynthesis. We note that another potential mechanism is size related differences in CO_2 diffusion, as

observed in various groups of marine phytoplankton (*Popp et al.*, 1998). Diffusion in larger foraminifer individuals is likely to be faster and more efficient than in small individuals due to their larger surface area, which is expected to minimize the CO_2 (and pH) differential between ambient seawater and internal microenvironment i.e. closer to equilibrium.

2.7 Summary and Conclusions

This study underscores the importance of using different approaches for calibrating geochemical proxies (i.e., cultures, sediment traps and core tops). The results show that B/Ca variability of 30-40 μmol/mol in the surface dwelling planktonic foraminifer *G. ruber* from OFP sediment trap samples (Sargasso Sea) that follows the changes in mixed-layer temperature and inversely correlates with ambient pH. The observed variability cannot be attributed to changes in the mixed layer $\left[B(OH)_4^-/HCO_3^-\right]_{sw}$ ratio, which remains relatively constant throughout the year. Furthermore, the apparent covariation with temperature is inconsistent with results from controlled culture experiments that suggest a negligible temperature influence on B/Ca variability in *G. ruber*, and other planktonic foraminifera species (*Allen et al.*, 2012; *Allen et al.*, 2011). Instead, we suggest that the B/Ca variability reflects the changes in the internal pH within the foraminifera calcifying fluid, rather than the surrounding ambient seawater. The internal pH is likely modified by the balance between the photosynthetic symbiont activity and respiration, which are influenced by seasonal changes in light and temperature. Support for this hypothesis can be seen in the increase of B/Ca with increasing test size despite constant Mg/Ca and $\delta^{18}O$ ratios and the size-dependent B/Ca offset as reflecting higher photosynthetic activity due to greater

abundance of symbionts in larger foraminifera (i.e., higher microenvironment pH). Although our results imply that B/Ca (and possibly $\delta^{11}B$) ratios reflect primarily the internal pH as biologically mediated by light and temperature, we note that on annual and greater time scales this variability averages out and thus B/Ca may reflect seawater pH as the offset between the internal pH and ambient seawater remains relatively constant. This is borne out by culture experiments that see clear evidence for increasing B/Ca and $\delta^{11}B$ at elevated seawater pH. Variations in test size distribution within samples and temperature could, however, introduce significant noise into reconstructions using this proxy due to their influence on the internal pH. We speculate that geologic intervals in which pH changes are less than 0.1-0.2 units such as Pleistocene glacial-interglacial timescales are at the limit of the reliability of the B/Ca proxy and therefore the interpretation of such records should be treated with caution (*Allen and Hönisch* 2012). It is possible, however, that major climate transitions during the Cenozoic such as the Eocene-Oligocene and Paleocene-Eocene boundaries where the expected pH changes are greater than 0.1 units will be reflected in the foraminiferal B/Ca records (*Allen and Hönisch* 2012). In these cases, the comparison between changes in Mg/Ca (as a temperature proxy) and B/Ca recorded in the same samples may be used to discern temporal relationships between perturbations in the carbon cycle and Earth's climate.

2.8 Acknowledgements

We would like to thank JC Weber at MBL for laboratory assistance. Nick Bates for providing carbonate chemistry data at BATS and Tommy Dickey for light data from the BTM. Katherine Allen and Bärbel Hönisch for helpful discussions that improved the manuscript. This work was funded by ACS-PRF grant 47994-AC2 awarded to YR.

2.9 References

Al-Ammar, A.S., Gupta, R.K., and Barnes, R.M. (2000), Elimination of boron memory effect in inductively coupled plasma-mass spectrometry by ammonia gas injection into the spray chamber during analysis, *Spectrochimica Acta B*, *55*(6), 629-635.

Allen, K.A., and Hönisch, B. (2012a), The planktic foraminiferal B/Ca proxy for seawater carbonate chemistry: A critical evaluation, *Earth and Planetary Science Letters*, *345–348*(0), 203-211.

Allen, K.A., Hönisch, B., Eggins, S.M., and Rosenthal, Y. (2012b), Environmental controls on B/Ca in calcite tests of the tropical planktic foraminifer species Globigerinoides ruber and Globigerinoides sacculifer, *Earth and Planetary Science Letters*, *351–352*(0), 270-280.

Allen, K.A., et al. (2011), Controls on boron incorporation in cultured tests of the planktic foraminifer Orbulina universa, *Earth and Planetary Science Letters*, *309*(3–4), 291-301.

Anand, P., Elderfield, H., and Conte, M.H. (2003), Calibration of Mg/Ca thermometry in planktonic foraminifera from a sediment trap time series, *Paleoceanography*, *18*(2), 1050.

Arbuszewski, J., deMenocal, P., Kaplan, A., and Farmer, E.C. (2010), On the fidelity of shell-derived [delta]18Oseawater estimates, *Earth and Planetary Science Letters*, *300*(3-4), 185-196.

Barker, S., Greaves, M., and Elderfield, H. (2003), A study of cleaning procedures used for foraminiferal Mg/Ca paleothermometry, *Geochemistry Geophysics Geosystems*, *4*(9), 8407.

Bates, N.R. (2007), Interannual variability of the oceanic CO2 sink in the subtropical gyre of the North Atlantic Ocean over the last 2 decades, *J. Geophys. Res.*, *112*(C9), C09013.

Bates, N.R., Michaels, A.F., and Knap, A.H. (1996), Seasonal and interannual variability of oceanic carbon dioxide species at the U.S. JGOFS Bermuda Atlantic Time-series Study (BATS) site, *Deep Sea Research Part II: Topical Studies in Oceanography*, *43*(2–3), 347-383.

Bates, N.R., Takahashi, T., Chipman, D.W., and Knap, A.H. (1998), Variability of pCO2 on diel to seasonal timescales in the Sargasso Sea near Bermuda, *Journal of Geophysical Research: Oceans*, *103*(C8), 15567-15585.

Bé, A.W.H., and Tolderlund, D.S. (1971), Distribution and Ecology of Living Planktonic Foraminifera in Surface Waters of the Atlantic and Indian Oceans, *In Funnel, B.M., and Riedel, W.R. (Eds.), he Micropaleontology of Oceans: Cambridge (Cambridge Univ. Press)*, 105-1449.

Bemis, B.E., Spero, H.J., Bijma, J., and Lea, D.W. (1998), Reevaluation of the Oxygen Isotopic Composition of Planktonic Foraminifera: Experimental Results and Revised Paleotemperature Equations, *Paleoceanography*, *13*(2), 150-160.

Brown, R.E., Anderson, L.D., Thomas, E., and Zachos, J.C. (2011), A core-top calibration of B/Ca in the benthic foraminifers Nuttallides umbonifera and Oridorsalis umbonatus: A proxy for Cenozoic bottom water carbonate saturation, *Earth and Planetary Science Letters*, *310*(3–4), 360-368.

Conte, M.H., Ralph, N., and Ross, E.H. (2001), Seasonal and interannual variability in deep ocean particle fluxes at the Oceanic Flux Program (OFP)/Bermuda Atlantic Time Series (BATS) site in the western Sargasso Sea near Bermuda, *Deep Sea Research Part II: Topical Studies in Oceanography*, *48*(8–9), 1471-1505.

Deuser, W.G. (1987), Seasonal variations in isotopic composition and deep-water fluxes of the tests of perennially abundant planktonic foraminifera of the Sargasso Sea; results from sediment-trap collections and their paleoceanographic significance, *The Journal of Foraminiferal Research*, *17*(1), 14-27.

Deuser, W.G., Ross, E.H., Hemleben, C., and Spindler, M. (1981), Seasonal changes in species composition, numbers, mass, size, and isotopic composition of planktonic foraminifera settling into the deep sargasso sea, *Palaeogeography, Palaeoclimatology, Palaeoecology*, *33*(1–3), 103-127.

Dickson, A.G., and Millero, F.J. (1987), A comparison of the equilibrium constants for the dissociation of carbonic acid in seawater media, *Deep Sea Research Part A. Oceanographic Research Papers*, *34*(10), 1733-1743.

Elderfield, H., Vautravers, M., and Cooper, M. (2002), The relationship between shell size and Mg/Ca, Sr/Ca, $\delta^{18}O$, and $\delta^{13}C$ of species of planktonic foraminifera, *Geochemistry, Geophysics, Geosystems*, *3*(8), 1052.

Erez, J., and Honjo, S. (1981), Comparison of isotopic composition of planktonic foraminifera in plankton tows, sediment traps and sediments, *Palaeogeography, Palaeoclimatology, Palaeoecology*, *33*(1–3), 129-156.

Foster, G.L. (2008), Seawater pH, pCO2 and [CO2-3] variations in the Caribbean Sea over the last 130 kyr: A boron isotope and B/Ca study of planktic foraminifera, *Earth and Planetary Science Letters*, *271*(1-4), 254-266.

Gastrich, M.D., and Bartha, R. (1988), Primary Productivity in the Planktonic Foraminifer Globigerinoides ruber (D'Orbigny), *Journal of Foraminiferal Research*, *18*, 137-142.

Hemleben, C., Spindler, M., and Anderson, O.R. (1989), Modern Planktonic Foraminifera, *Berlin (Springer-Verlag)*.

Hemming, N.G., and Hanson, G.N. (1992), Boron isotopic composition and concentration in modern marine carbonates, *Geochimica Cosmochimica Acta*, *56*, 537-543.

Hendry, K.R., Rickaby, R.E.M., Meredith, M.P., and Elderfield, H. (2009), Controls on stable isotope and trace metal uptake in Neogloboquadrina pachyderma (sinistral) from an Antarctic sea-ice environment, *Earth and Planetary Science Letters*, *278*(1-2), 67-77.

Henehan, M.J., et al. (2013), Calibration of the boron isotope proxy in the planktonic foraminifera Globigerinoides ruber for use in palaeo-CO2 reconstruction, *Earth and Planetary Science Letters*, *364*(0), 111-122.

Hönisch, B., et al. (2009), Atmospheric carbon dioxide concentration across the Mid-Pleistocene transition, *Science*, *324*(5934), 1551-1554.

Hönisch, B., et al. (2003), The influence of symbiont photosynthesis on the boron isotopic composition of foraminifera shells, *Marine Micropaleontology*, *49*(1-2), 87-96.

Huang, S., and Conte, M.H. (2009), Source/process apportionment of major and trace elements in sinking particles in the Sargasso sea, *Geochimica et Cosmochimica Acta*, *73*(1), 65-90.

Jœrgensen, B.B., Erez, J., Revsbech, N.P., and Cohe, Y. (1985), Symbiotic photosynthesis in a planktonic foraminiferan, Globeriginoides sacculifer (Brady), studied with microelectrodes, *Limnology and Oceanography*, *30*(6), 1253-1267.

Klochko, K., et al. (2009), Re-Evaluating boron speciation in biogenic calcite and aragonite using 11B mas NMR, *Geochim. Cosmochim. Acta*, *73*, 1890-1900.

Lee, K., et al. (2010), The universal ratio of boron to chlorinity for the North Pacific and North Atlantic oceans, *Geochimica et Cosmochimica Acta*, *74*(6), 1801-1811.

Lombard, F., Erez, J., Michel, E., and Labeyrie, L. (2009), Temperature effect on respiration and photosynthesis of the symbiont-bearing planktonic foraminifera Globigerinoides ruber, Orbulina universa, and Globigerinella siphonifera, *Limnology and Oceanography*, *54*(1), 210-218.

McGillicuddy, D.J., et al. (1999), Mesoscale variations of biogeochemical properties in the Sargasso Sea, *Journal of Geophysical Research: Oceans*, *104*(C6), 13381-13394.

Mehrbach, C., Culberson, C.H., Hawley, J.E., and Pytkowicz, R.M. (1973), Measurement of the Apparent Dissociation Constants of Carbonic Acid in Seawater at Atmospheric Pressure, *Limnology and Oceanography*, *18*(6), 897-907.

Ni, Y., et al. (2007), A core top assessment of proxies for the ocean carbonate system in surface-dwelling foraminifers, *Paleoceanography*, *22*, PA3212.

Pak, D.K., Lea, D.W., and Kennett, J.P. (2004), Seasonal and interannual variation in Santa Barbara Basin water temperatures observed in sediment trap foraminiferal Mg/Ca, *Geochemistry, Geophysics, Geosystems*, *5*(12), Q12008.

Pearson, P.N., and Palmer, M.R. (2000), Atmospheric carbon dioxide concentrations over the past 60 million years, *Nature*, *406*(6797), 695-699.

Pearson, P.N., et al. (2006), Atlas of Eocene Planktonic Foraminifera, *Cushman Foundation Special Publication*, *41*, 257-326.

Pelletier, G., Lewis, E., and D., W. (2007), CO_2sys.xls: a calculator for the CO_2 system in seawater for Microsoft Excel/VBA, *Washington State Department of Ecology, Olympia, WA, USA.*

Popp, B.N., et al. (1998), Effect of Phytoplankton Cell Geometry on Carbon Isotopic Fractionation, *Geochimica et Cosmochimica Acta*, *62*(1), 69-77.

Rae, J.W.B., Foster, G.L., Schmidt, D.N., and Elliott, T. (2011), Boron isotopes and B/Ca in benthic foraminifera: Proxies for the deep ocean carbonate system, *Earth and Planetary Science Letters*, *302*(3–4), 403-413.

Ravelo, A.C., and Fairbanks, R.G. (1995), Carbon isotopic fractionation in multiple species of planktonic foraminifera from core-tops in the tropical Atlantic *Journal of Foraminiferal Research*, *25*(1), 53-74.

Rink, S., Kühl, M., Bijma, J., and Spero, H.J. (1998), Microsensor studies of photosynthesis and respiration in the symbiotic foraminifer <i>Orbulina universa</i&gt, *Marine Biology*, *131*(4), 583-595.

Rosenthal, Y., Field, M.P., and Sherrell, R.M. (1999), Precise determination of element/calcium ratios in calcareous samples using Sector Field Inductively Couple Plasma Mass Spectrometry, *Analytical Chemistry 71*, 3248-3253.

Ruiz-Agudo, E., et al. (2012), Boron incorporation into calcite during growth: Implications for the use of boron in carbonates as a pH proxy, *Earth and Planetary Science Letters*, *345–348*(0), 9-17.

Sanyal, A., Bijma, J., Spero, H., and Lea, D.W. (2001), Empirical relationship between pH and the boron isotopic composition of *Globigerinoides sacculifer*: Implications for the boron isotope paleo-pH proxy, *Paleoceanography*, *16*, 515-519.

Sanyal, A., et al. (1996), Oceanic pH control on the boron isotopic composition of foraminifera: Evidence from culture experiments, *Paleoceanography*, *11*, 513-517.

Schmidt, G.A., Bigg, G.R., and Rohling., E.J. (1999), Global Seawater Oxygen-18 Database - v1.21.

Shatova, O., Koweek, D., Conte, M.H., and Weber, J.C. (2012), Contribution of zooplankton fecal pellets to deep ocean particle flux in the Sargasso Sea assessed using quantitative image analysis, *Journal of Plankton Research*, *34*(10), 905-921.

Spero, H.J., and Parker, S.L. (1985), Photosynthesis in the symbiotic planktonic foraminifer Orbulina universa, and its potential contribution to oceanic primary productivity, *The Journal of Foraminiferal Research*, *15*(4), 273-281.

Spivack, A.J., You, C.-F., and Smith, H.J. (1993), Foraminiferal boron isotope ratios as a proxy for surface ocean pH over the past 21 Myr, *Nature*, *363*(6425), 149.

Tripati, A.K., Roberts, C.D., and Eagle, R.A. (2009), Coupling of CO2 and Ice Sheet Stability Over Major Climate Transitions of the Last 20 Million Years *Science*, *326*(5958), 1394-1397.

Williams, D.F., Bé, A.W.H., and Fairbanks, R.G. (1981), Seasonal stable isotopic variations in living planktonic foraminifera from bermuda plankton tows, *Palaeogeography, Palaeoclimatology, Palaeoecology*, *33*(1–3), 71-102.

Wolf-Gladrow, D.A., Bijma, J., and Zeebe, R.E. (1999), Model simulation of the carbonate chemistry in the microenvironment of symbiont bearing foraminifera, *Marine Chemistry*, *64*(3), 181-198.

Yu, J., and Elderfield, H. (2007a), Benthic foraminiferal B/Ca ratios reflect deep water carbonate saturation state, *Earth and Planetary Science Letters*, *258*(1-2), 73-86.

Yu, J., Elderfield, H., and Hönisch, B. (2007b), B/Ca in planktonic foraminifera as a proxy for surface seawater pH, *Paleoceanography*, *22*(2), PA2202.

Yu, J., Elderfield, H., Greaves, M., and Day, J. (2007c), Preferential dissolution of benthic foraminiferal calcite during laboratory reductive cleaning, *Geochem. Geophys. Geosyst.*, *8*(6), Q06016.

Zeebe, R.E., Wolf-Gladrow, D.A., Bijma, J., and Hönisch, B. (2003), Vital effects in foraminifera do not compromise the use of $\delta^{11}B$ as a paleo-pH indicator: Evidence from modelling, *Paleoceanography*, *18*, 1043, doi: 1010.1029/2003PA000881.

Table 2.1 Long-term analytical precision of laboratory internal consistency standards from February to August 2010.

Consistency Standards	Statistics	Mg/Ca mmol/mol	B/Ca µmol/mol
CS1	Expected	1.240	20.656
	Mean	1.265	24.671
	± 1σ	0.011	1.112
	% RSD	**0.90%**	**4.51%**
	Δ (meas-exp) %	1.99%	19.44%
CS2	Expected	3.318	115.433
	Mean	3.379	120.931
	± 1σ	0.014	3.970
	% RSD	**0.41%**	**3.28%**
	Δ (meas-exp) %	1.83%	4.76%
CS3	Expected	7.506	242.541
	Mean	7.673	250.078
	± 1σ	0.055	7.584
	% RSD	**0.71%**	**3.03%**
	Δ (meas-exp) %	2.23%	3.11%

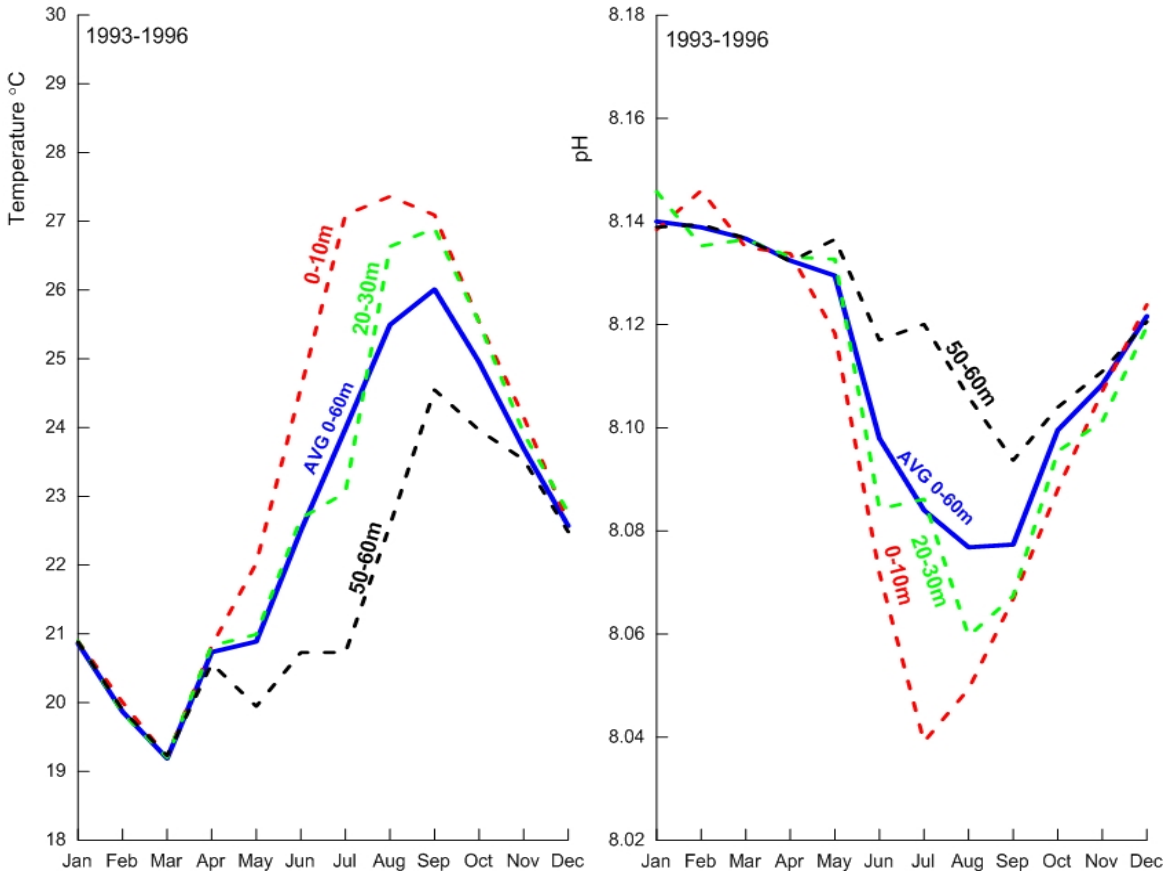

Figure 2.1 Measurements of ocean temperature (°C) and pH (derived from DIC and ALK) at BATS (31°40'N 64°10'W) for the upper 60 meters of the water column from 1993-1995. Plotted are monthly averaged temperature and pH values at discrete ocean depth ranges (0-10, 20-30 and 50-60m; colored dashed lines) and averaged from 0-60m.

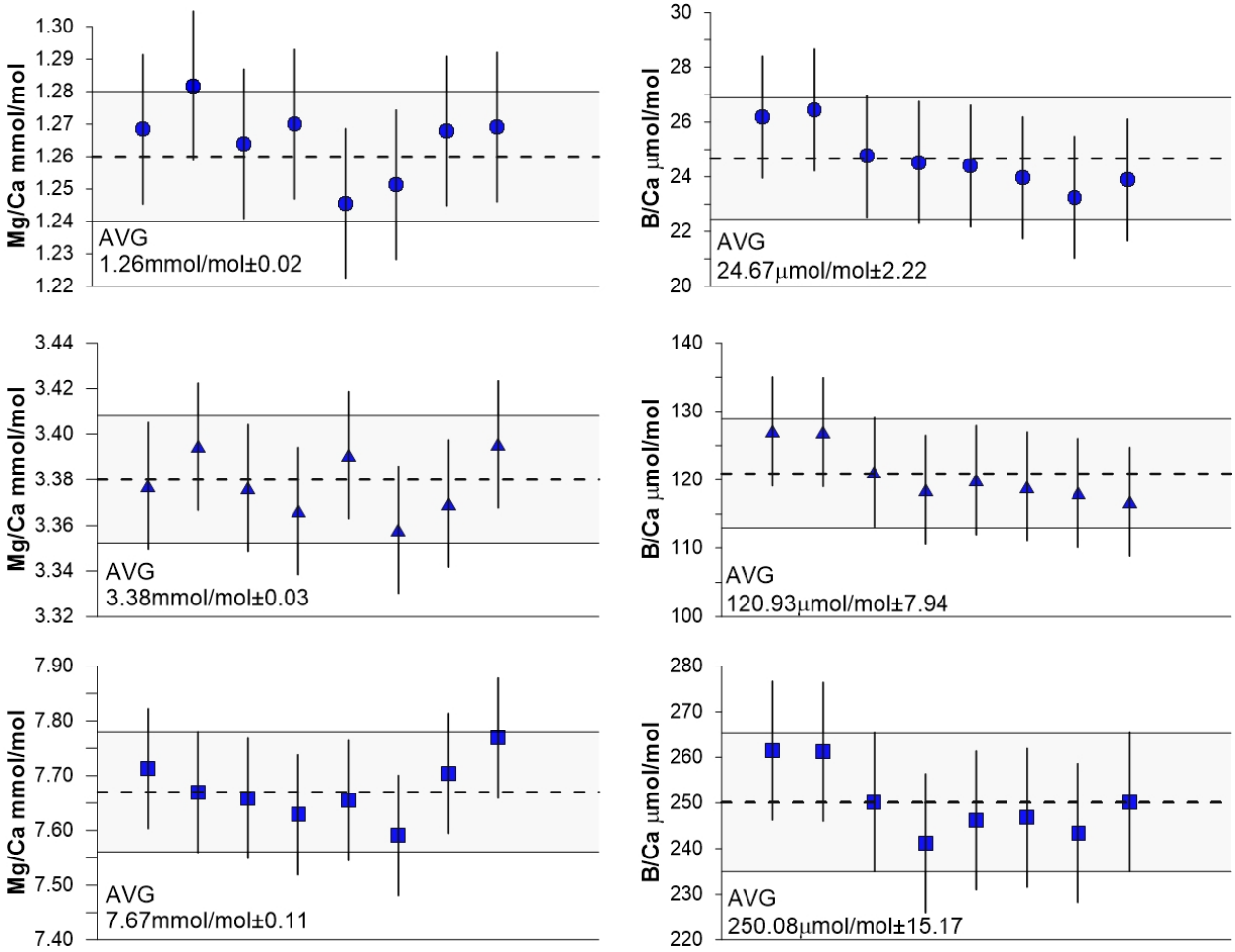

Figure 2.2 Measurements of Mg/Ca (mmol/mol) and B/Ca (µmol/mol) for in house consistency standards plotted during the data acquisition for this study (February to August 2010). Average values and with uncertainty are reported as 2σ.

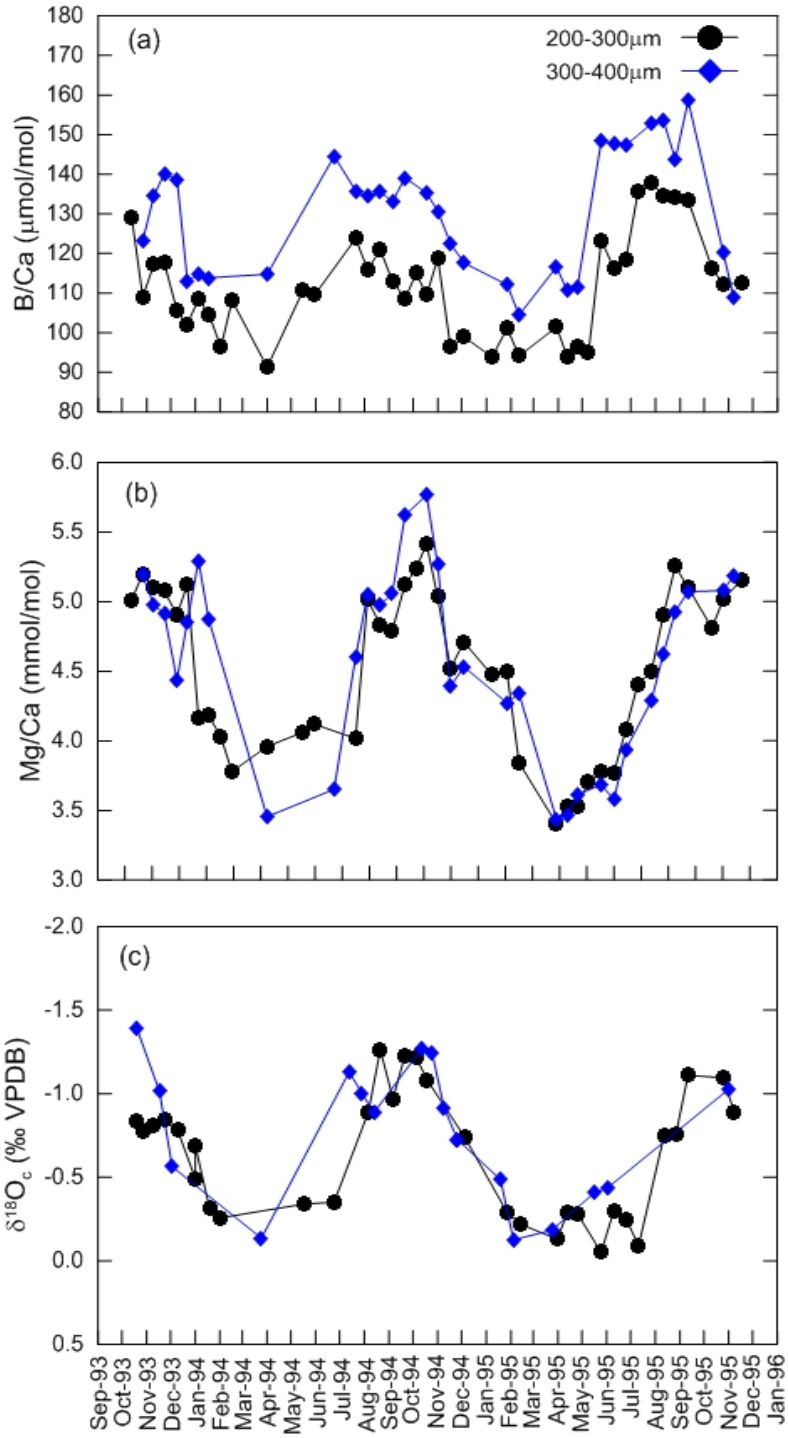

Figure 2.3 Biweekly measurements of (a) B/Ca (µmol/mol) (b) Mg/Ca (mmol/mol) and (c) $\delta^{18}O$ (‰ VPDB) of *G. ruber* white in two size fractions: 200-300µm (black circle) and 300-400µm (blue diamond).

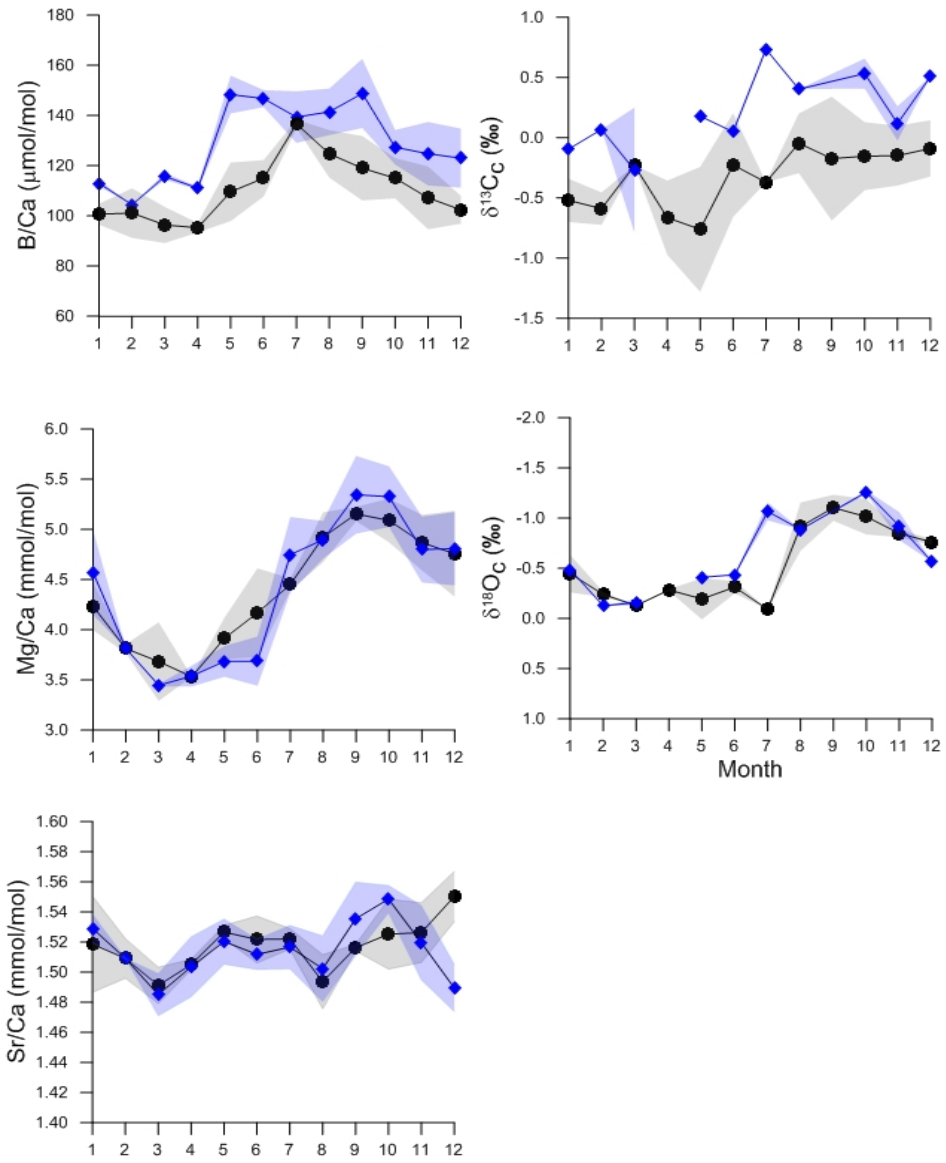

Figure 2.4 Annual values of B/Ca (µmol/mol), $\delta^{13}C_c$ (‰ VPDB), Mg/Ca (mmol/mol), $\delta^{18}O_c$ (‰ VPDB) and Sr/Ca (mmol/mol) of *G. ruber* white in two size fractions: 200-300µm (black circle) and 300-400µm (blue diamond). Monthly values are averaged monthly measurements from 1993-1995 (interval used in this study) and shaded regions represent the monthly standard deviation. Note that only B/Ca and $\delta^{13}C_c$ exhibit an offset between the two size fractions.

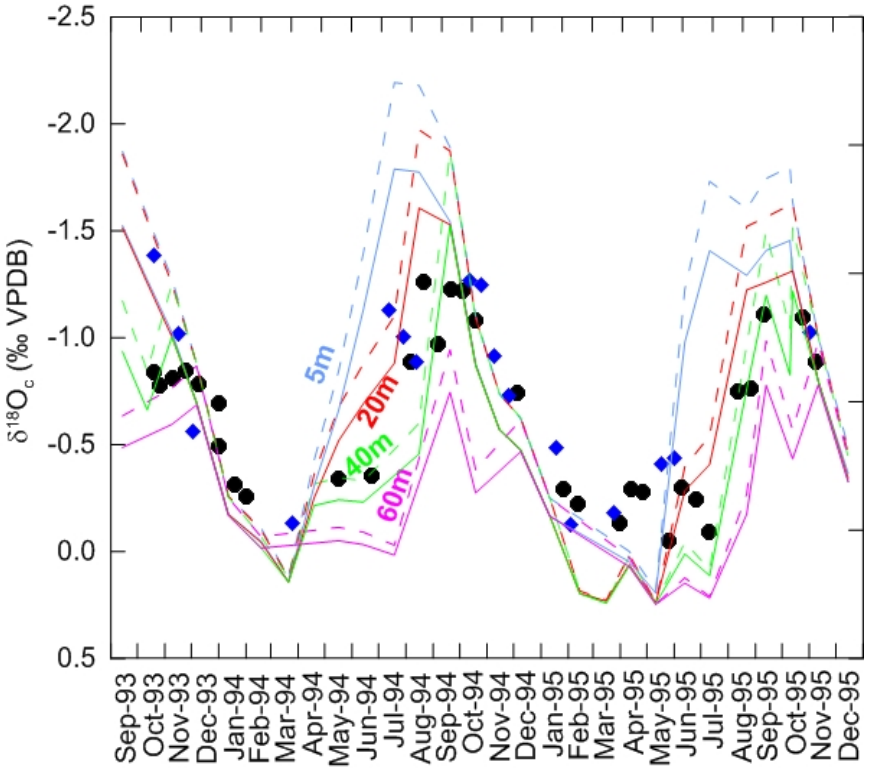

Figure 2.5 Monthly values of $\delta^{18}O_c$ (‰ VPDB) estimated based on equilibrium with seawater using temperature and salinity measurements obtained from BATS for ocean depth intervals (5, 20, 40 and 60m). Solid line is the predicted $\delta^{18}O_c$ based on the paleotemperature of *Bemis et al*., (1998) and the dashed line is computed from the *Shackleton et al*., 1974 equation. *G. ruber* white $\delta^{18}O_c$ (‰ VPDB) measurement are plotted in two size fractions: 200-300µm (black circle) and 300-400µm (blue diamond).

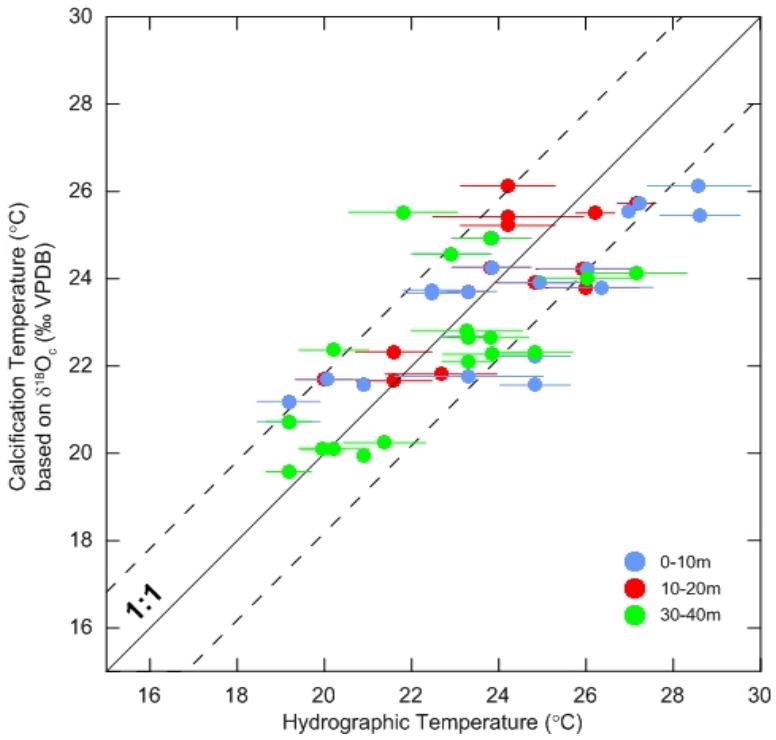

Figure 2.6 Temperature based on $\delta^{18}O_c$ (‰ VPDB) for *G. ruber* white plotted versus contemporaneous hydrographic sea temperatures (°C) (0-10m, blue; 10-20m, red; 30-40m, green). Error bars represent the standard deviation of monthly temperature values during 1993-1995 and the dashed lines represent the 95% confidence interval for 20-40m values.

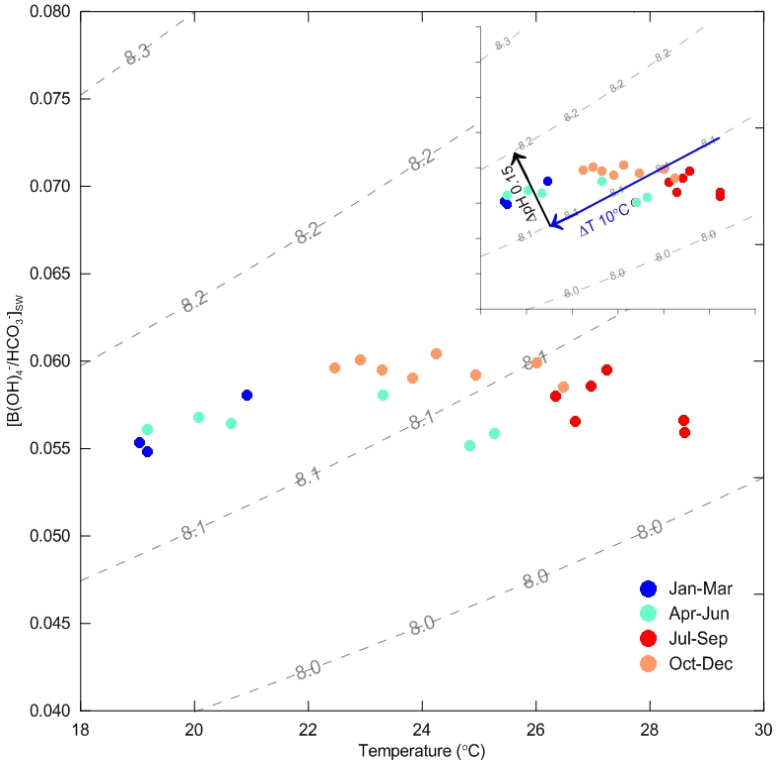

Figure 2.7 Seawater temperature versus $\left[B(OH)_4^-/HCO_3^-\right]_{sw}$ crossplotted with pH calculated using a constant alkalinity (2400µmol/kg), salinity (36) and total seawater boron (445µmol/kg). Seasonal surface (0-5m) $\left[B(OH)_4^-/HCO_3^-\right]_{sw}$ versus SST derived from BATS hydrographic data (1993-1995).

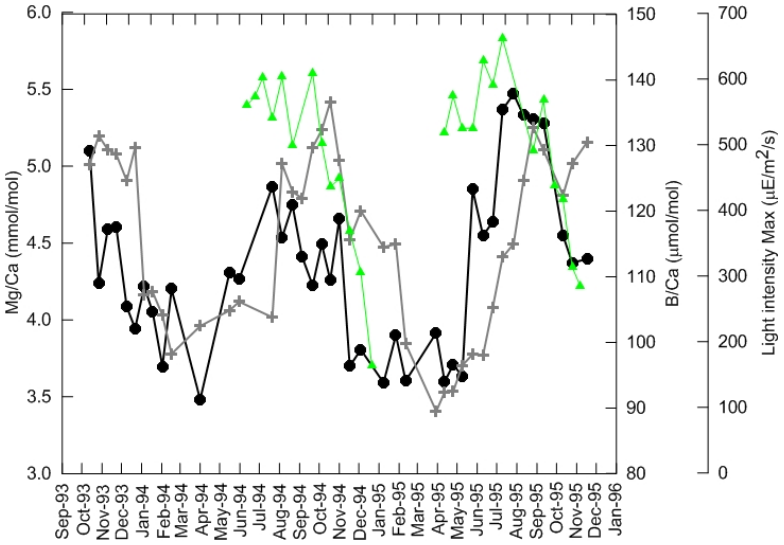

Figure 2.8 *G. ruber* white for 200-300 µm for B/Ca ratios (µmol/mol, black circle) and Mg/Ca ratios (mmol/mol, gray cross). Maximum light intensities (µE/m^2/s, green triangle) at 20m during the sediment trap deployment intervals are averaged from hourly measurements. Data collected from the Bermuda Mooring Testbed courtsey of Tommy Dickey UCSB.

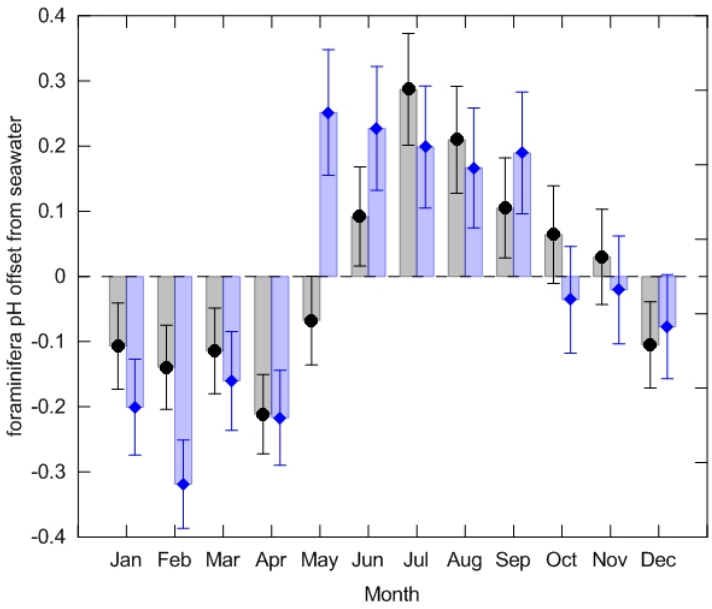

Figure 2.9 Monthly average offset of foraminifera pH from seawater (annual average = 8.1 at 25m) estimated from B/Ca µmol/mol (200-300m - black circle; and 300-400m - blue diamond) using the sensitivity from *Allen* et al., 2012. Error bars (y-axis) are the standard deviation of monthly pH values.

3.0 Chapter Three

Boron geochemistry in planktonic foraminifera from core top sediments

3.1 Abstract

Boron/Calcium (B/Ca) and boron isotope ($\delta^{11}B$) ratio measurements in 11 planktonic foraminifera species from globally distributed surface sediments were used to evaluate the relative influences of carbonate chemistry, temperature and vital effects on boron incorporation into foraminiferal calcite. With the understanding that planktonic foraminifera calcify their tests at different depths within the water column, depth profiles of B/Ca and $\delta^{11}B$ were constructed. B/Ca values exhibit a decreasing trend with increasing water depth and $\delta^{11}B$ shift towards lower values. B/Ca ratios in surface dwelling *Globigerinoides* spp. are offset from equilibrium values likely due to the effect of their photosymbionts. Support for this vital effect comes from the observations that B/Ca in *Globigerinoides* spp. increases with test size, temperature and light levels (Chapter Two) which influence symbiont activity. Temperature and vital effects on B/Ca in thermocline and deep dwelling planktonic foraminifera are found to be minimal. Core-top calibrations based on the comparison of B/Ca and seawater $\left[B(OH)_4^-/HCO_3^-\right]$ hydrographic data in thermocline (*N. dutertrei* and *P. obliquiloculata*) and deep dwelling *Globorotalia* spp. are presented. $\delta^{11}B$ in all planktonic foraminifera species are offset from calculated $\delta^{11}B$ of $B(OH)_4^-$ assuming equilibrium with ambient seawater. While the application of a temperature correction on the fractionation factor between borate and boric acid (α_B) yielded $\delta^{11}B$ foraminieral results that are more consistent with predicted equilibrium values, offsets remained. Interspecies differences and vital effects may account for the disequilibrium of foraminiferal $\delta^{11}B$ from predicted seawater values

through the modification of carbonate chemistry within the calcifying fluid. It is recommended that the observed vital effects be considered when utilizing the $\delta^{11}B$ proxy in planktonic foraminfera in paleoceanographic studies.

3.2 Introduction

In seawater boron exists as two species, boric acid $B(OH)_3$ and borate $B(OH)_4^-$ and their relative concentrations and isotopic composition are dependent on pH (Figure 3.1). Boron has two stable isotopes, ^{10}B and ^{11}B and the differences in coordination at vibration frequencies results in an isotopic fractionation ($\alpha_B = 1/ {}^{11\text{-}10}K_B$) between the boron species. Analysis of modern marine carbonates yields isotopic values consistent with that of borate in seawater leading *Hemming and Hanson* (1992) to suggest that borate is likely the species incorporated into carbonates. Based on this model of borate incorporation, proposed the following equation *Hemming and Hanson* (1992)

$$CaCO_3 + B(OH)_4^- \leftrightarrow Ca(HBO)_3 + HCO_3^- + H_2O$$

Yu et al., (2007) modified the above equation to define B/Ca in planktonic foraminifera using a partition coefficient K_D, between incorporated seawater $B(OH)_4^-$ and $CaCO_3$ as:

$$K_D \approx \frac{[B/Ca]_{CaCO_3}}{[B(OH)_4^-/HCO_3^-]_{seawater}}$$

The proposed theoretical basis for boron incorporation (*Hemming and Hanson* 1992; *Yu et al.*, 2007) in planktonic foraminifera is supported by empirically derived relationships from culture experiments (*Allen et al.*, 2012; *Allen et al.*, 2011).

Planktonic foraminifera B/Ca records across Pleistocene glacial-interglacial cycles in *Globigerinoides ruber* and *Globigerinoides sacculifer* decrease by ~10-

15µmol/mol from interglacial to glacial periods (*Foster*, 2008; *Tripati et al.*, 2009; *Yu et al.*, 2007), inconsistent with the expectation of higher B/Ca at higher glacial pH (based on boron isotope measurements in the same cores) (*Foster*, 2008; *Yu et al.*, 2007). In contrast, high latitude records of *Globorotalia inflata* show invariant B/Ca values (*Yu et al.*, 2007) and *Neogloboquadrina pachyderma* (sinistral) increase by ~20µmol/mol (*Yu et al.*, 2013) . Core-top and down-core calibrations on *G. ruber, G. sacculifer, N. dutertrei* and *G. inflata* indicate that K_D is not constant and suggest that temperature (*Yu et al.*, 2007) or $[CO_3^{2-}]$ (*Foster*, 2008) may influence K_D. *Allen and Hönisch* (2012) argue that the K_D derived calibrations from core-top (*Foster*, 2008) and down-core (*Yu et al.*, 2007) studies can be driven by independent relationship(s) with $[B(OH)_4^-/HCO_3^-]_{sw}$ and other environmental variables, not related to B/Ca. For this reason *Allen and Hönisch* (2012) suggest that K_D derived calibrations do not necessarily apply to B/Ca and can be misleading.

Culture studies (*Allen et al.*, 2012; *Allen et al.*, 2011) in symbiotic planktonic foraminifera species do not show a significant temperature effect on boron incorporation into foraminiferal tests for B/Ca. Sediment-trap *G. ruber* results (Chapter Two), however, indicates that light intensity and temperature may influence rates of symbiotic activity which can modify the pH within the foraminiferal calcifying pool and therefore, B/Ca recorded in the test. Based on the potential influence of temperature on photosynthetic activity in *G. ruber* (Chapter Two) it is hypothesized that the trends in the Pleistocene B/Ca records may be due to differences in the relative contribution(s) of temperature influencing boron incorporation, which varies between the tropical (*Foster*, 2008; *Tripati et al.*, 2009; *Yu et al.*, 2007) and polar ocean sites (*Yu et al.*, 2007; *Yu et al.*, 2013). To

test the hypothesis put forth in Chapter Two, symbiotic and asymbiotic species were analyzed from core-top sediments to evaluate the influence(s) of $[B(OH)_4^-/HCO_3^-]_{sw}$ and temperature on B/Ca.

Core-top sediments provide the opportunity to evaluate the controls on B/Ca in planktonic foraminifera to ambient seawater environmental parameters. More importantly core-top samples undergo similar sediment depositional processes that occur in down core records making them valuable analogs. A disadvantage of using core-tops is that in the ocean, salinity, temperature and pH often covary making it difficult to discern their independent influences on test geochemistry. In order to assess the influence of ocean carbonate chemistry and temperature on the boron geochemistry of foraminifera, B/Ca and $\delta^{11}B$ measurements in different species of planktonic foraminifera are compared to the proposed environmental variables at their ambient calcification depths.

3.3 Materials and Methods

3.3.1 Sample Collection

Modern and Holocene core-top sediment samples from Cape Hatteras, Gulf of Mexico, the Galapagos Platform, Indonesia, New Zealand, and Sierra Leone Rise locations were used in this study (Figure 3.2; Table 3.1). Cape Hatteras samples were collected during the R/V Knorr 178 cruise in 2004 in the Western Sargasso Sea using a multi-corer during the cruise. The Gulf of Mexico was a subsample from a box core collected as a part of the Deepwater Program: Northern Gulf of Mexico Continental Slope Habitats and Benthic Ecology (DGoMB) project (Gilbert T. Rowe, TAMU, 2000). Core-top samples from the Galapagos platform were collected during the R/V Knorr 195

cruise in 2009 using a multi-corer. The core-top samples from Indonesia in the Southern Maskassar Straits were collected using a multi-corer on the R/V Baruna Jaya VIII in 2003. New Zealand core-top samples were collected from the Bay of Plenty and Chatham Rise using a multi-corer on the R/V Roger Revelle cruise in 2003. Sierra Leone rise core-top samples were collected using gravity cores on the R/V Endeavor cruise in 1996 and reflect late-Holocene conditions (*Rosenthal et al.*, 1997). Radiocarbon dates for Knorr 178 core tops yielding modern values (<1000 years) (Lloyd Keigwin, personal communication) (*Keigwin et al.*, 2009). Samples from Gulf of Mexico, Galapagos Platform, Indonesia and New Zealand are assumed to reflect modern to late Holocene conditions.

3.3.2 Oceanographic parameters

Core-top planktonic foraminiferal B/Ca and $\delta^{11}B$ were compared with modern seawater environmental variables. World Ocean Atlas 2009 (WOA09) database was used to generate temperature, salinity and nutrient (phosphate, silicate) profiles at each core-top location. To calculate ocean pH (seawater scale), dissolved inorganic carbon (DIC) and alkalinity (ALK) measurements were compiled from the Global Ocean Data Analysis Project (GLODAP) (*Key et al.*, 2004). Pre-industrial DIC values were estimated by removing the recent addition of anthropogenic DIC (*Key et al.*, 2004; *Sabine et al.*, 2004). Carbonate system calculations were made using CO_2sys (*Pelletier et al.*, 2007) and K_1, K_2 equilibrium constants from (*Mehrbach et al.*, 1973) as refit by (*Dickson et al.*, 1987). Total seawater boron concentrations are related to surface ocean salinity as calculated from the globally defined equation of (*Lee et al.*, 2010): [B] = 432.6 μmol/kg x

(S/35). Seawater $\delta^{11}B_{B(OH)_4^-}$ was calculated using K_B equation from (*Dickson*, 1990) with the pressure correction from (*Culberson et al.*, 1968). Using the following equation:

$$\delta^{11}B_{B(OH)_4^-} = \delta^{11}B_{sw} * B_T - 1000\ (\alpha_B - 1)\ [B(OH)_3]/[B(OH)_4^-] + \alpha_B\ [B(OH)_3]$$

$B(OH)_4^-$ and $B(OH)_3$ concentrations were calculated using equations from (*Zeebe et al.*, 2001) and $\delta^{11}B_{sw}$ value of 39.61‰ (*Foster et al.*, 2010).

3.3.3 Estimation of calcification depth

Calcification depths were estimated by comparing the measured foraminiferal $\delta^{18}O$ of calcite from core top sediments to the predicted $\delta^{18}O$ by assuming equilibrium with seawater. Depth profiles of predicted $\delta^{18}O$ were compiled from $\delta^{18}O_{sw}$ model dataset from (*LeGrande et al.*, 2006) salinity and temperature from the World Ocean Atlas 2009. Because of the limited spatial resolution of $\delta^{18}O_{sw}$ measurements the model data set from (*LeGrande et al.*, 2006) was used in order to minimize potential bias related to the time of year samples were collected and variable quantity of available data at each core top site. The $\delta^{18}O_{sw}$ was converted from standard mean ocean water (SMOW) to the Pee Dee Belemnite (PDB) scale by subtracting 0.27‰. Predicted $\delta^{18}O$ was calculated using the general paleo temperature from *Shackleton*. (1974). Species specific paleo temperature equations (*Bemis et al.*, 1998; *Farmer et al.*, 2007; *Mulitza et al.*, 2003) were considered and resulted in < 2 °C differences in temperature when compared with the *Shackleton*. (1974) equation and did not significantly influence the calcification depth estimates. Calcification depth and temperature was determined by comparing the measured foraminiferal $\delta^{18}O$ to predicted $\delta^{18}O$ by assuming equilibrium with seawater. *G.ruber*

white $\delta^{18}O$ from Cape Hatteras and Gulf of Mexico yielded calcification temperatures that were warmer than recorded sea surface temperatures from nearby hydrostations and were assigned a calcification depth of 5m.

3.3.4 Elemental Analysis

Individual foraminifer specimens (20-50 individuals yielding ~300-400 μg of $CaCO_3$) were picked disaggregated sediments from 212-250, 250-300-355, 355-425, 425-500 and 500-600 μm size fractions. Foraminiferal tests were gently crushed between two glass plates in order to open individual chambers and facilitate the chemical cleaning procedure. Visible contaminants such as volcaniclastic sediments adhered to foraminifer fragments were removed when possible. Crushed samples were transferred into acid-leached 0.5 mL centrifuge tubes and chemically cleaned following the Cd-cleaning protocol (*Boyle et al.*, 1985/1986) later modified by (*Rosenthal et al.*, 1997). The full reductive oxidative cleaning was included in this study to obtain Mg/Ca data and should not influence the B/Ca ratios. All reagents and acids were prepared using Milli-Q water passed through a boron Q-gard purification filter to obtain low boron water. Samples were rinsed with Milli-Q water and glass distilled methanol to remove surficial clays on the tests. Reductive and oxidative cleaning steps were conducted to reduce contaminate metal oxides and organics from foraminiferal tests. A final dilute acid (0.001 N HNO_3) leach was done before completely dissolving samples using 100 μL 0.065 N OPTIMA® HNO_3. Samples were diluted with ~100-200 μL (depending on the sample size) with 0.5N OPTIMA® HNO_3 to a final calcium concentration of 4 mmol/L. Samples were monitored for potential contamination from clay and metal oxides by measuring Mn/Ca, Al/Ca and Fe/Ca. Typical Mn/Ca values were ~20-40 μmol/mol, Al/Ca ~175-400

μmol/mol and Fe/Ca ~80-200 μmol/mol depending on the site. No significant correlation between B/Ca and Mn/Ca, Al/Ca or Fe/Ca was observed.

Trace element ratios (B/Ca, Mg/Ca, Mn/Ca, Al/Ca and Fe/Ca) were measured at the Institute of Marine and Coastal Sciences at Rutgers University on a Thermo Finnigan Element XR Sector Field Inductively Coupled Plasma Mass Spectrometer (SF-ICP-MS) operated at low resolution ($m/\Delta m$ =300) (B/Ca, Mg/Ca, Al/Ca) and medium resolution ($m/\Delta m$ =4300) (Mn/Ca and Fe/Ca) settings outlined in the protocol of (*Rosenthal et al.*, 1999). Elemental B analysis required several modifications to the (*Rosenthal et al.*, 1999) method to address potentially high [B] blanks and instrumental memory effect. The boron memory effect in the ICP introduction system is caused by the tendency of boric acid to volatilize and form droplets that accumulate in the spray chamber during the course of an analytical run (*Al-Ammar et al.*, 2000). To reduce the boron memory effect and improve washout efficiency anhydrous ammonia gas was injected into a high purity quartz cyclonic spray chamber (Elemental Scientific, ESI), thus raising the pH of the injected sample, converting boric acid to ammonium borate which is soluble and is removed during rinsing. Typical B blank levels were ~0.15 ppb (<3 % of [B] of planktonic foraminifera samples) and remained stable (±1 %) throughout an analytical run.

Elemental ratios were monitored and corrected for matrix effects for each analytical run by analyzing a suite of standards using an internal spiked gravimetric standard (SGS) with the same elemental ratios but varying [Ca] (1.5 mmol/L to 8 mmol/L) (*Rosenthal et al.*, 1999). [Ca] concentrations in sample solutions were typically maintained in the range of 1.5 to 4 mmol/L to minimize matrix effects on Mg/Ca and B/Ca. Typical matrix corrections are <1% for Mg/Ca and <2% for B/Ca. Analytical

precision of B/Ca 115.43 μmol/mol was ± 2.18 (2σ) and for Mg/Ca 3.32 mmol/mol ± 0.09 (2σ) based on repeated analysis of laboratory consistency standards throughout the length of the study (Figure 3.3; Table 3.2).

3.3.5 Stable Isotopes

Stable carbon and oxygen isotopes were measured at the Department of Earth and Planetary Sciences using an Optima mass spectrometer with an attached multi-prep device (Appendix 2.1). Carbonate samples were reacted with phosphoric acid at 90 °C for 15 minutes. Measurements are reported Vienna-Pee Dee Belemenite (VPDB) with precision values of ±0.05 ‰ $\delta^{13}C$ and ±0.08 ‰ $\delta^{18}O$ for NBS19 standard throughout the analysis of this study. Approximately 5-10 whole tests were used for stable isotopes.

3.3.6 Boron Isotopes

3.3.7 Sample preparation

Foraminifera cleaning and sample preparation was conducted in a designated pressure hood with a B-free hepa filter at National Cheng Kung University, Taiwan (method outlined Appendix 2.2). All reagents and acids were prepared using Milli-Q water passed through a boron Q-gard purification filter to obtain low concentration boron water. Individual foraminifer specimen were picked from disaggregated sediments in the 355-425 μm sieve fraction yielding typical sample sizes for $\delta^{11}B$ of ~2-4 mg to yield a target [B] of 10-20 ppb. Reductive step was omitted from the foraminifera cleaning following previous protocols for $\delta^{11}B$ measurement in foraminifera (*Foster*, 2008; *Hönisch et al.*, 2005; *Ni et al.*, 2010; *Ni et al.*, 2007; *Rae et al.*, 2011). Oxidative cleaning consisted of 0.1M sodium hydroxide in a 1% hydrogen peroxide solution to remove

organic matter. A procedural blank was included with each set of samples to monitor boron blank levels which were typically less than ~1 ppb [B].

Boron separation from $CaCO_3$ matrices (i.e. foraminifera) was achieved using micro-sublimation methodology (*Anagnostou et al.*, 2012; *Wang et al.*, 2010). Cleaned foraminifera samples were dissolved with 60 µL of 1 N HNO_3 and 50 µL of solution was transferred onto the screw top lid of a conical Teflon vials (Savillex Corporation). The vials were closed and placed upside down on a thermostatic hotplate coated with Teflon graphite. Samples were heated on the hotplate at 98°C for 12 hours the duration determined for complete B recovery (*Wang et al.*, 2010). The sublimated droplet was recovered from the top of the conical vial and diluted with 100-300 µL of 0.3 N HNO_3 for a target [B] of 20 ppb (range 10-20 ppb [B]). Given the lack of an accepted $\delta^{11}B$ reference standard the JCp-1 carbonate standard (Geological Society of Japan) was analyzed with each analytical run (*Aggarwal et al.*, 2009; *Anagnostou et al.*, 2012; *Douville et al.*, 2010; *Wang et al.*, 2010). Reproducibility of JCp-1 during this study is 24.61±0.61‰, 2σ; n=11) in agreement with previously reported for MC-ICPMS studies (Table 3.3). In addition to JCp-1 an in house high purity boron solution standard (Alfa-Aesar) was analyzed and we report a long term precision based on repeated measurements of (-5.44±0.93‰, 2σ; n = 28) (Figure 3.4).

3.3.8 MC-ICPMS analytical approach

Boron isotope analyzes were carried out on a ThermoFinnigan Neptune Multi-Collector Inductively Coupled Plasma Mass Spectrometer (MC-ICPMS) at National Cheng Kung University, Taiwan. Standard instrumental operating conditions were summarized in Table 3.3. The instrument was tuned prior to sample analysis for

optimized $^{11}B/^{10}B$ ratio stability by the adjustment of the sample gas flow rate. Instrumental mass bias was corrected using the standard-sample bracketing technique using NIST SRM 951 boric acid standards at 20ppb [B] or 0.4-0.5 V ^{11}B signal intensity (*Foster*, 2008; *Wang et al.*, 2010). To address the instrumental memory effect of B (*Al-Ammar et al.*, 2000) samples and standards were introduced in 0.1 M HNO_3 which is the same as the rinse and blanks were monitored throughout an analytical run (<3% of 20ppb [B] NIST 951).

3.4 Results

3.4.1 Foraminiferal B/Ca

Mixed-layer *Globigerinoides* spp. B/Ca values range from 80-140 μmol/mol, thermocline species range from 60-80 μmol/mol and deep dwelling *Globorotalia* spp. B/Ca ratios range from 40-60 μmol/mol (Figure 3.5) (Appendix 2.3). Planktonic foraminiferal B/Ca ratios decrease with increasing water depth. Comparison with $[B(OH)_4^-/HCO_3^-]_{sw}$ profiles *Globigerinoides* spp. reveal that B/Ca ratios are higher than the predicted $[B(OH)_4^-/HCO_3^-]_{sw}$, assuming equilibrium between calcite and seawater (Figure 3.5). B/Ca ratios of thermocline dwellers *N. dutertrei* and *P. obliquiloculata* and deep dwelling *Globorotalia* spp. exhibit a close match with seawater $[B(OH)_4^-/HCO_3^-]_{sw}$ (Figure 3.5).

3.4.2 Foraminiferal $\delta^{11}B$

Planktonic foraminiferal $\delta^{11}B$ values are offset from the predicted seawater $\delta^{11}B_{B(OH)_4^-}$ profiles with a trend towards lower values with increasing water depth (Figure 3.6) (Appendix 2.3). $\delta^{11}B$ values in surface dwelling *Globigerinoides* spp. range from 16-

20 ‰, thermocline species and deep dwelling *Globorotalia* spp. range from 14-16 ‰. *Globigerinoides* spp. from the Indonesian core top are offset by 1 to 3‰ from the calculated $\delta^{11}B_{B(OH)_4^-}$ of ambient seawater (Figure 3.6). At the other ocean sites, *Globigerinoides* spp. $\delta^{11}B$ values are close to predicted values at equilibrium. $\delta^{11}B$ values of *N. dutertrei*, *P. obliquiloculata, G. siphonifera* and *Globorotalia* spp. are -1 to -3‰ offset by the predicted seawater $\delta^{11}B_{B(OH)_4^-}$ (Figure 3.6).

3.5 Discussion

3.5.1 Controls on B/Ca

Planktonic foraminifera B/Ca profiles (Figure 3.5) show that *Globigerinoides* spp. are not in equilibrium with seawater, assuming $K_D = 1$. Based on *G. ruber* sediment-trap results (Chapter Two), the disequilibrium of foraminiferal B/Ca from seawater is attributed to the presence of photosymbionts. Furthermore, *Globigerinoides* spp. show that B/Ca increases with increasing test size (Figure 3.7; Appendix 2.4), consistent with the results from Chapter Two and *Ni et al.*, (2007) which indicate that photosynthetic activity influences B/Ca ratio in symbiont bearing taxa. It was suggested that larger individuals incorporate more boron compared with smaller individuals due to enhanced calcite precipitation (*Elderfield et al.*, 2002; *Ni et al.*, 2007; *Ruiz-Agudo et al.*, 2012). An alternative explanation is that larger individuals compared to smaller foraminifera can host more symbionts (*Spero et al.*, 1985) amplifying the proposed vital effect on B/Ca in *Globigerinoides* spp. (for more discussion see Chapter Two). Assuming that calcification rate influences boron incorporation similarly between symbiotic and asymbiotic species it is expected that the influence on test size would exhibit similar behavior. However,

thermocline and deep dwelling species (*N. dutertrei*, *P. obliquiloculata* and *Globorotalia* spp.) exhibit no significant relationship between B/Ca and test size arguing against a calcification rate effect and for a vital effect (Figure 3.8) (Appendix 2.4).

To explain the presence of a vital effect in *Globigerinoides* spp. and lack thereof in thermocline and deep dwelling species it is suggested that a depth related environmental parameter either light levels or temperature acts to amplify the observed disequilibrium and test size effect. For further discussion on the influence of light on pH modification and boron incorporation see Chapter Two. Evidence for temperature influence on symbiotic activity is supported by culture experiments that show that calcification temperature in symbiotic species can influence rates of photosynthesis and respiration (*Lombard et al.*, 2009).

It is not straightforward to assess the influence of temperature on B/Ca in planktonic foraminifera using core-top sediments. This is because both temperature and pH influence the equilibrium constants, K_1, K_2 and K_B which in turn control $[B(OH)_4^-/HCO_3^-]_{sw}$ making it difficult to separate their individual effect(s). To address this covariance, $[B(OH)_4^-/HCO_3^-]_{sw}$ is compared with temperature and calculated seawater pH at the various core top sites (Figure 3.9). At the surface, temperature variability among sites is large (~5 °C). The temperature variability among sites is significantly lower in deeper waters; in the upper thermocline (75-100 m) temperature varies by about 2 °C whereas at the depth range of deep dwelling planktonic foraminifera (typically calcifying at the depth range of 100-500 m) temperature variability is <1 °C). In contrast pH in deeper waters (100-500 m) changes considerably among sites (~0.4-0.5)

(Figure 3.9). *Globigerinoides* spp. shows an intra- species co-variance between B/Ca and temperature (Figure 3.10a). With the exception of *G. siphonifera*, no inter- or intra-species relationship between temperature and B/Ca is observed (Figure 3.10a).

The comparison of B/Ca in thermocline and deep dwelling planktonic foraminifera with temperature suggest a negligible temperature influence (Figure 3.10a) Given the lack of discernible temperature effect on the deep dwelling foraminifera, B/Ca ratios of *N. dutertrei*, *P. obliquiloculata*, *G. menardii* and *G. truncatulinoides* are compared with seawater $[B(OH)_4^-/HCO_3^-]_{sw}$ at the depth of calcification estimated from nearby hydrographic stations (see methods). Based on observations from hydrographic data at the core-top locations (Figure 3.9) it is argued that the calibration of thermocline and deep dwelling foraminifera is not significantly biased by a possible influence of temperature on $[B(OH)_4^-/HCO_3^-]_{sw}$. Linear regressions are computed for data from Gulf of Mexico, Cape Hatteras, Galapagos platform, Indonesia and New Zealand with additional sites from the Caribbean, Sierra Leone Rise and Ceara Rise for *N.dutertrei* analyzed by (*Foster*, 2008). Simple linear regressions are reported as the following (Appendix 2.5):

P. obliquiloculata

$B/Ca = (658\pm198) * [B(OH)_4^-/HCO_3^-]_{sw} + (33\pm11)$, $r^2=0.85$, n=4 Figure 3.11 (Eq.1)

N. dutertrei

$B/Ca = (326\pm100) * [B(OH)_4^-/HCO_3^-]_{sw} + (39\pm5)$, $r^2=0.60$, n=9 Figure 3.11 (Eq.2)

G. truncatulinoides

$B/Ca = (528 \pm 228) * [B(OH)_4^-/HCO_3^-]_{sw} + (47 \pm 8)$, $r^2=0.47$, n=8 Figure 3.12 (Eq.1)

G. menardii

$B/Ca = (471 \pm 158) * [B(OH)_4^-/HCO_3^-]_{sw} + (35 \pm 8)$, $r^2=0.60$, n=6 Figure 3.12 (Eq.2)

B/Ca is in μmol/mol and $[B(OH)_4^-/HCO_3^-]_{sw}$ is without units. The number of data points used in the regression is represented by n and standard errors are reported next to the given parameters (Appendix 2.6).

3.5.2 Controls on $\delta^{11}B$

The isotopic fractionation factor (α_B) between boric acid and borate was determined experimentally and estimated based on vibrational frequencies yielding a range of values of 1.019-1.035 (*Kakihana et al.*, 1977; *Klochko et al.*, 2006). It is hypothesized that α_B is dependent on temperature (*Zeebe*, 2005), however the experimental work of *Klochko et al*., (2006) exhibited no difference between results conducted at 25°C and 40°C leading *Klochko et al*., (2006), leading them to conclude that the temperature influence on α_B was negligible. *Zeebe* (2005) used a theoretical approach to estimate the temperature influence on α_B and concluded that the temperature sensitivities depend on the specific α_B value. If a temperature effect on α_B accounts for the entire observed isotopic offset of foraminifera $\delta^{11}B$ from predicted $\delta^{11}B_{B(OH)_4^-}$, then the temperature-α_B relationship estimated here suggests a higher sensitivity than published results (*Hönisch et al.*, 2004; *Zeebe*, 2005) (Figure 3.13). It seems unlikely, however, that

the temperature effect on α_B was the only factor for the observed isotopic offset and that vital effects are not a contributing factor to the observed $\delta^{11}B$ disequilibrium. Instead, a more conservative approach was applied to correct for the temperature effect on α_B by using *Klochko* et al., 2006 ($\alpha_B = 1.027$) temperature equation estimated from *Hönisch et al.*, (2008). The applied temperature correction yielded foraminifer $\delta^{11}B$ values that are more consistent with the predicted $\delta^{11}B_{B(OH)_4^-}$ equilibrium values with seawater (Figure 3.14) however isotopic offsets remain. This observation does not compromise the utility of $\delta^{11}B$ as a seawater pH proxy (*Zeebe et al.*, 2003). It highlights, however, the necessity to apply empirically derived species specific calibrations in order to accurately account for interspecies vital effects.

The offset of $\delta^{11}B$ from equilibrium values and the depth-related trend may be due to vital or depth related effects. The argument used here to explain the influence of test size on B/Ca is consistent with previous $\delta^{11}B$ studies that attributed the variable positive isotopic offsets from predicted equilibrium to the presence of symbionts (*Foster*, 2008; *Henehan et al.*, 2013; *Hönisch et al.*, 2003; *Sanyal et al.*, 2001; *Sanyal et al.*, 1996). The presence of photosymbionts and, therefore, photosynthetic activity leads to an elevation of pH, increasing $B(OH)_4^-$ ion within the calcifying fluid resulting in more positive $\delta^{11}B$ recorded in foraminifera tests relative to predicted equilibrium values (*Henehan et al.*, 2013; *Hönisch et al.*, 2003; *Sanyal et al.*, 2001; *Sanyal et al.*, 1996). Likewise, respiration acts to decrease the internal pH and the $B(OH)_4^-$ ratio within the calcifying pool, which may led to $\delta^{11}B$ values that are negatively offset from the expected values when assuming equilibrium with the ambient seawater (*Foster*, 2008; *Hönisch et al.*, 2003). In

photosymbiont bearing species, both processes of photosynthesis and respiration can modify ocean pH and therefore foraminiferal $\delta^{11}B$ likely represents the combined effects.

3.6 Conclusions

Measurements of B/Ca and $\delta^{11}B$ in 11 species of planktonic foraminifera from globally distributed modern to late-Holocene sediments were offset from predicted seawater $[B(OH)^-_4/HCO^-_3]$ and $\delta^{11}B_{B(OH)^-_4}$ respectively and vital effects are invoked to explain the observed disequilibria. The core top B/Ca results of *P. obliquiloculata*, *N. dutertrei, G. truncatulinoides* and *G. menardii* indicated a positive relationship with seawater $[B(OH)^-_4/HCO^-_3]$. B/Ca increased with test size in *Globigerinoides* species and exerted negligible influence on asymbiotic species. The good agreement between B/Ca and seawater $[B(OH)^-_4/HCO^-_3]$ encourages the application of thermocline and deep dwelling planktonic species for paleo reconstructions of the oceanic carbonate chemistry as temperature and vital effects were minimal.

Another implication of the $\delta^{11}B$ results was that the observation that foraminifera values were not in equilibrium with seawater. Within the limited size fraction used in this study it remains uncertain whether the isotopic offset observed holds for all size fractions in the species considered. A more thorough study of the size influence on $\delta^{11}B$ in asymbiotic species is needed to address these concerns. Paleo records over which temperature variations are likely, such as Pleistocene glaciations, a temperature correction on α_B may be needed. Studies that aim to derive absolute carbonate chemistry should consider empirical species specific calibration relationships to best estimate past seawater conditions.

3.7 References

Aggarwal, S.K., Wang, B.-S., You, C.-F., and Chung, C.-H. (2009), Fractionation Correction Methodology for Precise and Accurate Isotopic Analysis of Boron by Negative Thermal Ionization Mass Spectrometry Based on BO2− Ions and Using the 18O/16O Ratio from ReO4− for Internal Normalization, *Analytical Chemistry*, *81*(17), 7420-7427.

Al-Ammar, A.S., Gupta, R.K., and Barnes, R.M. (2000), Elimination of boron memory effect in inductively coupled plasma-mass spectrometry by ammonia gas injection into the spray chamber during analysis, *Spectrochimica Acta B*, *55*(6), 629-635.

Allen, K.A., and Hönisch, B. (2012), The planktic foraminiferal B/Ca proxy for seawater carbonate chemistry: A critical evaluation, *Earth and Planetary Science Letters*, *345–348*(0), 203-211.

Allen, K.A., Hönisch, B., Eggins, S.M., and Rosenthal, Y. (2012), Environmental controls on B/Ca in calcite tests of the tropical planktic foraminifer species Globigerinoides ruber and Globigerinoides sacculifer, *Earth and Planetary Science Letters*, *351–352*(0), 270-280.

Allen, K.A., et al. (2011), Controls on boron incorporation in cultured tests of the planktic foraminifer Orbulina universa, *Earth and Planetary Science Letters*, *309*(3–4), 291-301.

Anagnostou, E., et al. (2012), Evaluation of boron isotope ratio as a pH proxy in the deep sea coral Desmophyllum dianthus: Evidence of physiological pH adjustment, *Earth and Planetary Science Letters*, *349–350*(0), 251-260.

Bemis, B.E., Spero, H.J., Bijma, J., and Lea, D.W. (1998), Reevaluation of the Oxygen Isotopic Composition of Planktonic Foraminifera: Experimental Results and Revised Paleotemperature Equations, *Paleoceanography*, *13*(2), 150-160.

Boyle, E.A., and Keigwin, L.D. (1985/1986), Comparison of Atlantic and Pacific paleochemical records for the last 215,000 years: changes in deep ocean circulation and chemical inventories, *Earth and Planetary Science Letters*, *76*(1-2), 135-150.

Culberson, C.H., and Pytkowicz, R.M. (1968), Effect of pressure on carbonic acid, boric acid, and the pH in seawater, *Limnology and Oceanography*, *13*(3), 403-417.

Dickson, A.G. (1990), Thermodynamics of the dissociation of boric acid in synthetic seawater from 273.15 to 318.15 K, *Deep Sea Research Part A. Oceanographic Research Papers*, *37*(5), 755-766.

Dickson, A.G., and Millero, F.J. (1987), A comparison of the equilibrium constants for the dissociation of carbonic acid in seawater media, *Deep Sea Research Part A. Oceanographic Research Papers*, *34*(10), 1733-1743.

Douville, E., et al. (2010), Abrupt sea surface pH change at the end of the Younger Dryas in the central sub-equatorial Pacific inferred from boron isotope abundance in corals (Porites), *Biogeosciences*, *7*(2).

Elderfield, H., Vautravers, M., and Cooper, M. (2002), The relationship between shell size and Mg/Ca, Sr/Ca, $\delta^{18}O$, and $\delta^{13}C$ of species of planktonic foraminifera, *Geochemistry, Geophysics, Geosystems*, *3*(8), 1052.

Farmer, E.C., Kaplan, A., de Menocal, P.B., and Lynch-Stieglitz, J. (2007), Corroborating ecological depth preferences of planktonic foraminifera in the

tropical Atlantic with the stable oxygen isotope ratios of core top specimens, *Paleoceanography*, *22*(3), PA3205.

Foster, G.L. (2008), Seawater pH, pCO2 and [CO2-3] variations in the Caribbean Sea over the last 130 kyr: A boron isotope and B/Ca study of planktic foraminifera, *Earth and Planetary Science Letters*, *271*(1-4), 254-266.

Foster, G.L., Pogge von Strandmann, P.A.E., and Rae, J.W.B. (2010), Boron and magnesium isotopic composition of seawater, *Geochemistry, Geophysics, Geosystems*, *11*(8), Q08015.

Hemming, N.G., and Hanson, G.N. (1992), Boron isotopic composition and concentration in modern marine carbonates, *Geochim. Cosmochim. Acta*, *56*, 537-543.

Henehan, M.J., et al. (2013), Calibration of the boron isotope proxy in the planktonic foraminifera Globigerinoides ruber for use in palaeo-CO2 reconstruction, *Earth and Planetary Science Letters*, *364*(0), 111-122.

Hönisch, B., and Hemming, N.G. (2004), Ground-truthing the boron isotope-paleo-pH proxy in planktonic foraminifera shells: Partial dissolution and shell size effects, *Paleoceanography*, *19*(4), PA4010.

Hönisch, B., and Hemming, N.G. (2005), Surface ocean pH response to variations in pCO_2 through two full glacial cycles, *Earth Plan. Sci. Lett.*, *236*(1-2), 305-314.

Hönisch, B., Bickert, T., and Hemming, N.G. (2008), Modern and Pleistocene boron isotope composition of the benthic foraminifer *Cibicidoides wuellerstorfi*, *Earth Plan. Sci. Lett.*, *272*(1-2), 309-318.

Hönisch, B., et al. (2003), The influence of symbiont photosynthesis on the boron isotopic composition of foraminifera shells, *Marine Micropaleontology*, *49*(1-2), 87-96.

Kakihana, H., et al. (1977), Fundamental studies on the ion-exchange separation of boron isotopes, *Chem. Soc. Jpn., B*, *50*, 158-163.

Keigwin, L.D., and Guilderson, T.P. (2009), Bioturbation artifacts in zero-age sediments, *Paleoceanography*, *24*(4), PA4212.

Key, R.M., et al. (2004), A global ocean carbon climatology: Results from Global Data Analysis Project (GLODAP), *Global Biogeochem. Cycles*, *18*(4), GB4031.

Klochko, K., et al. (2006), Experimental measurement of boron isotope fractionation in seawater, *Earth and Planetary Science Letters*, *248*(1–2), 276-285.

Lee, K., et al. (2010), The universal ratio of boron to chlorinity for the North Pacific and North Atlantic oceans, *Geochimica et Cosmochimica Acta*, *74*(6), 1801-1811.

LeGrande, A.N., and Schmidt, G.A. (2006), Global gridded data set of the oxygen isotopic composition in seawater, *Geophys. Res. Lett.*, *33*(12), L12604.

Lombard, F., Erez, J., Michel, E., and Labeyrie, L. (2009), Temperature effect on respiration and photosynthesis of the symbiont-bearing planktonic foraminifera Globigerinoides ruber, Orbulina universa, and Globigerinella siphonifera, *Limnology and Oceanography*, *54*(1), 210-218.

Mehrbach, C., Culberson, C.H., Hawley, J.E., and Pytkowicz, R.M. (1973), Measurement of the Apparent Dissociation Constants of Carbonic Acid in Seawater at Atmospheric Pressure, *Limnology and Oceanography*, *18*(6), 897-907.

Mulitza, S., et al. (2003), Temperature δ18O relationships of planktonic foraminifera collected from surface waters, *Palaeogeography, Palaeoclimatology, Palaeoecology*, *202*(1–2), 143-152.

Ni, Y., Foster, G.L., and Elliott, T. (2010), The accuracy of [delta]11B measurements of foraminifers, *Chemical Geology*, *274*(3-4), 187-195.

Ni, Y., et al. (2007), A core top assessment of proxies for the ocean carbonate system in surface-dwelling foraminifers, *Paleoceanography*, *22*, PA3212.

Pelletier, G., Lewis, E., and D., W. (2007), CO_2sys.xls: a calculator for the CO_2 system in seawater for Microsoft Excel/VBA, *Washington State Department of Ecology, Olympia, WA, USA*.

Rae, J.W.B., Foster, G.L., Schmidt, D.N., and Elliott, T. (2011), Boron isotopes and B/Ca in benthic foraminifera: Proxies for the deep ocean carbonate system, *Earth and Planetary Science Letters*, *302*(3–4), 403-413.

Rosenthal, Y., Boyle, E.A., and Slowey, N. (1997), Temperature control on the incorporation of magnesium, strontium, fluorine, and cadmium into benthic foraminiferal shells from Little Bahama Bank: Prospects for thermocline paleoceanography, *Geochimica et Cosmochimica Acta*, *61*(17), 3633-3643.

Rosenthal, Y., Field, M.P., and Sherrell, R.M. (1999), Precise determination of element/calcium ratios in calcareous samples using Sector Field Inductively Couple Plasma Mass Spectrometry, *Analytical Chemistry 71*, 3248-3253.

Ruiz-Agudo, E., et al. (2012), Boron incorporation into calcite during growth: Implications for the use of boron in carbonates as a pH proxy, *Earth and Planetary Science Letters*, *345–348*(0), 9-17.

Sabine, C.L., et al. (2004), The Oceanic Sink for Anthropogenic CO2, *Science*, *305*(5682), 367-371.

Sanyal, A., Bijma, J., Spero, H., and Lea, D.W. (2001), Empirical relationship between pH and the boron isotopic composition of *Globigerinoides sacculifer*: Implications for the boron isotope paleo-pH proxy, *Paleoceanography*, *16*, 515-519.

Sanyal, A., et al. (1996), Oceanic pH control on the boron isotopic composition of foraminifera: Evidence from culture experiments, *Paleoceanography*, *11*, 513-517.

Shackleton, N.J. (1974), Attainment of isotopic equilibrium between ocean water and benthonic foraminiferal genus Uvigerina: Isotopic changes in the ocean during the last glacial *Colloques Internationaux du Centre National du Recherche Scientifique*, *219*, 203-209.

Spero, H.J., and Parker, S.L. (1985), Photosynthesis in the symbiotic planktonic foraminifer Orbulina universa, and its potential contribution to oceanic primary productivity, *The Journal of Foraminiferal Research*, *15*(4), 273-281.

Tripati, A.K., Roberts, C.D., and Eagle, R.A. (2009), Coupling of CO2 and Ice Sheet Stability Over Major Climate Transitions of the Last 20 Million Years *Science*, *326*(5958), 1394-1397.

Wang, B.-S., et al. (2010), Direct separation of boron from Na- and Ca-rich matrices by sublimation for stable isotope measurements by MC-ICP-MS, *Talanta*, *82*, 1378-1384.

Yu, J., Elderfield, H., and Hönisch, B. (2007), B/Ca in planktonic foraminifera as a proxy for surface seawater pH, *Paleoceanography*, *22*(2), PA2202.

Yu, J., Thornalley, D.J.R., Rae, J.W.B., and McCave, N.I. (2013), Calibration and application of B/Ca, Cd/Ca, and δ11B in Neogloboquadrina pachyderma (sinistral) to constrain CO2 uptake in the subpolar North Atlantic during the last deglaciation, *Paleoceanography*, *28*(2), 237-252.

Zeebe, R. (2005), Stable boron isotope fractionation between dissolved $B(OH)_3$ and $B(OH)^{-4}$ *Geochim. Cosmochim. Acta*, *69*, 2753-2766.

Zeebe, R.E., and Wolf-Gladrow, D. (2001), *CO_2 in Seawater: Equilibrium, Kinetics, Isotopes*, Amsterdam.

Zeebe, R.E., Wolf-Gladrow, D.A., Bijma, J., and Hönisch, B. (2003), Vital effects in foraminifera do not compromise the use of $\delta^{11}B$ as a paleo-pH indicator: Evidence from modelling, *Paleoceanography*, *18*, 1043, doi: 1010.1029/2003PA000881.

Table 3.1 Sample site locations for analyzed in this study.

Core	Latitude	Longitude	Water Depth, m	Depth, cm	Core Type[1]
Cape Hatteras					
KN178 46	35.76 N	74.44 W	2000	0-1	MC
KN178 1	36.12 N	72.29 W	3979	0-1	MC
Gulf of Mexico					
DGoM RW5-3	26.95 N	95.00 W	1620	0-1	BC
Sierra Leone Rise					
EN66 30	02 28N	19 46W	5224	0-1	GGC
EN66 39	05 04N	20 52W	2818	0-1	GGC
Galapagos					
KN195-5 42	01.25 S	89.69 W	615	0-1	MC
KN195-5 9	00.83 S	87.91 W	1563	0-1	MC
KN195-5 12	03.71 S	81.12 W	378	0-1	MC
New Zealand					
RR05-03 118	36.37 S	177.45 E	2252	0-1	MC
RR05-03 12	44.80 S	179.66 W	1335	0-1	MC
Indonesia					
BJ8-03 24	05.06 S	117.45 E	832	1-2	MC
BJ8-03 20	06.77 S	116.97 E	419	0-1	MC

[1] MC, multicore, BC, box core and GGC, giant gravity core

Table 3.2 Long-term analytical precision of laboratory internal consistency standards from July 2009 to November 2011.

Consistency Standards	Statistics	Mg/Ca mmol/mol	B/Ca µmol/mol
CS1	Expected	1.240	20.656
	Mean	1.258	23.103
	± 1σ	0.009	0.880
	% RSD	**0.68%**	**3.81%**
	% Δ (meas-exp)	1.44%	11.85%
CS2	Expected	3.318	115.433
	Mean	3.324	114.286
	± 1σ	0.011	0.849
	% RSD	**0.33%**	**0.74%**
	% Δ (meas-exp)	0.17%	-0.99%
CS3	Expected	7.506	242.541
	Mean	7.513	233.713
	± 1σ	0.040	1.537
	% RSD	**0.53%**	**0.66%**
	% Δ (meas-exp)	0.09%	-3.64%

Table 3.3 $\delta^{11}B$ of routinely measured standards and reported published error values.

Standard	n	[B] ppb	Average	2 SD	2 SE
SRM NIST 951	57	20	0.00	0.47	0.06
Alfa-Aesar	28	20	-5.44	0.93	0.18
			-5.41	0.19	*Anagnostou* et al., 2012
JCp-1	11	20	24.61	0.61	0.18
			24.42	0.10	*Dissard* et al., 2012
			24.41	0.30	*Anagnostou* et al., 2012
			24.22	0.28	*Wang* et al., 2010
			24.50	0.20	*Douville* et al., 2010

Table 3.4 Instrumental (Neptune, MC-ICPMS Thermo Scientific) operating conditions for the duration of this study (June-August 2011).

Neptune MC-ICPMS operating conditions	
RF power	1200 W
Ar cooling gas flow rate	15 L min^{-1}
Ar sampling gas flow rate	1.1 L min^{-1}
Ar auxiliary gas flow rate	0.7 L min^{-1}
Interface cones	Ni-Sampler, X-Skimmer
Nebulizer type	PFA microflow 100µL min^{-1} (Elemental Scientific)
Inlet system	Stable inlet system with dual-quartz spray chamber
Resolution	Low
Faraday cup	H3 (^{11}B) and L3 (^{10}B)
Intergration time	1.049 s

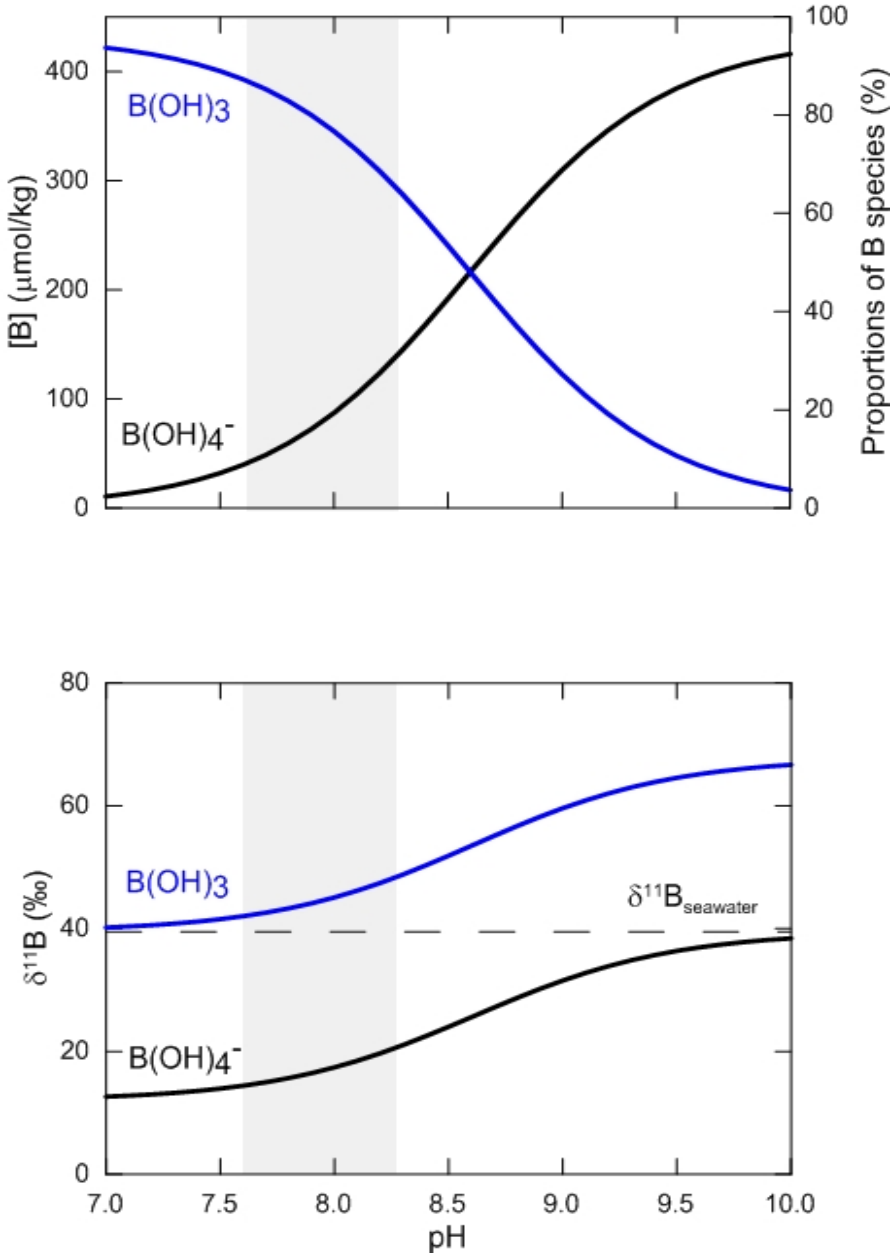

Figure 3.1 Concentration and isotopic composition of borate ion $B(OH)_4^-$ and boric acid $B(OH)_3$ relative to seawater pH. Values were calculated for surface conditions using a temperature of 25°C, salinity of 35 psu and isotopic fractionation factor, α_B of 1.027(*Klochko et al.*, 2006). Grey bar signifies typical seawater pH for the upper water column for the ocean sites used in this study.

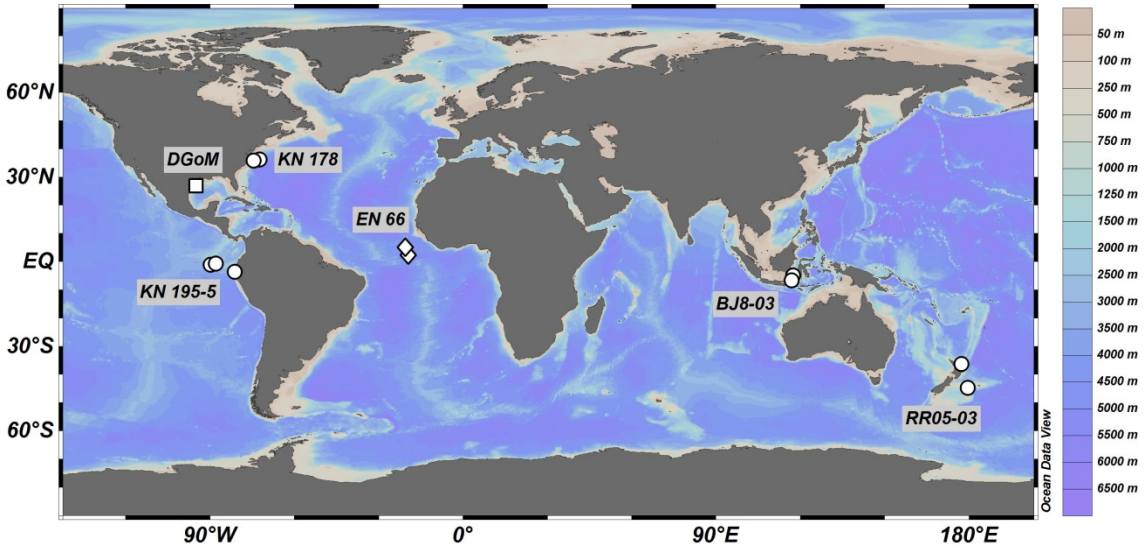

Figure 3.2 Map of sediment core-top samples analyzed in this study (http://odv.awi.de/) [circle-multicore, square-box core and diamond-giant gravity core]. Color bar represents ocean bathymetry.

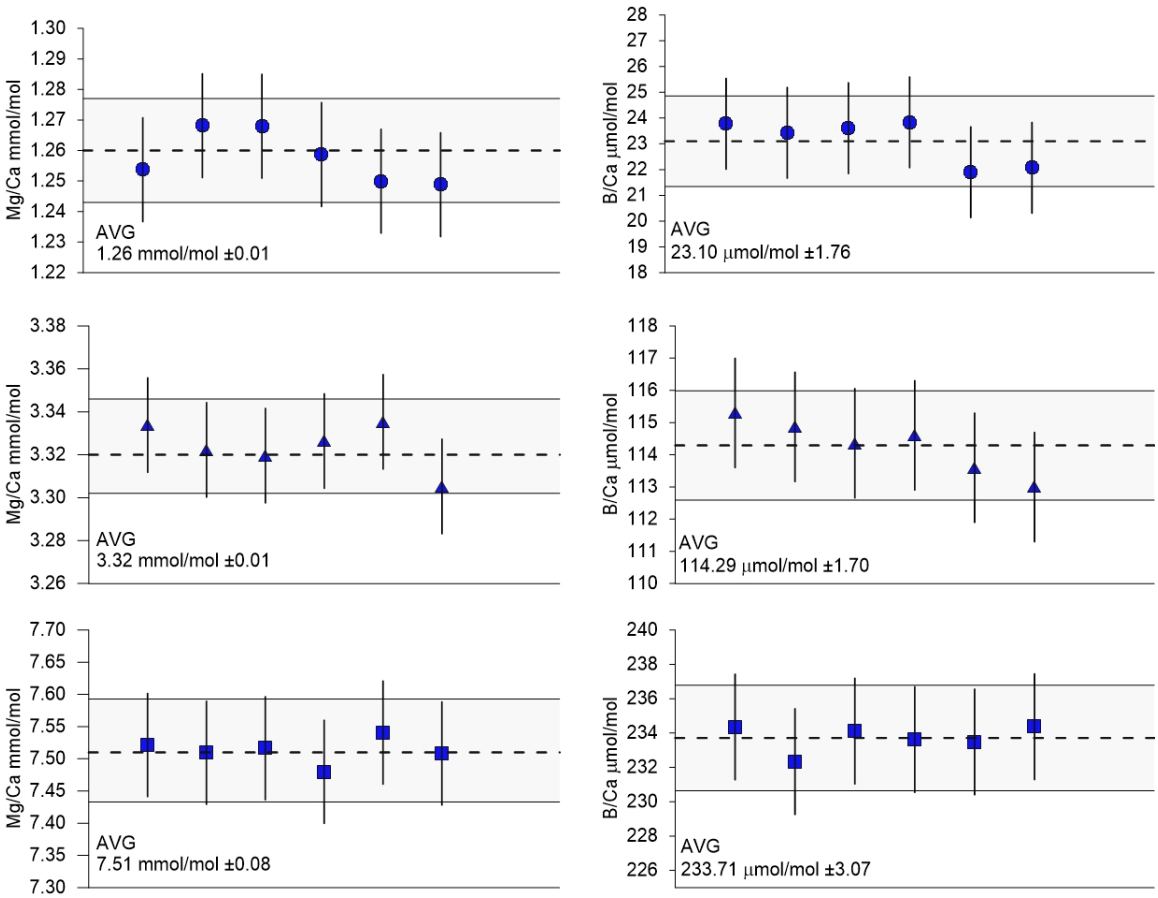

Figure 3.3 Measurements of Mg/Ca (mmol/mol) and B/Ca (µmol/mol) for in house consistency standards plotted during the data acquisition for this study (July 2009 to November 2011). Average values and with uncertainty are reported as 2σ.

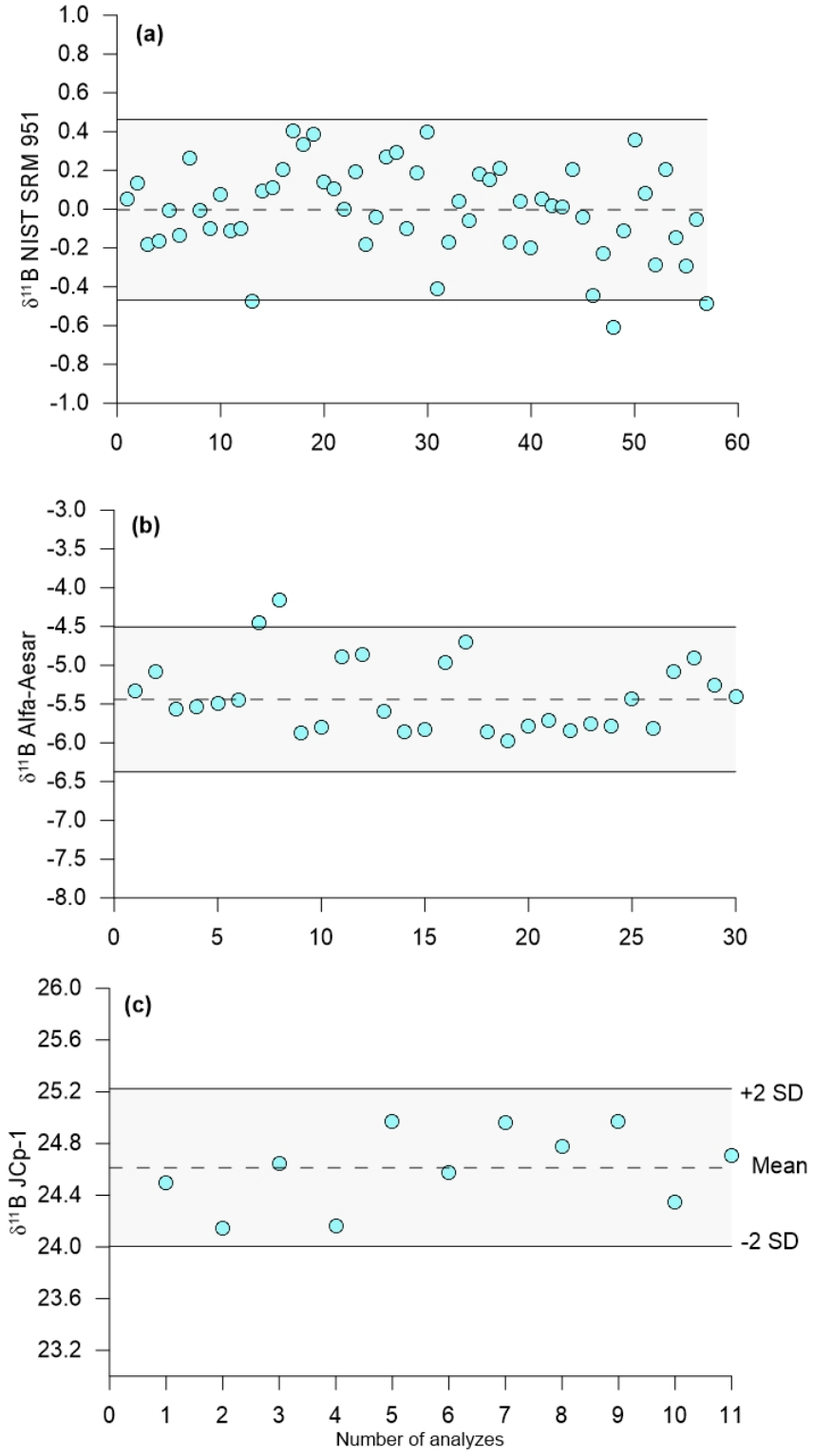

Figure 3.4 Repeated analyzes of solution and carbonate standards: (a) NIST SRM 951, (b) Alfa-Aesar and (c) JCp-1.

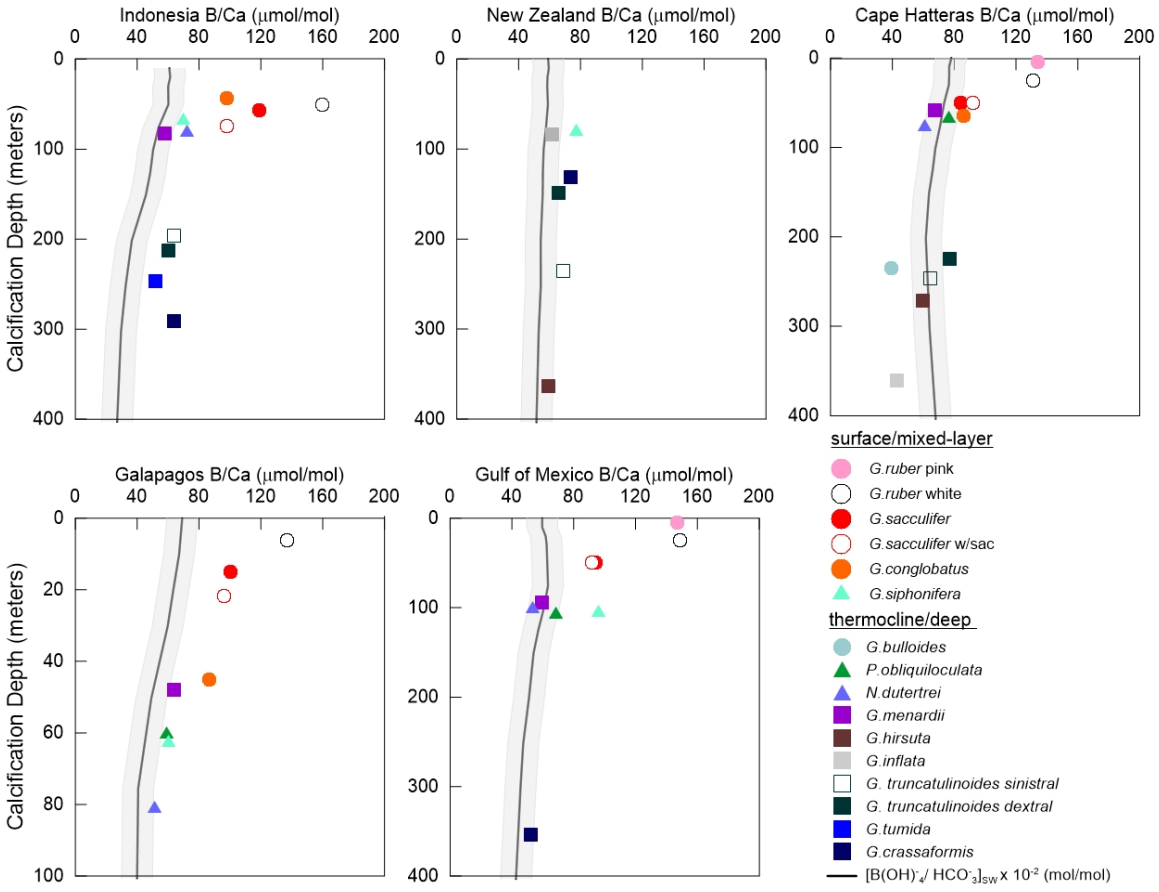

Figure 3.5 Depth profiles of measured B/Ca of planktonic foraminifera (355-425µm) and calculated annual $[B(OH)_4^-/HCO_3^-]_{sw}$ (x 10^{-2} mol/mol) computed from nearby GLODAP and World Ocean Atlas 2009 stations. Foraminifer calcification depths were derived by comparing measurements of $\delta^{18}O$ calcite and predicted $\delta^{18}O$ based on assuming equilibrium with seawater. Gray bands indicate typical seasonal range of $[B(OH)_4^-/HCO_3^-]_{sw}$ of 0.01 µmol/mol based on seasonal variations in temperature and salinity. B/Ca error bars are smaller than the symbol size.

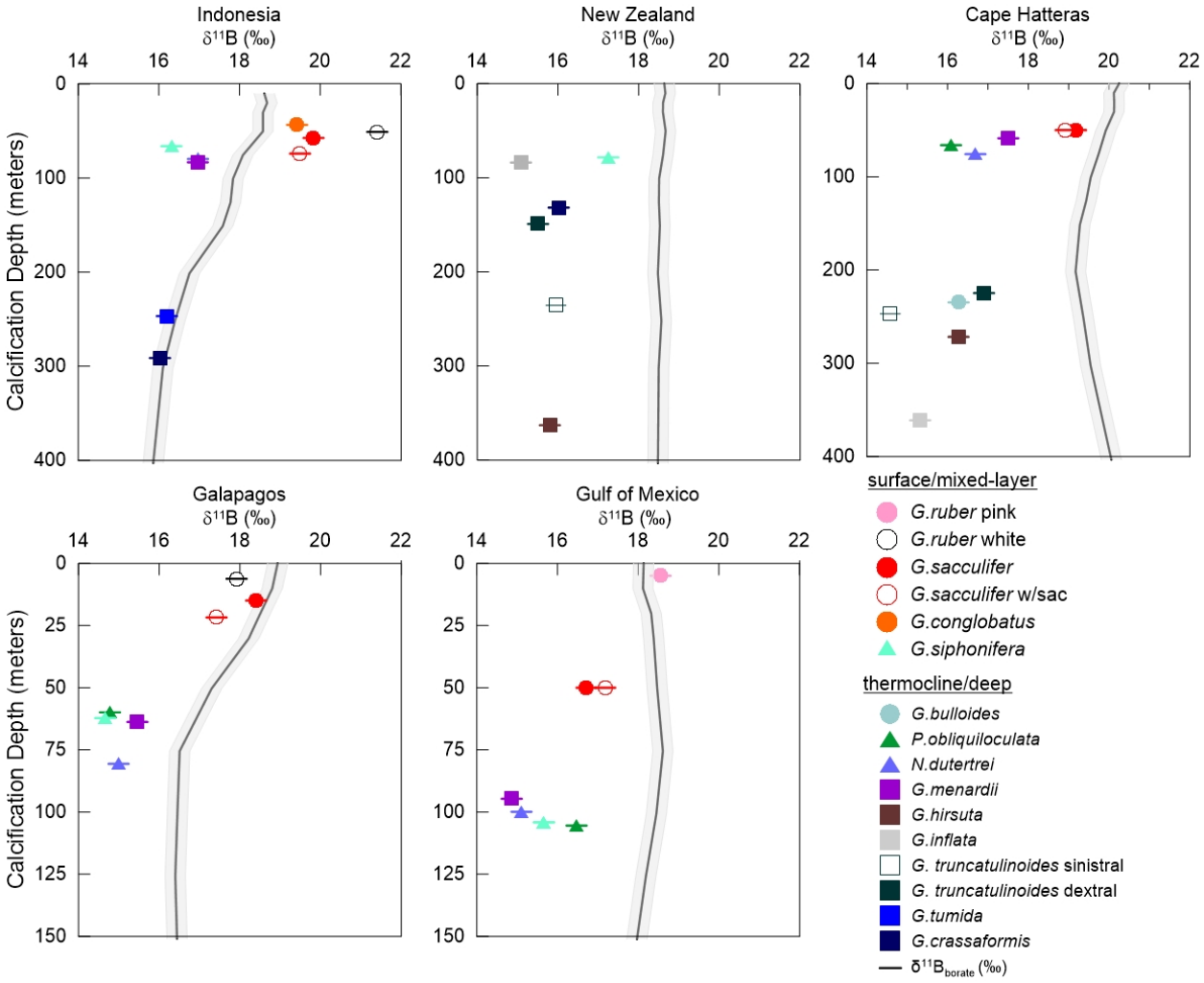

Figure 3.6 Depth profiles showing measured $\delta^{11}B$ of planktonic foraminifera (355-425µm) and calculated annual $\delta^{11}B$ of borate in seawater computed from nearby GLODAP and World Ocean Atlas 2009 stations. Foraminifer calcification depths were derived by comparing measurements of $\delta^{18}O$ calcite and predicted $\delta^{18}O$ based on assuming equilibrium with seawater. Gray bands indicate typical uncertainty on $\delta^{11}B_{B(OH)_4^-}$ of 0.25‰ based on seasonal variations in temperature and salinity.

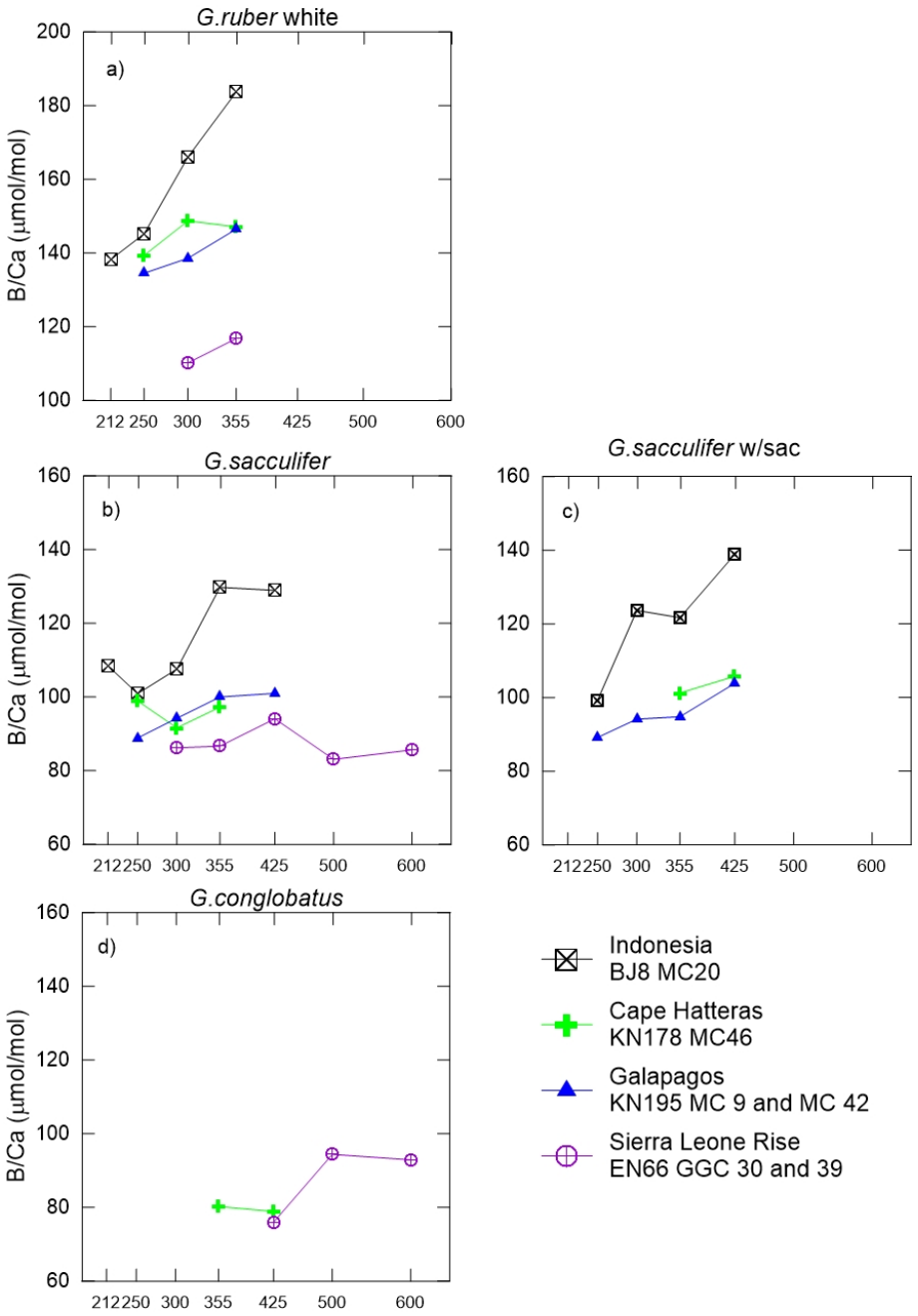

Figure 3.7 Measured B/Ca ratios of symbiotic foraminifer species *Globigerinoides ruber* (white) sensu stricto, *Globigerinoides sacculifer*, *Globigerinoides sacculifer* with sac-like chamber and *Globigerinoides conglobatus* plotted against the minima test size (µm) along the x-axis for the following ranges: 212-250, 250-300, 355-425, 425-500 and 500-600µm from globally distributed core-top sediments.

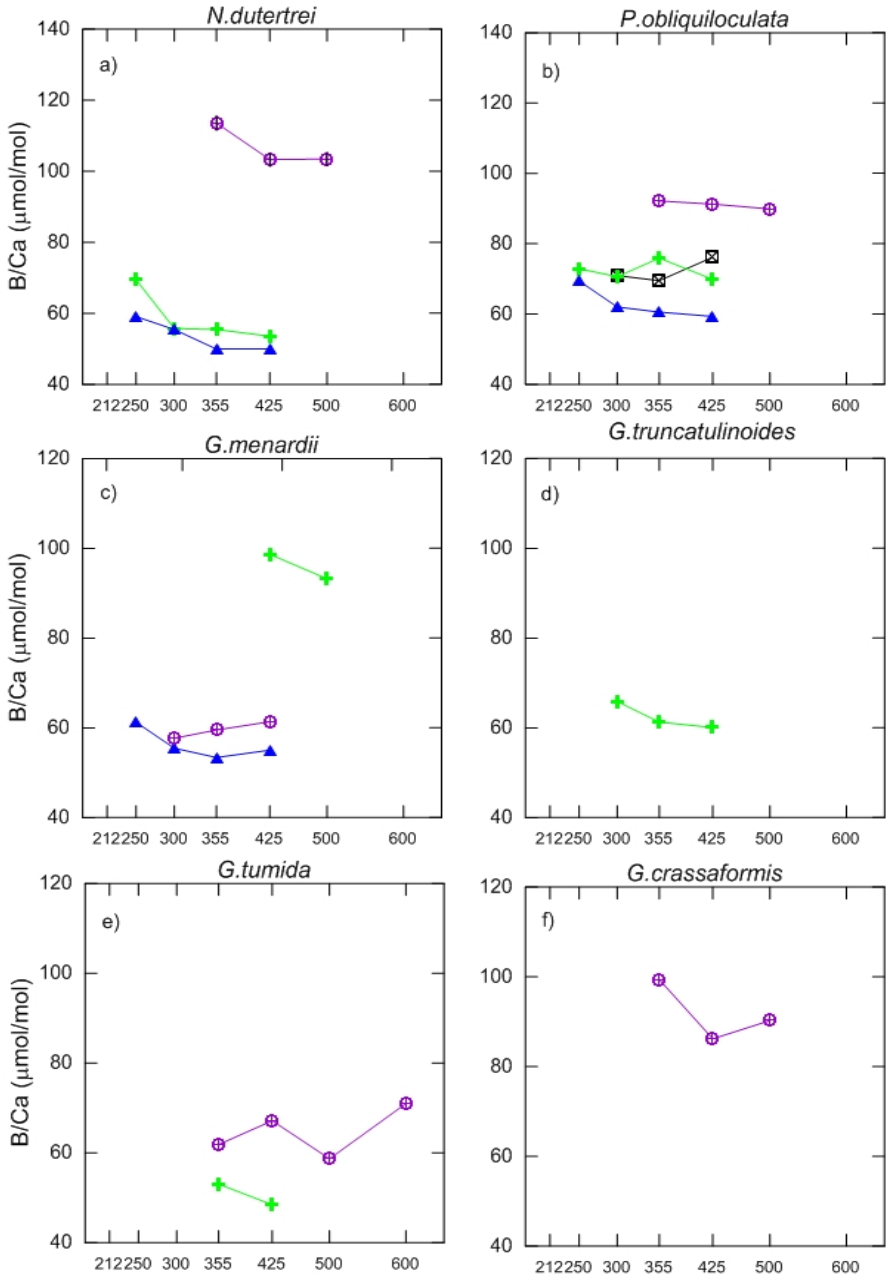

Figure 3.8 Measured B/Ca ratios of asymbiotic foraminifer species *Neogloboquadrina dutertrei* and *Pulleniatina obliquiloculata*, *Globorotalia menardii*, *Globorotalia truncatulinoides* (sinistral and dextral), *Globorotalia tumida* and *Globorotalia crassaformis* plotted against the minima test size (µm) along the x-axis for the following ranges: 212-250, 250-300, 355-425, 425-500 and 500-600µm from globally distributed core-top sediments.

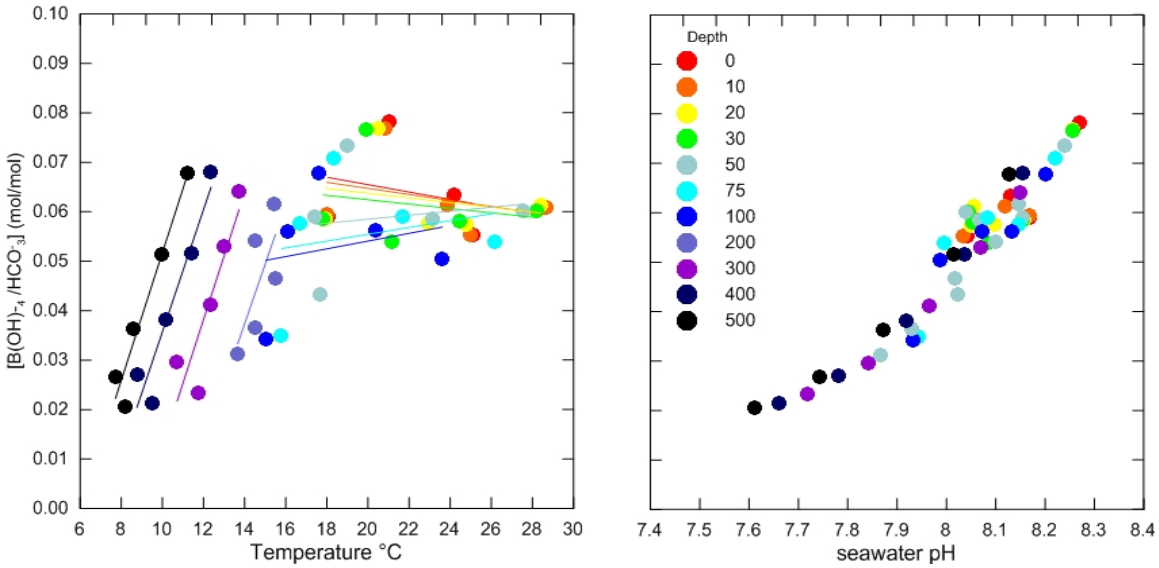

Figure 3.9 Estimated $[B(OH)_4^-/HCO_3^-]_{sw}$ from 0 to 500m depth was compared to temperature and pH from the various core top sites.

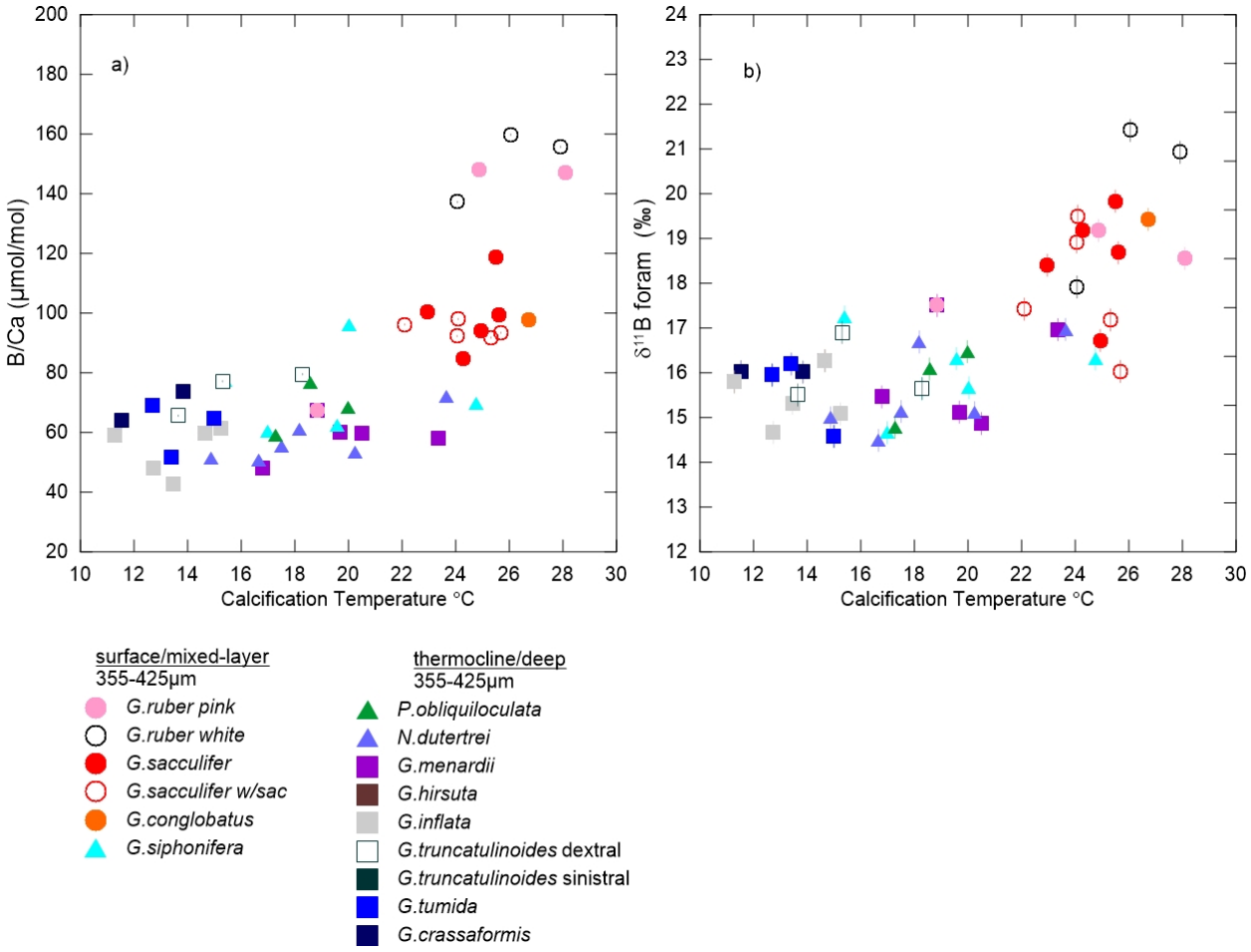

Figure 3.10 (a) B/Ca and (b) $\delta^{11}B$ measurements in planktonic foraminifera are compared to calcification temperature derived from paired $\delta^{18}O$ measurements. Error bars on $\delta^{11}B$ are 0.25‰.

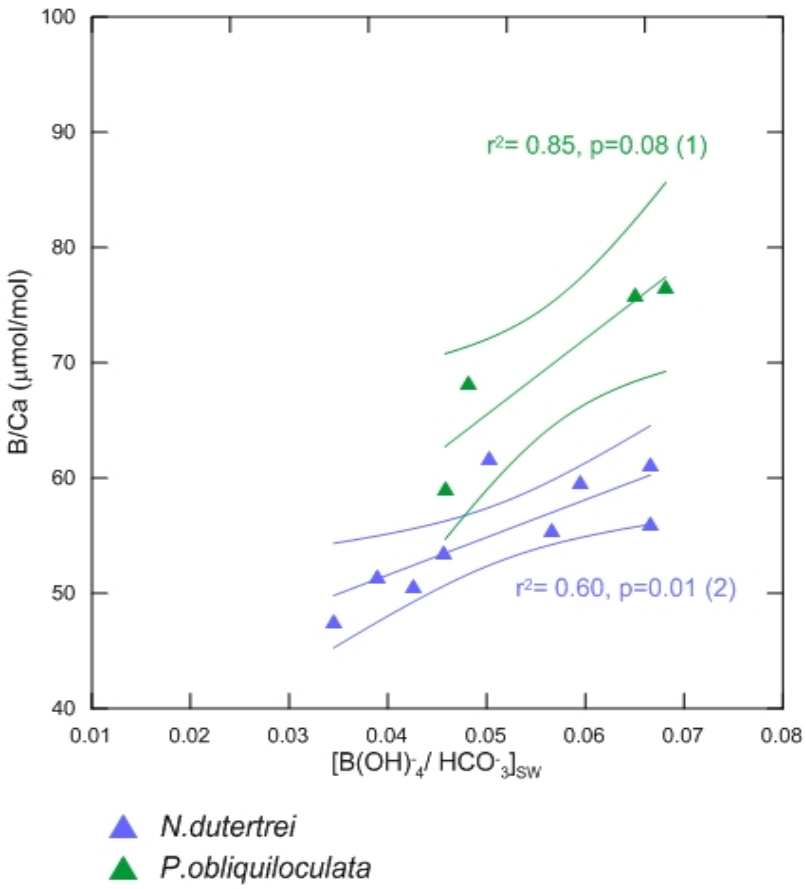

Figure 3.11 B/Ca ratios of asymbiotic planktonic foraminifer species *Neogloboquadrina dutertrei* and *Pulleniatina obliquiloculata* (355-425µm) with $[B(OH)_4^-/HCO_3^-]_{sw}$ computed from nearby GLODAP and WOA09 stations at the depth of calcification determined from paired $\delta^{18}O$ measurements. *N.dutertrei* includes measurements analyzed in this study and from core top sediments analyzed in (*Foster*, 2008) from the size fraction of 425-500µm. Solid lines represent linear regressions of the plotted data with 95% confidence intervals.

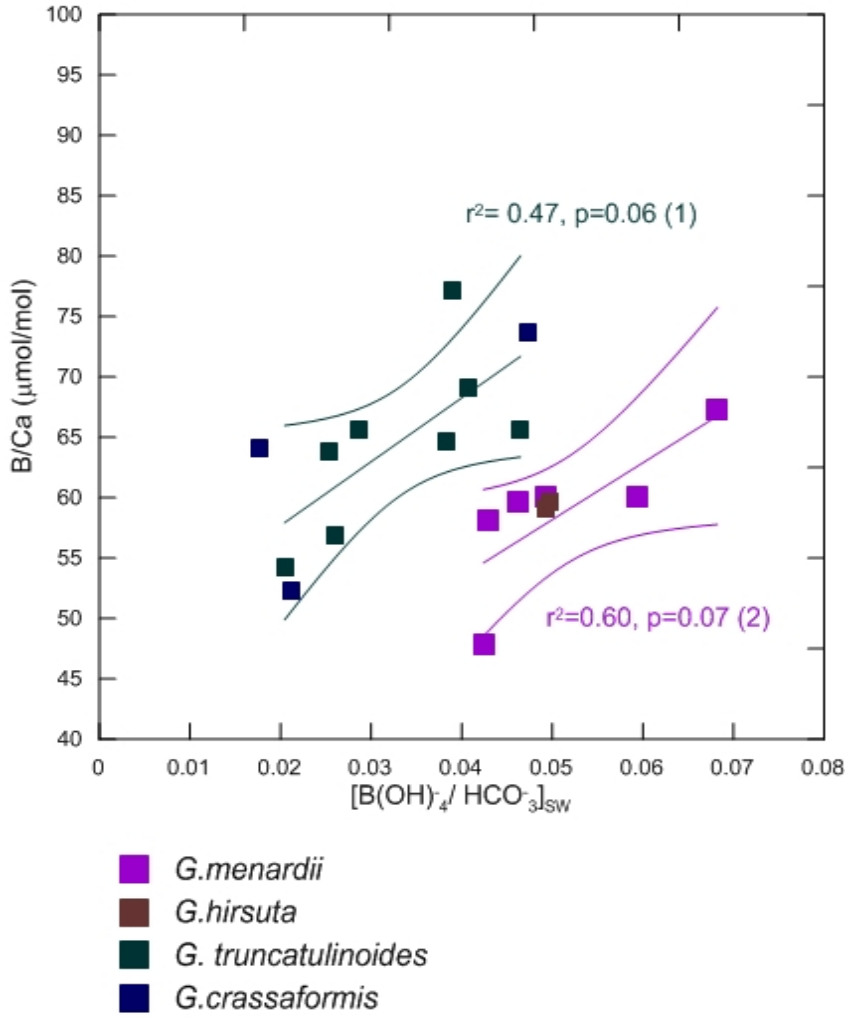

Figure 3.12 B/Ca ratios of asymbiotic planktonic foraminifer species *Globorotalia menardii, G. hirsuta G.truncatulinoides* (dextral and sinistral) and *G. crassaformis* (355-425µm) with $[B(OH)_4^-/HCO_3^-]_{sw}$ computed from nearby GLODAP and WOA09 stations at the depth of calcification determined from paired $\delta^{18}O$ measurements. (a) Solid lines represent linear regressions of the plotted data with 95% confidence intervals.

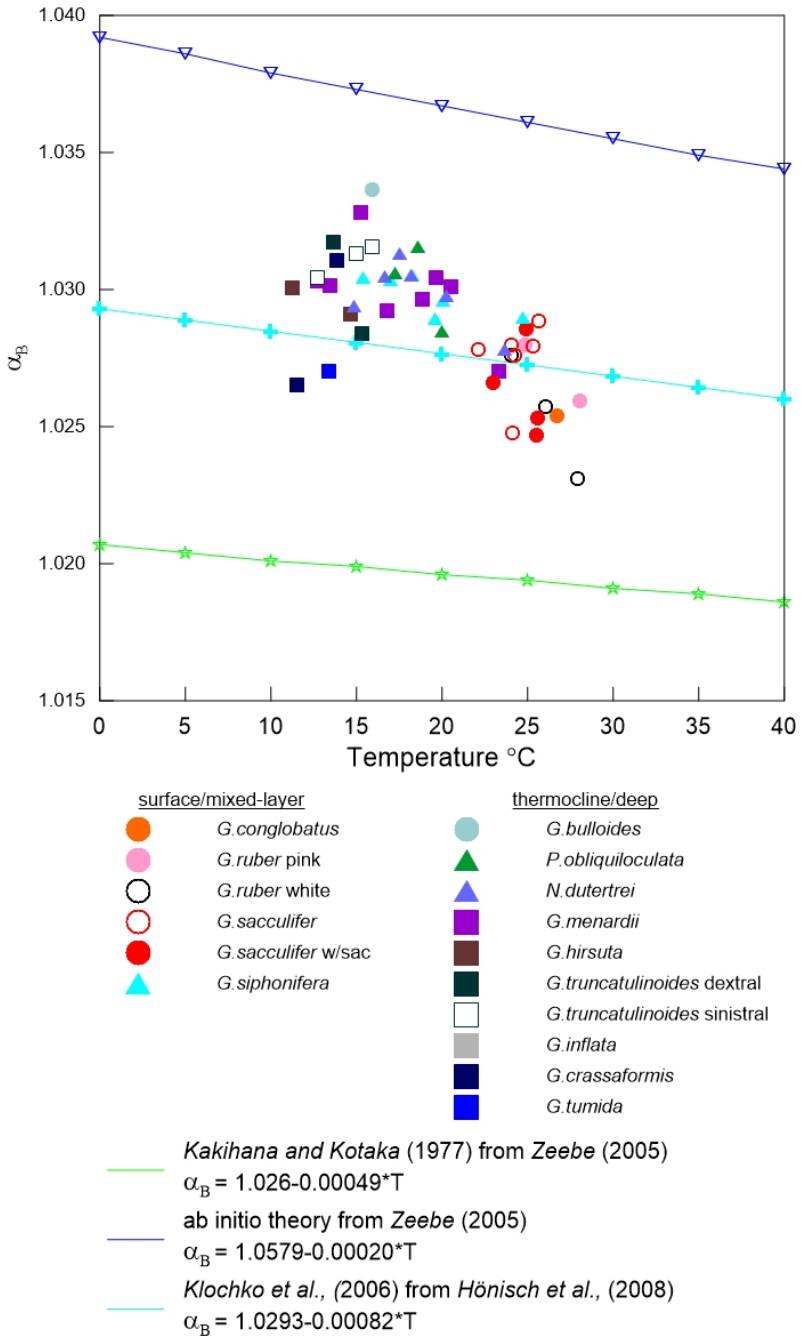

Figure 3.13 Temperature dependence of α_B, fractionation factor between $B(OH)_3$ and $B(OH)^-_4$ from (*Kakihana et al.*, 1977), ab initio theory computed in (*Zeebe*, 2005) and modified for *Klochko* et al., 2006 from (*Hönisch et al.*, 2008). Foraminifer α_B was computed by following the assumption of equilibrium between the measured foraminifera $\delta^{11}B$ and predicted seawater $\delta^{11}B_{B(OH)^-_4}$ compared to temperature derived from $\delta^{18}O$.

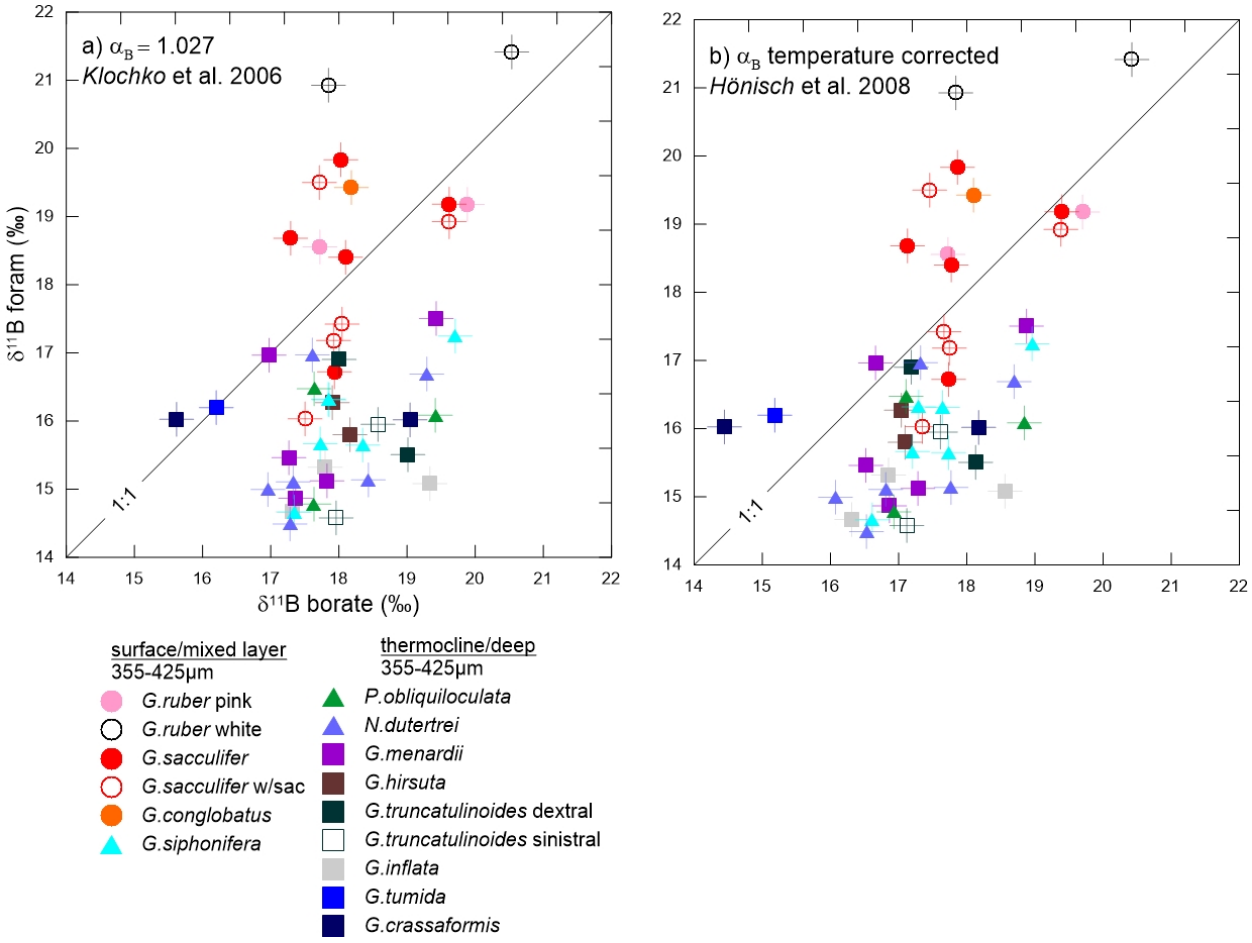

Figure 3.14 $\delta^{11}B$ of planktonic foraminifera plotted against predicted $\delta^{11}B_{B(OH)_4^-}$ at the depth of calcification. Black solid line represents isotopic equilibrium. a) $\delta^{11}B_{B(OH)_4^-}$ was computed using α_B from *Klochko* et al., (2006) assuming no correction for temperature and b) $\delta^{11}B_{B(OH)_4^-}$ was computed using the temperature corrected *Klochko* et al., (2006) estimated in (*Hönisch et al.*, 2008).

4.0 Chapter Four

Rapid surface ocean acidification and warming along the NJ coastal plain during the PETM

4.1 Abstract

The Paleocene Eocene thermal maximum (PETM) (~55.8 Myr) is characterized by a negative carbon isotope excursion (CIE) representing a large and rapid injection of carbon into the ocean-atmosphere reservoirs. Whereas acidification of the deep-ocean at the PETM is inferred from ocean sediment cores that record a widespread dissolution of carbonate sediments, there is no direct evidence for acidification in the surface ocean. A recently developed Boron/Calcium (B/Ca) proxy in planktonic foraminifera was applied to reconstruct surface ocean carbonate chemistry during the PETM. ODP Leg 174AX cores from the New Jersey coastal plain recovered expanded (up to 15 m thick) PETM sections deposited in middle shelf paleodepths (30-100 m). Coupled measurements of isotopic ($\delta^{13}C$, $\delta^{18}O$) B/Ca and Magnesium/Calcium (Mg/Ca) ratios were used to evaluate the magnitude and relative timing of ocean carbonate chemistry and temperature across the Paleocene-Eocene (P/E) boundary. Mg/Ca and B/Ca in mixed layer (*Morozovella* spp. and *Acarinina soldadoensis*) and deep dwelling (*Subbotina* spp.) planktonic foraminifera at Bass River and Ancora documented significant changes across the P/E boundary signifying warming and acidification of surface waters. Within the resolution of the New Jersey PETM records, the decrease in B/Ca is coincident with carbon isotope records suggesting that the carbon released during the PETM was linked to the change in surface ocean carbonate chemistry. The $\delta^{13}C$, B/Ca and % $CaCO_3$ records exhibit a step-wise change at the P/E boundary interpreted as evidence of abrupt acidification of coastal waters. Given that species specific calibrations are not possible for the extinct PETM taxa, a range of modern sensitivities for Mg/Ca and B/Ca were considered. The surface ocean temperature record

as inferred from Mg/Ca indicates a 5-7 ºC warming. Oceanic carbonate chemistry record based on B/Ca indicates a decrease in pH of 0.2-0.5 units across the P/E boundary. Determining the surface ocean carbonate chemistry during the PETM may provide a constraint on atmospheric pCO_2 levels and ultimately the amount of carbon released during the event.

4.2 Introduction

During the greenhouse world of the early Cenozoic (~40-65 Myr), pCO_2 concentrations arguably were high, with estimates exceeding 1,800 parts per million, six times pre-industrial values (*Lowenstein et al.*, 2006; *Pagani et al.*, 2005; *Pearson et al.*, 2000; *Royer et al.*, 2001) and the polar regions were generally ice-free (*Cramer et al.*, 2011; *Miller et al.*, 1987; *Zachos et al.*, 2005). Rapid warming events known as hyperthermals characterized by carbon cycle perturbations are superimposed on a longer term warming culminating at the Early Eocene Climatic Optimum (~51-53 Myr). The Paleocene-Eocene Thermal Maximum (PETM), the largest Eocene hyperthermals, is associated with a warming of global ocean temperatures of 5-6 °C (*Kennett et al.*, 1991; *Tripati et al.*, 2005; *Zachos et al.*, 2003) and up to 8 °C in the Arctic region (*Sluijs et al.*, 2009). Terrestrial and marine PETM sections record a negative carbon isotopic excursion indicating that a substantial addition of $\delta^{13}C$- depleted carbon into the atmosphere and ocean reservoirs (*Kennett et al.*, 1991; *Koch et al.*, 1992) establishing the CIE as a global event and chronostratigraphic marker of the initiation of the PETM (*Aubry*, 2002). Additional evidence for an abrupt and large carbon release comes from the occurrence of a clay horizon throughout the deep ocean interpreted as evidence of a rapid shoaling of the calcite compensation depth (CCD), followed by a gradual recovery (*Zachos et al.*, 2005). Several carbon sources have been proposed to explain the PETM perturbation, including burning of peat and coal deposits (*Kurtz et al.*, 2003) volcanism (*Storey et al.*, 2007), thermogenic methane

(*Svensen et al.*, 2004), bolide impact (*Kent et al.*, 2003) oxidation of terrestrial organic matter (*Higgins et al.*, 2006), permafrost carbon (*DeConto et al.*, 2012), and destabilization of continental shelf methane hydrates (*Dickens et al.*, 1995).

Records of $\delta^{13}C$ across P/E boundary provide evidence for the carbon perturbation and converge on the magnitude of the CIE to be ~3.5-5 ‰ in the surface ocean (*John et al.*, 2008; *Kennett et al.*, 1991; *Thomas et al.*, 2002; *Zachos et al.*, 2007; *Zachos et al.*, 2003). Using the magnitude of the CIE, models simulate a range from 2500 Pg to 10,000 Pg of carbon released during the PETM. The range of estimates relies on the assumed carbon source and its isotopic composition (*Dunkley Jones et al.*, 2010; *Ridgwell et al.*, 2010; *Zeebe et al.*, 2009). It is predicted that the geologically rapid and large carbon injection overwhelmed the ocean buffering capacity, resulting in the decline of pH and carbonate ion saturation (*Ridgwell et al.*, 2007). Model studies agree that surface ocean pH decreased during the PETM however, the rate and extent of acidification is contingent upon the mass of the carbon into the global reservoirs. The lithologic evidence of acidification (*Robinson*, 2011; *Zachos et al.*, 2005) supports model predictions of changes in carbonate chemistry that would ensue from the absorption of thousands of petagrams of carbon (*Panchuk et al.*, 2008; *Zeebe et al.*, 2009). However, quantitative evidence of the pH decline/carbonate ion saturation which can validate current estimates of the magnitude of the carbon release and its consequences to the ocean is still lacking.

Currently debated is whether the abrupt carbon input was a response to or the initial cause of the global warming at the PETM (*Sluijs et al.*, 2007). Increased input of greenhouse gases such as CH_4 or CO_2 is an appealing trigger for the warming as it provides both a carbon source and positive feedback mechanism to explain the sustained warming throughout the CIE (*Dickens et al.*, 1995). Determining the sequence of events at the onset of the PETM is, however,

challenging because of the briefness of the event and dissolution driven gap in deep-ocean cores. Nonetheless, expanded sections at sites with high sediment accumulation rates such as those along continental margins preserve the onset of the CIE allowing for detailed paleo reconstructions. *Sluijs et al.*, (2007) use the ODP Leg 174AX Bass River and the United States Geologic Survey Wilson Lake (USGS) core sites along the New Jersey shelf margin to argue that warming of sea surface temperature (SST) by about 3-4 °C preceded the carbon isotopic excursion, which accounts for 50-60 % of the entire SST warming observed in most records. It was further argued that the initial warming that preceded the CIE by several thousand years provided a precursor for the release of $\delta^{13}C$-depeleted carbon. The pre-CIE warming is apparently observed in other marine and terrestrial records (*Secord et al.*, 2010; *Sluijs et al.*, 2007; *Thomas et al.*, 2002), thus supporting the hypothesis that ocean warming might have acted as a trigger mechanism for the dissociation of submarine methane hydrates which caused further warming (*Dickens et al.*, 1995). Orbital forcing was suggested as a mechanism to trigger the warming, possibly by modulated release of oceanic methane hydrates (*Dickens et al.*, 1995) observed for several Eocene hyperthermal events (*Lourens et al.*, 2005) but appears out of phase at the PETM suggesting that other processes must have triggered the warming (*Zachos et al.*, 2010). Alternatively, an increase in greenhouse gas concentrations perhaps pCO_2 could produce the observed warming (*Sluijs et al.*, 2007) without altering the $\delta^{13}C$ of the exogenic carbon pool and the foraminifer $\delta^{13}C$ records at Bass River (*Cramer et al.*, 1999; *John et al.*, 2008).

Concerns arise regarding the reliability of the temperature records presented by *Sluijs et al.*, (2007) and question the presumed pre-CIE warming. The proxy carriers for the temperature proxies (i.e. TEX_{86}, % *Apectodinium acme*) were not the same as the records of $\delta^{13}C$ and may also be influenced by terrestrial inputs (*Crouch et al.*, 2003; *Kender et al.*, 2012) presenting

uncertainty regarding the relative timing of warming versus the carbon release. Also, the interpretation of changes in *Apectodinium acme* as solely a recorder of temperature is questioned. Here, I present records of temperature and ocean carbonate chemistry changes across the P/E boundary estimated using Magnesium/Calcium (Mg/Ca), B/Ca and $\delta^{13}C$ of planktonic foraminifera from Bass River (studied by *Sluijs et al., 2007*) and Ancora core sites drilled as part of ODP Leg 174AX. In principle, paired measurements (B/Ca, Mg/Ca, $\delta^{13}C$ and $\delta^{18}O$) in the same signal carrier are used in this study as it can be assumed that any post-depositional processes are influencing the proxy records similarly. Furthermore, use of autochthonous sediments (i.e. planktonic foraminifera) assumes that reconstructions of temperature and carbonate chemistry are reflecting a true marine signature. These records are used to test the hypothesis that a pre-CIE warming as measured along the shelf in New Jersey put forth by *Sluijs et al.*, (2007) and evaluate relative timing amongst the CIE, temperature and carbonate chemistry records at the PETM.

4.3 Geologic Setting

ODP Leg 174AX core sites located at Ancora and Bass River New Jersey were analyzed in this study (Figure 4.1). The Vincentown formation and Marlboro member comprise the upper Paleocene and lower Eocene section along the NJ coastal plain. The Paleocene-Eocene (P/E) boundary at Ancora and Bass River is associated although not coeval with the lithologic transition from glauconitic sand to the rapidly deposited kaolinitic-rich Marlboro clay similarly observed at Maryland and Delaware sections (*Gibson et al.*, 1993; *John et al.*, 2012; *Kopp et al.*, 2009). The P/E boundary is characterized by the decrease in $\delta^{13}C$ identified in bulk carbonate ($CaCO_3$) and foraminifera records occurring 1172.6-1172.2 ft (357.4-357.3 m) at Bass River (*Cramer et al.*, 1999; *John et al.*, 2008; *Zachos et al.*, 2007) and 563-562.1 ft (171.6-171.3 m) at

Ancora (*Cramer et al.*, 2005; *Kent et al.*, 2003). The CIE occurs within planktonic foraminiferal Zone P5, calcareous nannoplankton Zone NP9b and magnetic polarity Chron C24r (*Berggren*, 1995). Paleodepth estimates during the CIE based on benthic foraminifera biofacies and lithofacies at Ancora and Bass River were ~60 to 110 m and ~80-145 m, respectively and interpreted as middle to outer shelf environments (*Harris et al.*, 2010).

4.4 Material and Methods

4.4.1 Sample preparation

Individual foraminifer specimens were picked from disaggregated sediments from 250-300 and 300-355 μm sieve fractions and combined to obtain ~200-400 μg $CaCO_3$ material. Foraminiferal tests were gently crushed between two glass plates in order to open the chambers and facilitate the chemical cleaning procedure. Visible siliciclastic and glauconitic grains were removed when possible. Crushed foraminifera samples were transferred into acid-leached 0.5 mL centrifuge vials and rinsed with Milli-Q water (x3) and separated into trace element (100-400 μg) and stable isotope (50-100 μg) aliquots.

Stable isotope and trace element analysis were carried out on various planktonic foraminifera species from the *Subbotina*, *Morozovella* and *Acarinina* genera (see Appendix 3.1-3.4). Based on stable isotope measurements, *Morozovella* spp. are interpreted to represent the surface mixed-layer (low $\delta^{18}O$ and high $\delta^{13}C$ values), *Acarinina* spp. are estimated to represent the top of the thermocline (high $\delta^{18}O$ and high $\delta^{13}C$) and *Subbotina* spp. are estimated to reflect deeper waters (high $\delta^{18}O$ and low $\delta^{13}C$). Mixed-layer and symbiotic species included *A. soldadoensis, M. aequa*, *M. velascoensis* and *M. acuta (D'Hondt et al., 1994).* Somewhat deeper dwelling asymbiotic species included *S. velascoensis, S. patagonica, S. triangularis,* and *S.*

roesnaesensis (D'Hondt et al., 1994). Single species Mg/Ca and B/Ca records were not possibly from *Morozovella* and *Subbotina* as they were not available in sufficient abundances throughout the section. No differences in Mg/Ca and B/Ca between the different *Morozovella* species and *Subbotina* species analyzed throughout the section were observed (Figure 4.2). Therefore, species measurements were compiled to yield single genera records (i.e. *Subbotina* spp. and *Morozovella* spp.) with the exception of analysis of *Acarinina* spp. which is based on the species *A.soldadoensis.*

4.4.2 Elemental Analysis

Crushed foraminiferal samples were chemically cleaned following the Cd-cleaning protocol (*Boyle et al.*, 1985/1986) later modified by *Rosenthal et al.*, (1997). All reagents and acids were prepared using Milli-Q water passed through a boron Q-gard purification filter to obtain low boron water. Samples were rinsed with Milli-Q water and glass distilled methanol to remove adhered surficial clays on the tests. Reductive and oxidative cleaning steps were conducted to remove potential contaminate metal oxides and organics from foraminiferal tests. A final dilute acid (0.001 N HNO_3) leach was done before completely dissolving samples using 100 µL 0.065 N OPTIMA® HNO_3. Samples were diluted with ~100-200 µL (depending on the sample size) with 0.5 N OPTIMA® HNO_3 to a final volume of ~300-400 µL for a target calcium concentration of 4 mmol/L. Samples were monitored for potential contamination from clay and metal oxides by measuring Mn/Ca, Al/Ca and Fe/Ca to monitor for diagenetic coatings. Typical Mn/Ca values and Al/Ca values at Bass River and Ancora were ~200-800 µmol/mol ~200-600 µmol/mol, respectively. No significant correlation between B/Ca and Mn/Ca, Al/Ca or Fe/Ca was observed. Mg/Ca samples with high Fe/Ca (>10,000 µmol/mol) and Mn/Ca (>800 µmol/mol) were not included in the reconstructions.

Trace element analyses (B/Ca, Mg/Ca, Mn/Ca, Al/Ca and Fe/Ca) were measured at the Institute of Marine and Coastal Sciences at Rutgers University on a Thermo Finnigan Element XR Sector Field Inductively Coupled Plasma Mass Spectrometer (SF-ICP-MS) operated in low resolution ($m/\Delta m = 300$) and medium resolution ($m/\Delta m = 4300$) settings outline in the protocol of *Rosenthal et al.*, (1999). Elemental B analysis requires several modifications to the *Rosenthal et al.*, (1999) method to address potentially high [B] blanks and instrumental memory effect. The boron memory effect in the ICP introduction system is caused by the tendency of boric acid to volatilize and form droplets that accumulate in the spray chamber during the course of an analytical run (*Al-Ammar et al.*, 2000). To reduce the boron memory effect and improve washout efficiency, anhydrous ammonia gas was injected (into a high purity quartz cyclonic spray chamber (Elemental Scientific, ESI), raising the pH of the injected sample, converting boric acid to ammonium borate which solubilized and was removed during rinsing. Typical B blank levels were ~0.15ppb (<3% of [B] of foraminifera samples) and remained stable (±1%) throughout an analytical run.

Elemental ratios were monitored and corrected for matrix effects for each analytical run by analyzing a suite of standards using an internal spiked gravimetric standard (SGS) with the same elemental ratios but varying [Ca] (1.5 mmol/L to 8 mmol/L) (*Rosenthal et al.*, 1999). [Ca] concentrations in sample solutions were typically maintained in the range of 1.5 to 4mmol/L to minimize matrix effects on Mg/Ca and B/Ca. Analytical precision of B/Ca 115.43µmol/mol was ± 0.74% (RSD) and for Mg/Ca 3.32 mmol/mol ± 0.33% (RSD) based on repeated analysis of laboratory consistency standards throughout the length of the study (Figure 4.3).

4.4.3 Stable Isotopes

Stable carbon and oxygen isotopes were measured at the Department of Earth and Planetary Sciences using an Optima mass spectrometer. Measurements are reported in PDB with precision values of ±0.05‰ $\delta^{13}C$ and ±0.08‰ $\delta^{18}O$ for NBS19 standard throughout the analysis of this study.

4.5 Results

4.5.1 Bass River

B/Ca ratios of symbiotic mixed-layer *A. soldadoensis* and deep dwelling *Subbotina* spp. are ~60 µmol/mol and ~55 µmol/mol respectively below the P/E boundary (1172.2ft; 357.3m) (Figure 4.4). Above the P/E boundary, B/Ca ratios in *A. soldadoensis*, *Subbotina* spp. and *Morozovella* spp. are ~40 µmol/mol (Figure 4.4). Mg/Ca ratios of *A. soldadoensis* and *Subbotina* spp. below the P/E boundary are 2.49 and 2.48mmol/mol respectively (Figure 4.4). Above the P/E boundary (within the CIE) maximum Mg/Ca values are reached at ~1170ft (356.6m) of 3.32 and 4.21mmol/mol respectively (Figure 4.4).

4.5.2 Ancora

B/Ca ratios of *Subbotina* spp. below the P/E boundary (562.1ft; 171.3m) are ~50 µmol/mol (Figure 4.5). Above the P/E boundary, B/Ca ratios in *A. soldadoensis* and *Subbotina* spp. are ~40 µmol/mol and *Morozovella* spp. are ~50 µmol/mol (Figure 4.5). Above the unconformity (542.9 ft) B/Ca ratios are 50 µmol/mol in *Subbotina* spp., 60 µmol/mol in *A. soldadoensis* and 70 µmol/mol in *Morozovella* spp. (Figure 4.5). Below the P/E boundary (562.1ft; 171.3m), average Mg/Ca ratios for *Subbotina* spp. are 2.56mmol/mol (Figure 4.5).

Above the P/E boundary, Mg/Ca ratios are at maximum values at ~555ft (169.2m) of 5.48 mmol/mol in *Subbotina* spp., 4.64 mmol/mol in *A. soldadoensis* and 6.39 mmol/mol in *Morozovella* spp. (Figure 4.5). *Subbotina* spp. $\delta^{13}C$ and $\delta^{18}O$ change from average below the CIE values of -1.76 and 1.34 ‰ to maximum values of -1.70 and -3.55 ‰, respectively (Figure 4.5). CIE average values of $\delta^{13}C$ and $\delta^{18}O$ for *A. soldadoensis* and *Morozovella* spp. are -0.15 and -3.19 ‰ and 0 and -3.81 ‰, respectively (Figure 4.5).

4.6 Discussion

4.6.1 Preservation

Evidence of a CCD shoaling ~1 km across the P-E boundary and dissolution of carbonate sediments (i.e. foraminifera) (*Zachos et al.*, 2005) predicts that preservation of foraminifera tests during the PETM may be compromised in the deep ocean cores. Paleodepth estimates at Ancora and Bass River based on benthic foraminifera assemblages estimate ~50 and 100 m water depth lying well above the paleo-CCD. Dissolution influence on B/Ca in planktonic foraminiferal tests during post-depositional is largely uncharacterized. Observations from modern core top sediments demonstrate that B/Ca may be influenced by dissolution (*Coadic et al.*, 2013). Down-core records of B/Ca and planktonic foraminifera size normalized test weight, often used as an indication of dissolution, suggest that B/Ca may not be significantly influenced by preservation conditions (*Wara et al.*, 2003). Foraminiferal test weight at Bass River and Ancora exhibit no significant relationship with B/Ca suggesting negligible dissolution. Samples from Bass River and Ancora consist of both well-preserved tests with porcelain or glassy textures and poorly preserved tests.

To evaluate the preservation of foraminifera specimens using a high-resolution scanning electron microscope (SEM) images of *Subbotina* spp. were compared from below the CIE, within the CIE, and in the recovery intervals (Figure 4.6). Samples (Figure 4.6 a-c) from the Vincentown formation (below the CIE) exhibited the poorest preserved specimens when compared with those up section within the Marlboro Member (CIE interval) (Figure 4.6). The generally good preservation of the latter is attributed to the impermeable character of the clay-rich matrix (*Pearson et al.*, 2001). *Kozdon et al.*, (2013) suggest that Sr/Ca may be used as indication of diagenetic overprinting in planktonic foraminifera during the PETM (ODP 865). Sr/Ca measurements at Bass River are above 1.0mmol/mol, suggesting that diagensis is not influencing Mg/Ca ratios and therefore represent biogenic conditions with the exception of two sample depths which were not included due to possible diagensis (see Appendix). B/Ca records from Bass River (Figure 4.4) documented relatively constant values throughout the CIE despite the observation that variable degrees of test preservation were present throughout the section.

4.6.2 Mg/Ca, B/Ca and $\delta^{13}C$

To estimate ocean temperature, a multi-species calibration was applied as inter-species variability in Mg-temperature sensitivity is quite small for tropical and subtropical species planktonic foraminifera (*Anand et al.*, 2003). Because the seawater Mg/Ca composition of early Cenozoic seawater is not well constrained (compliation in *Evans et al.*, 2012; *Stanley et al.*, 1998; *Wilkinson et al.*, 1989) anomalies were computed relative to a pre-CIE baseline. Estimating temperature change rather than absolute values eliminates the uncertainty in the Mg/Ca ratio of seawater given the long residence time of Mg and Ca ions in the ocean relative to the short duration of the PETM (*Bates et al.*, 1998).

Mg/Ca based temperature in *A. soldadoensis* and *Subbotina* suggest a peak warming of 5 ºC and 7ºC, respectively (Figure 4.7). Warming across the P/E boundary based on Mg/Ca are within the TEX_{86} based estimate regardless of TEX_{86}^{H} or TEX_{86}^{L} calibration (*Kim et al.*, 2010). However, differences among proxies were observed in regards to the temporal relationship between the two paleotemperature proxy records relative to the CIE. Within the resolution of the record, Mg/Ca based sea surface warming occurred coincidently with the CIE as recorded in bulk inorganic and foraminifera carbonates (Figure 4.8). The Mg/Ca based temperature record do not record a pre-CIE warming in contrast with the TEX_{86} based temperature reconstruction from *Sluijs* et al., (2007) recording a SST warming preceding the CIE, recorded at Bass River and Wilson Lake core sites (Figure 4.8). While TEX_{86} based temperature records ~4 ºC warming starting at 1173.1 ft (357.6 m) below the CIE at 1172.2 ft (357.3 m) Mg/Ca remains unchanged (Figure 4.8).

Detailed reconstructions of the ocean carbonate system (B/Ca, $\delta^{13}C$ and % $CaCO_3$) and temperature (based on Mg/Ca) at Bass River allow for assessing the relative timing between warming and acidification. The drop in foraminiferal B/Ca ratios and $CaCO_3$, and inferred surface ocean acidification, were coincident with the negative CIE suggesting that the major carbon release during the PETM occurred at that time (Figure 4.8). Furthermore, the close coincidence between surface acidification and the initial rise in surface ocean temperature supports the idea that the released carbon was the cause for the PETM warming. This finding calls into question the hypothesis that warming preceded the CIE and that it was carbon induced (*Sluijs et al.*, 2007). Above the CIE at Bass River, $CaCO_3$ increases coincidently with a ~5 mol/mol B/Ca increase (*Subbotina* spp.) also observed at Ancora (*A.soldaoensis* and *Subbotina* spp.) (Figure 4.8). The increase in $CaCO_3$ and B/Ca ratios are interpreted as evidence of delivery

of alkalinity from rivers providing a buffering of NJ shelf waters. Enhanced hydrologic cycle during the PETM (*Bowen et al.*, 2004; *Pagani et al.*, 2006) may provide the catalyst for intense weathering (*John et al.*, 2012).

Sluijs et al., (2007) interpreted the pre-CIE warming as a potential trigger for the carbon release and evidence of thermal dissociation of methane hydrates during the PETM. The discrepancies between the two paleotemperature proxy records may be attributed to several factors including different mechanisms affecting the transport of proxies to the sediment, distinct ecologies of the signal carrying organisms and varying sediment digenesis histories. Evidence for intense weathering and terrestrial run off during the onset of the CIE was proposed to explain the delivery of ancient carbon organic matter or soils (*John et al.*, 2012; *Schneider-Mor et al.*, 2013) to the New Jersey coast below the CIE. The pre-CIE warming observed by the TEX_{86} record (*Sluijs et al.*, 2007) may be an artifact of terrestrial component possibly soil derived GDGTs and not representative of true oceanic conditions during the PETM. Mg/Ca and $\delta^{13}C$ in planktonic foraminifera both changed across the P/E boundary interpreted as evidence of simultaneous warming and carbon release into surface coastal waters along New Jersey (Figure 4.8).

4.6.3 Surface ocean acidification

If an increase in greenhouse gas emissions, pCO_2 or CH_4 caused the pre-CIE warming it is expected that surface ocean acidification should also precede the CIE. Seawater carbonate chemistry changes across the P/E boundary were estimated using the culture B/Ca sensitivities in planktonic foraminifera (*Allen et al.*, 2012; *Allen et al.*, 2011) and compared with model simulations. Given the long residence time of boron and calcium in the ocean, seawater [B]

within the duration of the PETM was assumed to be constant (*Bates et al.*, 1998). Knowledge of past seawater [B] and calibration errors are the primary uncertainties in determining past seawater pH values from B/Ca in planktonic foraminifera. To address those uncertainties the reconstructions of carbonate chemistry across the P/E boundary were focused on anomalies rather than determining absolute values.

Core-top and culture studies indicated that B/Ca ratios in planktonic foraminifera are controlled by the seawater carbonate chemistry from which their tests are precipitated (Chapter Three) (*Allen et al.*, 2012; *Allen et al.*, 2011; *Foster*, 2008; *Yu et al.*, 2007b). The basic mechanism controlling boron partitioning in modern foraminifera calcite is assumed to apply to the extinct PETM taxa and a range of B/Ca- $[B(OH)_4^-/HCO_3^-]_{sw}$ sensitivities were used to determine the magnitude of oceanic carbonate chemistry change across the P/E boundary. B/Ca- $[B(OH)_4^-/HCO_3^-]_{sw}$ sensitivities for symbiont bearing species *Globigerinoides ruber* and *G. sacculifer* (*Allen et al.*, 2012) were applied to mixed-layer *A. soldadoensis* species. For the *Subbotina* spp. asymbiotic thermocline dwelling equations from Chapter Three were applied. The culture sensitivities for the symbiotic species were used instead of the core-top calibrations (*Foster*, 2008; *Yu et al.*, 2007) because they are based on K_D derived relationships that likely are complicated by the multiple influences of temperature and carbonate chemistry (*Allen and Hönisch* 2012). Furthermore, the culture calibrations were preferred as they strictly represent the influence of $[B(OH)_4^-/HCO_3^-]_{sw}$ on B/Ca and are not biased by any potential temperature or dissolution effects. Based on the magnitude of the B/Ca anomalies (*A. soldadoensis* 25-30 µmol/mol*; Subbotina* spp. 15-20 µmol/mol) across the P/E boundary $[B(OH)_4^-/HCO_3^-]_{sw}$ was estimated to change by 0.04 ± 0.02 and 0.095 ±0.05 mol/mol equivalent to a pH change of 0.4 ±

0.02 units in the surface ocean (Figure 4.9 a) and 0.35 ± 0.15 units in the thermocline waters (Figure 4.9 b). The estimated influence of temperature on $[B(OH)_4^-/HCO_3^-]_{sw}$, assuming a warming of 5-7 ºC is small relative to the predicted change in ocean carbonate chemistry (Figure 4.10).

Carbon cycle model simulations during the PETM produce a coupled decline in the pH and carbonate saturation state in the surface and deep-ocean (***Ridgwell et al.***, 2010; ***Uchikawa et al.***, 2010). ***Uchikawa et al***., (2010) estimated an average surface ocean pH change during the PETM of 0.10-0.28 units. The magnitude of pH change estimated from B/Ca in this study was greater than the model result outputs. Assuming that the ***Uchikawa et al***., (2010) simulation reflects global surface ocean acidification it is hypothesized that the acidification, of coastal waters along NJ was greater than the global ocean. Alternatively, the amount or rate of carbon released in the model may be underestimating the magnitude of acidification as evident from the B/Ca reconstructions at Bass River. Support for the latter is a pelagic P/E section at ODP 1209 along Shatsky Rise in the central Pacific that records a similar B/Ca change in planktonic foraminifera to Bass River, suggesting a comparable degree of pH decline in the surface ocean (***Penman et al., 2011***).

The interpretation of B/Ca changes in terms of seawater carbonate chemistry may be complicated by the presence of symbionts that can influence boron incorporation (Chapter Two and Three). However, the possible loss of symbionts cannot account for the entire B/Ca anomaly at the P/E boundary as both asymbiotic *Subbotina* spp. and symbiotic ***A.soldadoensis*** species record a similar magnitude of change (Figure 4.4). The errors associated with the B/Ca calibrations yielded carbonate estimates that were similar between ***A.soldadoensis*** and *Subbotina* spp. suggesting the symbionts likely did not significantly bias the records (Figure 4.9).

Global evidence of enhanced hydrologic cycle during the PETM suggests an increased freshwater input into the oceans (*Kopp et al.*, 2009; *Pagani et al.*, 2006). Paired records sea surface temperature (SST) and foraminifera oxygen isotopes allow for the $\delta^{18}O_{sw}$ to be reconstructed and salinity to be estimated. Using the TEX_{86} sea surface temperature and foraminifera $\delta^{18}O$ values salinity anomalies across the P-E boundary at Wilson Lake record a surface ocean freshening (*Zachos et al.*, 2006).

Culture studies reveal a secondary influence of salinity boron incorporation (and hence B/Ca ratios) in planktonic foraminifera (*Allen et al.*, 2012; *Allen et al.*, 2011). Core-top studies do not provide evidence of a salinity effect on boron incorporation in planktonic foraminifera (*Foster*, 2008; *Yu et al.*, 2007). The paleodepth at Ancora is estimated to be shallower (~50 m) than Bass River and predicting that it would be more heavily influenced by freshwater inputs, due to its more proximal location to the continent. Both the absolute and magnitude of the B/Ca excursion recorded in *Subbotina* spp. at Ancora and Bass River are similar, arguing against a significant regional influence.

4.7 Conclusions

Records of planktonic foraminiferal B/Ca, and $\delta^{13}C$ along the NJ coastal plain demonstrate that the acidification of coastal surface waters at the PETM occurred at the CIE and were also coincident with the surface ocean warming as inferred from foraminiferal Mg/Ca. This finding questions the hypothesis that initial warming, suggested from a companion TEX_{86} record (Sluijs et al., 2007) was the precursor to the CIE and furthermore that it was forced by two carbon sources presumably with different $\delta^{13}C$ composition. While it is possible that the duration of the onset of CIE might have been shorter than previously proposed (<10,000 years), and

therefore the warming and acidification are geologically instantaneous, we see no evidence for ocean acidification nor for warming that support the previous findings of pre-CIE warming. It is argued that the virtually all the warming at the PETM was associated with a rapid carbon injection at the CIE with no evidence for a precursor to this event. Our estimates of ~5-8ºC surface ocean temperature warming at the CIE associated with ~0.2-0.4 pH reduction, and the absence of any change preceding the CIE, should put new constraints on the nature and magnitude of the carbon perturbation at that time.

4.8 References

Al-Ammar, A.S., Gupta, R.K., and Barnes, R.M. (2000), Elimination of boron memory effect in inductively coupled plasma-mass spectrometry by ammonia gas injection into the spray chamber during analysis, *Spectrochimica Acta B*, *55*(6), 629-635.

Allen, K.A., and Hönisch, B. (2012), The planktic foraminiferal B/Ca proxy for seawater carbonate chemistry: A critical evaluation, *Earth and Planetary Science Letters*, *345–348*(0), 203-211.

Allen, K.A., Hönisch, B., Eggins, S.M., and Rosenthal, Y. (2012), Environmental controls on B/Ca in calcite tests of the tropical planktic foraminifer species Globigerinoides ruber and Globigerinoides sacculifer, *Earth and Planetary Science Letters*, *351–352*(0), 270-280.

Allen, K.A., et al. (2011), Controls on boron incorporation in cultured tests of the planktic foraminifer Orbulina universa, *Earth and Planetary Science Letters*, *309*(3–4), 291-301.

Anand, P., Elderfield, H., and Conte, M.H. (2003), Calibration of Mg/Ca thermometry in planktonic foraminifera from a sediment trap time series, *Paleoceanography*, *18*(2), 1050.

Aubry, M.-P.a.t.W.G.o.t.P.E.B. (2002), The Paleocene/Eocene boundary global standard stratotype-section and point (GSSP): criteria for characterisation and correlation, *Tertiary Research*, *21*(1-4), 57-70.

Bates, N.R., Takahashi, T., Chipman, D.W., and Knap, A.H. (1998), Variability of pCO2 on diel to seasonal timescales in the Sargasso Sea near Bermuda, *Journal of Geophysical Research: Oceans*, *103*(C8), 15567-15585.

Berggren, W.A., Kent, D.V, Swisher, C.C, and Aubry, M.P (1995), A Revised Cenozoic Geochronology and Chronostratigraphy in Berggren, W. A., D.V. Kent, C.C., Swisher, M. Aubry, and J. Hardenbol (eds), Geochronology, Time Scales and Global Stratigraphic Correlation, *SEPM Special Publication 54*, 129-212.

Bowen, G.J., et al. (2004), A humid climate state during the Paleocene/Eocene thermal maximum, *Nature*, *432*, 495-499.

Boyle, E.A., and Keigwin, L.D. (1985/1986), Comparison of Atlantic and Pacific paleochemical records for the last 215,000 years: changes in deep ocean circulation and chemical inventories, *Earth and Planetary Science Letters*, *76*(1-2), 135-150.

Coadic, R., et al. (2013), A core-top study of dissolution effect on B/Ca in Globigerinoides sacculifer from the tropical Atlantic: Potential bias for paleo-reconstruction of seawater carbonate chemistry, *Geochemistry, Geophysics, Geosystems*, *14*(4), 1053-1068.

Cramer, B.S., and Kent, D.V. (2005), Bolide summer: The Paleocene/Eocene thermal maximum as a response to an extraterrestrial trigger, *Palaeogeography, Palaeoclimatology, Palaeoecology*, *224*(1-3), 144-166.

Cramer, B.S., Miller, K.G., Barrett, P.J., and Wright, J.D. (2011), Late Cretaceous–Neogene trends in deep ocean temperature and continental ice volume: Reconciling records of benthic foraminiferal geochemistry (δ18O and Mg/Ca) with sea level history, *Journal of Geophysical Research: Oceans*, *116*(C12), C12023.

Cramer, B.S., et al. (1999), An exceptional chronologic, isotopic, and clay mineralogic record of the latest Paleocene thermal maximum, Bass River, NJ, ODP 174AX, *Bulletin de la Societe Geologique de France*, *170*(6), 883-897.

Crouch, E.M., et al. (2003), The Apectodinium acme and terrestrial discharge during the Paleocene-Eocene thermal maximum: new palynological, geochemical and calcareous

nannoplankton observations at Tawanui, New Zealand, *Palaeogeography, Palaeoclimatology, Palaeoecology*, *194*(4), 387-403.
D'Hondt, S., Zachos, J.C., and Schultz, G. (1994), Stable Isotopic Signals and Photosymbiosis in Late Paleocene Planktic Foraminifera, *Paleobiology*, *20*(3), 391-406.
DeConto, R.M., et al. (2012), Past extreme warming events linked to massive carbon release from thawing permafrost, *Nature Geoscience*, *484*(7392), 87-91.
Dickens, G.R., O'Neil, J.R., Rea, D.K., and Owen, R.M. (1995), Dissociation of Oceanic Methane Hydrate as a Cause of the Carbon Isotope Excursion at the End of the Paleocene, *Paleoceanography*, *10*(6), 965-971.
Dunkley Jones, T., et al. (2010), A Palaeogene perspective on climate sensitivity and methane hydrate instability, *Philosophical Transactions of the Royal Society A: Mathematical, Physical and Engineering Sciences*, *368*(1919), 2395-2415.
Evans, D., and Müller, W. (2012), Deep time foraminifera Mg/Ca paleothermometry: Nonlinear correction for secular change in seawater Mg/Ca, *Paleoceanography*, *27*(4), PA4205.
Foster, G.L. (2008), Seawater pH, pCO2 and [CO2-3] variations in the Caribbean Sea over the last 130 kyr: A boron isotope and B/Ca study of planktic foraminifera, *Earth and Planetary Science Letters*, *271*(1-4), 254-266.
Gibson, T.G., Bybell, L.M., and Owens, J.P. (1993), Latest Paleocene lithologic and biotic events in neritic deposits of southwestern New Jersey, *Paleoceanography*, *8*(4), 495-514.
Harris, A.D., et al. (2010), Integrated stratigraphic studies of Paleocene-lowermost Eocene sequences, New Jersey Coastal Plain: Evidence for glacioeustatic control, *Paleoceanography*, *25*(3), PA3211.
Higgins, J.A., and Schrag, D.P. (2006), Beyond methane: Towards a theory for the Paleocene-Eocene Thermal Maximum, *Earth and Planetary Science Letters*, *245*(3-4), 523-537.
John, C.M., et al. (2012), Clay assemblage and oxygen isotopic constraints on the weathering response to the Paleocene-Eocene thermal maximum, east coast of North America, *Geology*, *40*(7), 591-594.
John, C.M., et al. (2008), North American continental margin records of the Paleocene-Eocene thermal maximum: Implications for global carbon and hydrological cycling, *Paleoceanography*, *23*(2), PA2217.
Kender, S., et al. (2012), Marine and terrestrial environmental changes in NW Europe preceding carbon release at the Paleocene–Eocene transition, *Earth and Planetary Science Letters*, *353–354*(0), 108-120.
Kennett, J.P., and Stott, L.D. (1991), Abrupt deep-sea warming, paleoceanographic changes and benthic extinctions at the end of the Paleocene, *Nature*, *353*, 225-229.
Kent, D.V., et al. (2003), A case for a comet impact trigger for the Paleocene/Eocene thermal maximum and carbon isotope excursion, *Earth and Planetary Science Letters*, *211*(1-2), 13-26.
Kim, J.-H., et al. (2010), New indices and calibrations derived from the distribution of crenarchaeal isoprenoid tetraether lipids: Implications for past sea surface temperature reconstructions, *Geochimica et Cosmochimica Acta*, *74*, 4639-4654.
Koch, P.L., Zachos, J.C., and Gingerich, P.D. (1992), Correlation between isotope records in marine and continental carbon reservoirs near the Palaeocene/Eocene boundary, *Nature*, *358*(6384), 319-322.

Kopp, R.E., et al. (2009), An Appalachian Amazon? Magnetofossil evidence for the development of a tropical river-like system in the mid-Atlantic United States during the Paleocene-Eocene thermal maximum, *Paleoceanography*, *24*(4).

Kozdon, R., et al. (2013), In situ δ18O and Mg/Ca analyses of diagenetic and planktic foraminiferal calcite preserved in a deep-sea record of the Paleocene-Eocene thermal maximum, *Paleoceanography*, *28*(3), 517-528.

Kurtz, A.C., et al. (2003), Early Cenozoic decoupling of the global carbon and sulfur cycles, *Paleoceanography*, *18*(4), 1090.

Lourens, L.J., et al. (2005), Astronomical pacing of late Palaeocene to early Eocene global warming events, *Nature*, *435*(7045), 1083-1087.

Lowenstein, T.K., and Demicco, R.V. (2006), Elevated Eocene Atmospheric CO2 and Its Subsequent Decline, *Science*, *313*(5795), 1928.

Miller, K.G., Janecek, T.R., Katz, M.E., and Keil, D.J. (1987), Abyssal Circulation and Benthic Foraminiferal Changes Near the Paleocene/Eocene Boundary, *Paleoceanography*, *2*(6), 741-761.

Pagani, M., et al. (2005), Marked Decline in Atmospheric Carbon Dioxide Concentrations During the Paleogene, *Science*, *309*(5734), 600-603.

Pagani, M., et al. (2006), Arctic hydrology during global warming at the Palaeocene/Eocene thermal maximum, *Nature*, *443*(7111), 598-598.

Panchuk, K., Ridgwell, A., and Kump, L.R. (2008), Sedimentary response to Paleocene-Eocene Thermal Maximum carbon release: A model-data comparison, *Geology*, *36*(4), 315-318.

Pearson, P.N., and Palmer, M.R. (2000), Atmospheric carbon dioxide concentrations over the past 60 million years, *Nature*, *406*(6797), 695-699.

Pearson, P.N., et al. (2001), Warm tropical sea surface temperatures in the Late Cretaceous and Eocene epochs, *Nature*, *413*(6855), 481-487.

Penman, D.E., et al. (*2011*), Boron proxy evidence for surface ocean acidification & elevated pCO2 during the PETM, *Mineralogical Magazine*, *75*(3), 1619.

Ridgwell, A., and Schmidt, D.N. (2010), Past constraints on the vulnerability of marine calcifiers to massive carbon dioxide release, *Nature Geoscience*, *3*(3), 196-200.

Ridgwell, A., et al. (2007), Marine geochemical data assimilation in an efficient Earth System Model of global biogeochemical cycling, *Biogeosciences*, *4*(1), 1726-4189.

Robinson, S.A. (2011), Shallow-water carbonate record of the Paleocene-Eocene Thermal Maximum from a Pacific Ocean guyot, *Geology*, *39*(1), 51-54.

Rosenthal, Y., Boyle, E.A., and Slowey, N. (1997), Temperature control on the incorporation of magnesium, strontium, fluorine, and cadmium into benthic foraminiferal shells from Little Bahama Bank: Prospects for thermocline paleoceanography, *Geochimica et Cosmochimica Acta*, *61*(17), 3633-3643.

Rosenthal, Y., Field, M.P., and Sherrell, R.M. (1999), Precise determination of element/calcium ratios in calcareous samples using Sector Field Inductively Couple Plasma Mass Spectrometry, *Analytical Chemistry 71*, 3248-3253.

Royer, D.L., et al. (2001), Paleobotanical Evidence for Near Present-Day Levels of Atmospheric CO2 During Part of the Tertiary, *Science*, *292*(5525), 2310-2313.

Schneider-Mor, A., and Bowen, G.J. (2013), Coupled and decoupled responses of continental and marine organic-sedimentary systems through the Paleocene-Eocene thermal maximum, New Jersey margin, USA, *Paleoceanography*, *28*(1), 105-115.

Secord, R., Gingerich, P.D., Lohmann, K.C., and MacLeod, K.G. (2010), Continental warming preceding the Palaeocene-Eocene thermal maximum, *Nature*, *467*(7318), 955-958.

Sluijs, A., et al. (2007), Environmental precursors to rapid light carbon injection at the Palaeocene/Eocene boundary, *Nature*, *450*(7173), 1218-1221.

Sluijs, A., et al. (2009), Warm and wet conditions in the Arctic region during Eocene Thermal Maximum 2, *Nature Geoscience*, *2*(11), 777-780.

Stanley, S.M., and Hardie, L.A. (1998), Secular oscillations in the carbonate mineralogy of reef-building and sediment-producing organisms driven by tectonically forced shifts in seawater chemistry, *Palaeogeography, Palaeoclimatology, Palaeoecology*, *144*(1–2), 3-19.

Storey, M., Duncan, R.A., and Swisher, C.C. (2007), Paleocene-Eocene Thermal Maximum and the Opening of the Northeast Atlantic, *Science*, *316*(5824), 587-589.

Svensen, H., et al. (2004), Release of methane from a volcanic basin as a mechanism for initial Eocene global warming, *Nature*, *429*(6991), 542-545.

Thomas, D.J., et al. (2002), Warming the fuel for the fire: Evidence for the thermal dissociation of methane hydrate during the Paleocene-Eocene thermal maximum, *Geology*, *30*(12), 1067-1070.

Tripati, A., and Elderfield, H. (2005), Deep-Sea Temperature and Circulation Changes at the Paleocene-Eocene Thermal Maximum, *Science*, *308*(5730), 1894-1898.

Uchikawa, J., and Zeebe, R.E. (2010), Examining possible effects of seawater pH decline on foraminiferal stable isotopes during the Paleocene-Eocene Thermal Maximum, *Paleoceanography*, *25*(2), PA2216.

Wara, M.W., Delaney, M.L., Bullen, T.D., and Ravelo, A.C. (2003), Possible roles of pH, temperature, and partial dissolution in determining boron concentration and isotopic composition in planktonic foraminifera, *Paleoceanography*, *18*(4), 1100.

Wilkinson, B.H., and Algeo, T.J. (1989), Sedimentary carbonate record of calcium-magnesium cycling, *American Journal of Science*, *289*(10), 1158-1194.

Yu, J., Elderfield, H., and Hönisch, B. (2007), B/Ca in planktonic foraminifera as a proxy for surface seawater pH, *Paleoceanography*, *22*(2), PA2202.

Zachos, J.C., et al. (2010), Tempo and scale of late Paleocene and early Eocene carbon isotope cycles: Implications for the origin of hyperthermals, *Earth and Planetary Science Letters*, *299*(1–2), 242-249.

Zachos, J.C., et al. (2007), The Palaeocene–Eocene carbon isotope excursion: constraints from individual shell planktonic foraminifer records, *Philosophical Transactions of the Royal Society A: Mathematical, Physical and Engineering Sciences*, *365*(1856), 1829-1842.

Zachos, J.C., et al. (2003), A Transient Rise in Tropical Sea Surface Temperature During the Paleocene-Eocene Thermal Maximum, *Science*, *302*(5650), 1551-1554.

Zachos, J.C., et al. (2006), Extreme warming of mid-latitude coastal ocean during the Paleocene-Eocene Thermal Maximum: Inferences from TEX86 and isotope data, *Geology*, *34*(9), 737-740.

Zachos, J.C., et al. (2005), Rapid Acidification of the Ocean During the Paleocene-Eocene Thermal Maximum, *Science*, *308*(5728), 1611-1615.

Zeebe, R.E., Zachos, J.C., and Dickens, G.R. (2009), Carbon dioxide forcing alone insufficient to explain Palaeocene-Eocene Thermal Maximum warming, *Nature Geoscience*, *2*(8), 576-580.

Table 4.1 Long-term analytical precision of laboratory internal consistency standards from April 2012 to May 2013.

Consistency Standards	Statistics	Mg/Ca mmol/mol	B/Ca µmol/mol
CS1	Expected	1.240	20.656
	Mean	1.265	20.503
	± 1σ	0.011	2.669
	% RSD	**0.86%**	**13.02%**
	% Δ (meas-exp)	2.02%	-0.74%
CS2	Expected	3.318	115.433
	Mean	3.327	110.437
	± 1σ	0.022	2.956
	% RSD	**0.67%**	**2.68%**
	% Δ (meas-exp)	0.27%	-4.33%
CS3	Expected	7.506	242.541
	Mean	7.543	229.508
	± 1σ	0.458	3.462
	% RSD	**0.46%**	**1.51%**
	% Δ (meas-exp)	0.50%	-5.37%

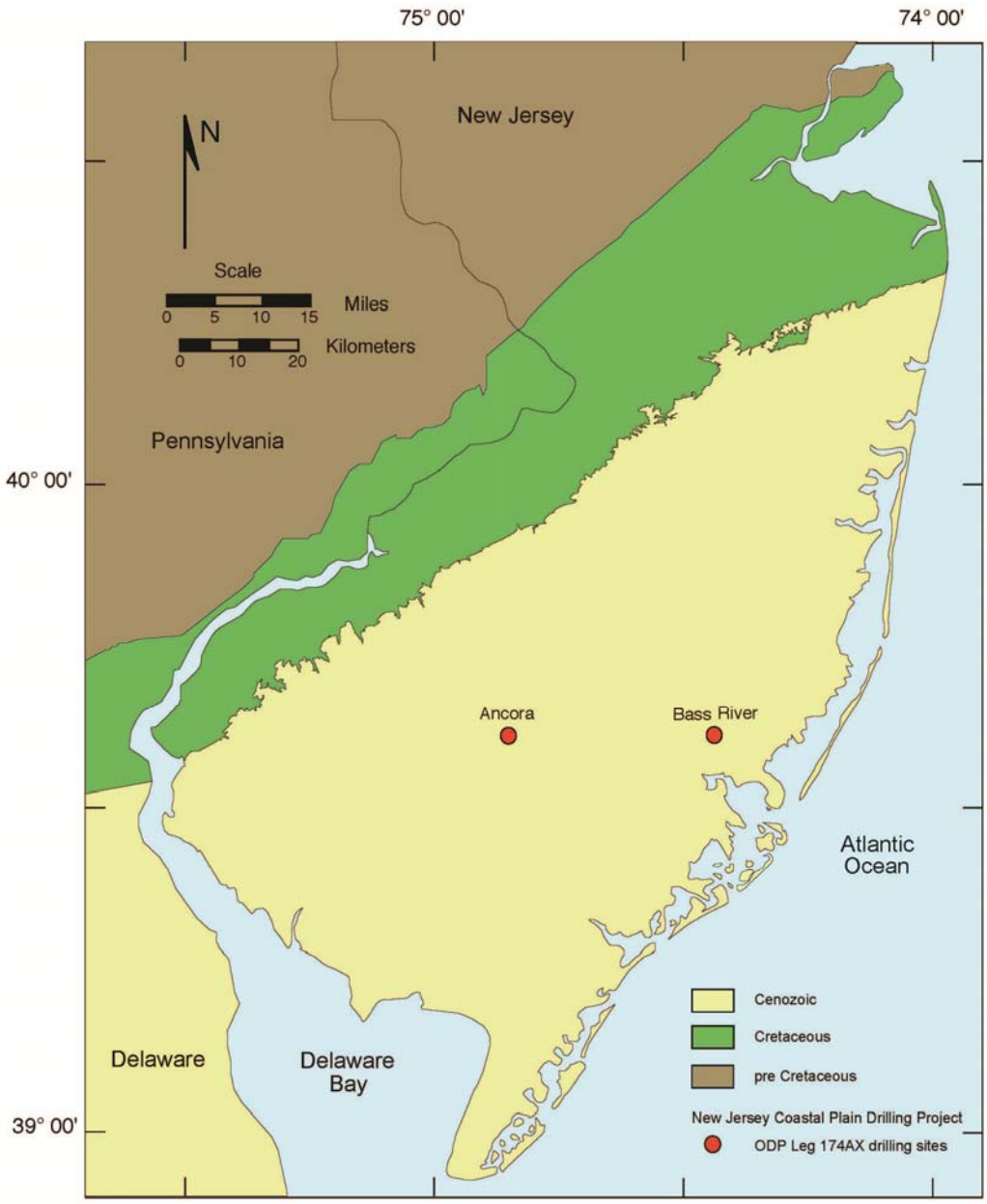

Figure 4.1 Location of Ancora and Bass River core sites used to generate geochemical records in this study from ODP Leg 174AX.

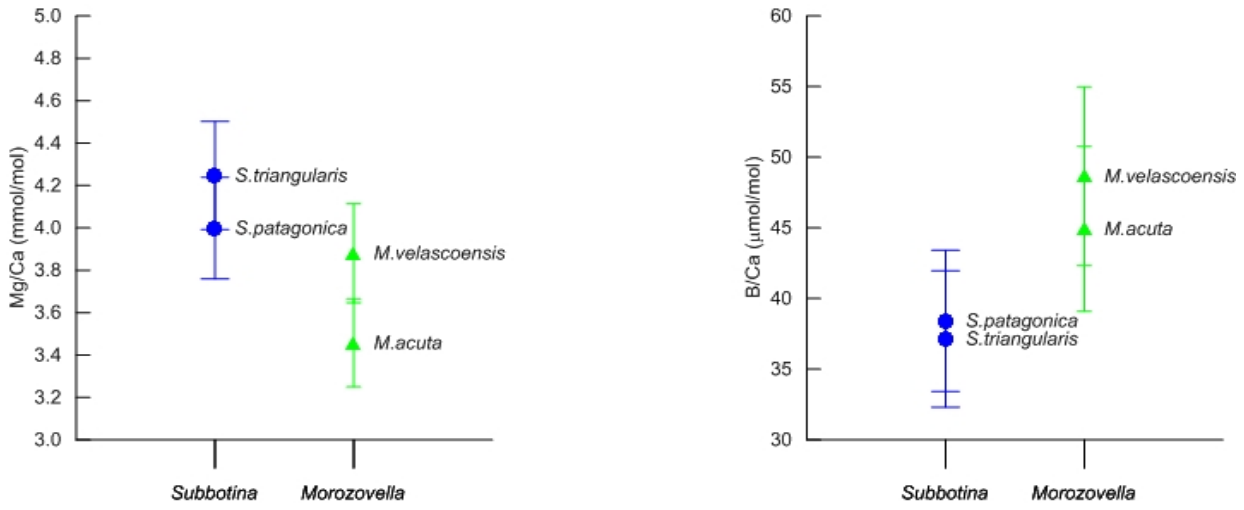

Figure 4.2 Comparison of Mg/Ca and B/Ca data for *S. patagonica*/*S. triangularis* (1171.5-1171.6 ft) and *M. acuta*/*M. velascoensis* (1167-1167.1 ft) species from the Bass River core site.

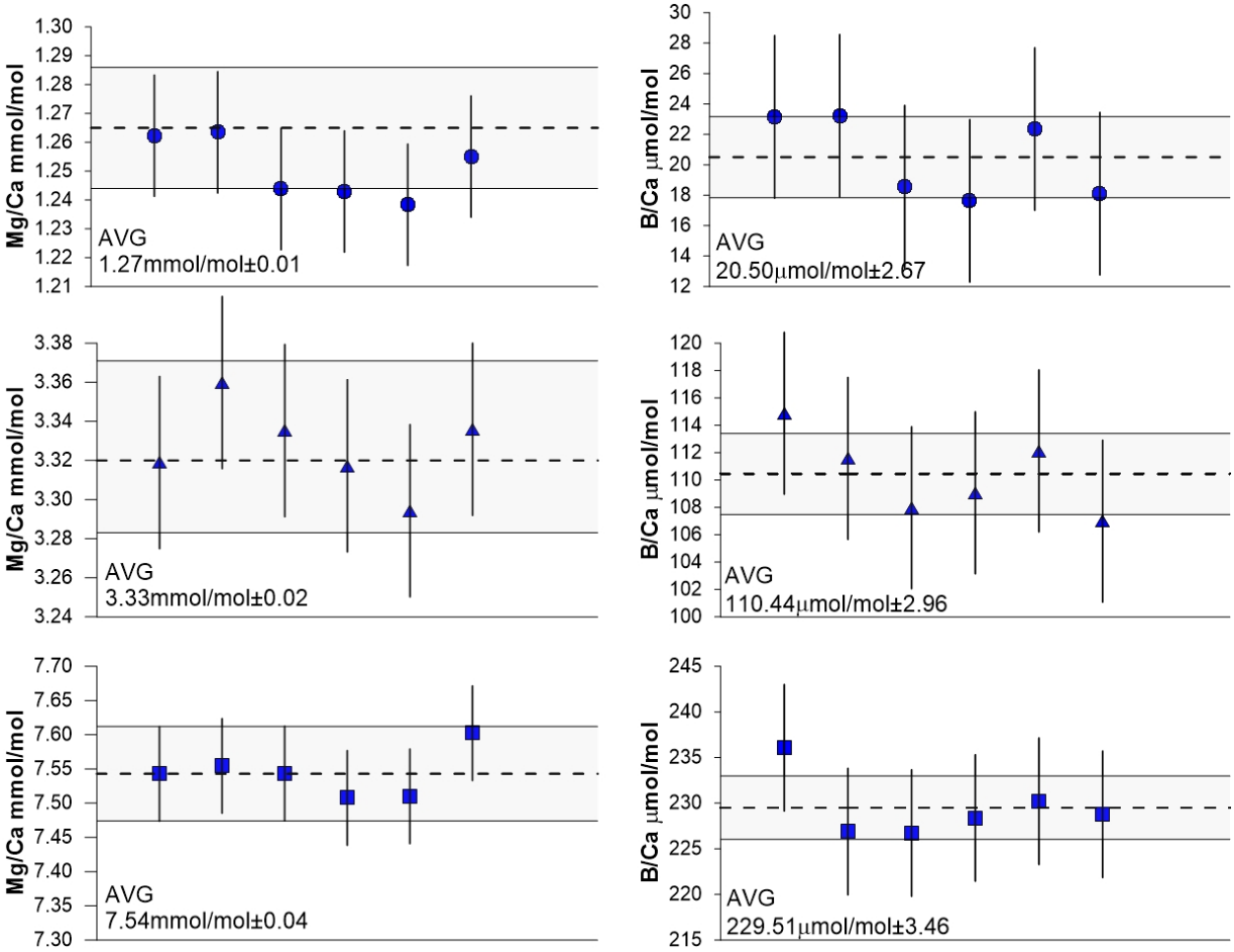

Figure 4.3 Measurements of Mg/Ca (mmol/mol) and B/Ca (µmol/mol) for in house consistency standards plotted during the data acquisition for this study (April 2012 to May 2013). Average values and with uncertainty are reported as 2σ.

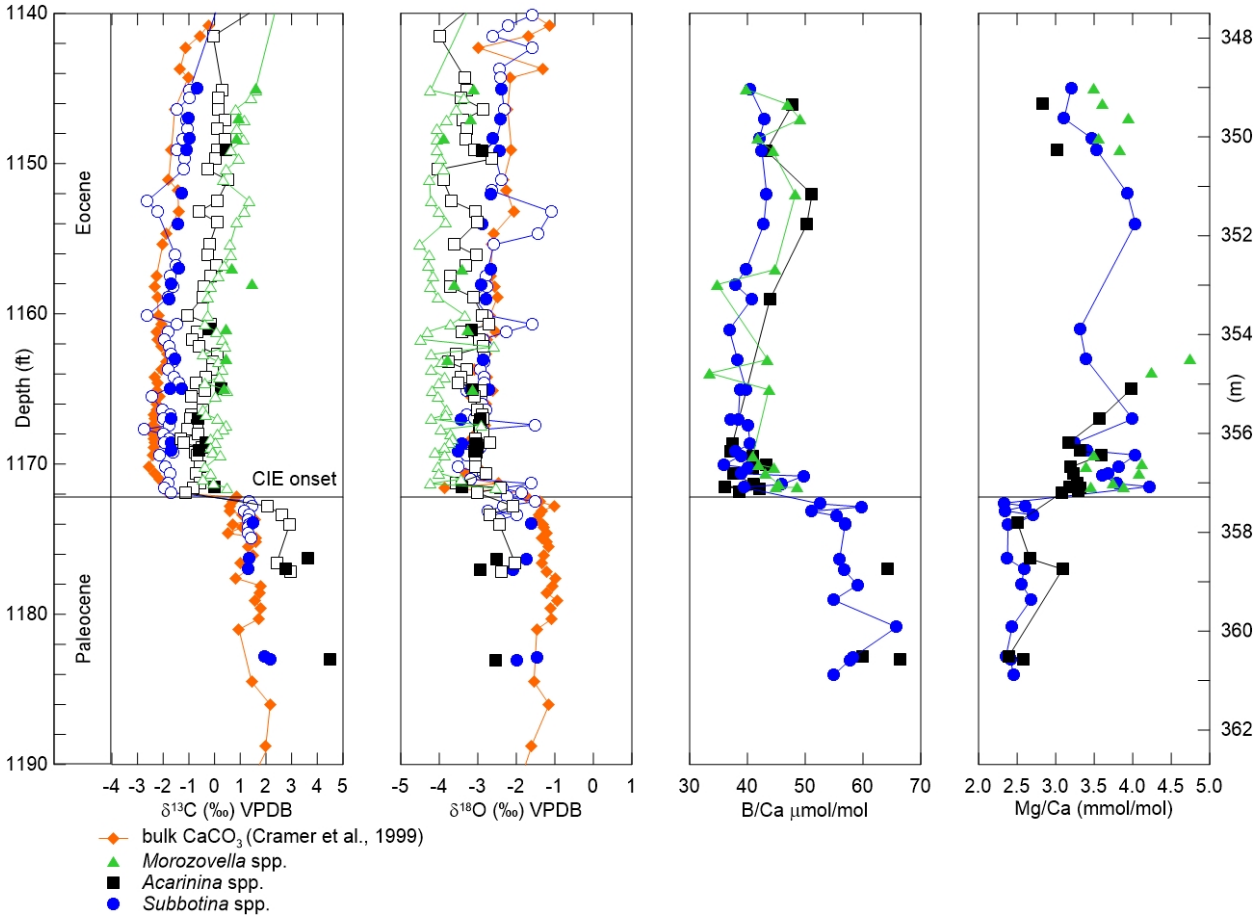

Figure 4.4 Results for Bass River core site. Solid horizontal line ~1172.2 ft (357.3 m) represents the onset of the CIE. Bulk carbonate $\delta^{13}C$ and $\delta^{18}O$ data are from (*Cramer et al.*, 1999) and foraminifera data are from this study (solid symbols) and *John et al.*, (2008) (open symbols) Mg/Ca and B/Ca µmol/mol ratios of foraminifera are from this study.

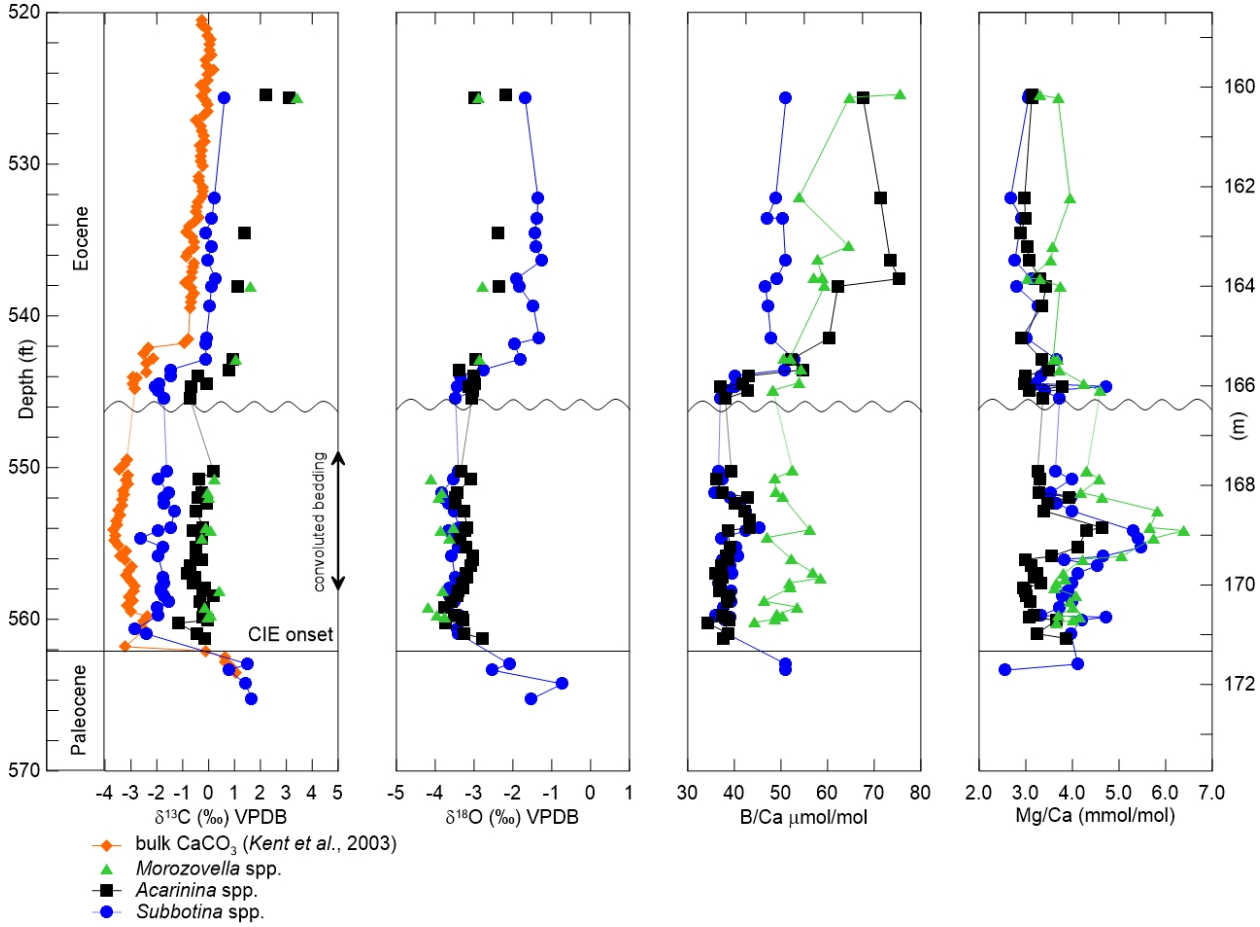

Figure 4.5 Results for Ancora core site A. Solid horizontal line ~562.1 ft (171.3 m) represents the onset of the CIE. Bulk carbonate $\delta^{13}C$ data are from *Kent et al.*, (2003). $\delta^{13}C$, $\delta^{18}O$, B/Ca and Mg/Ca records of planktonic foraminifera are from this study.

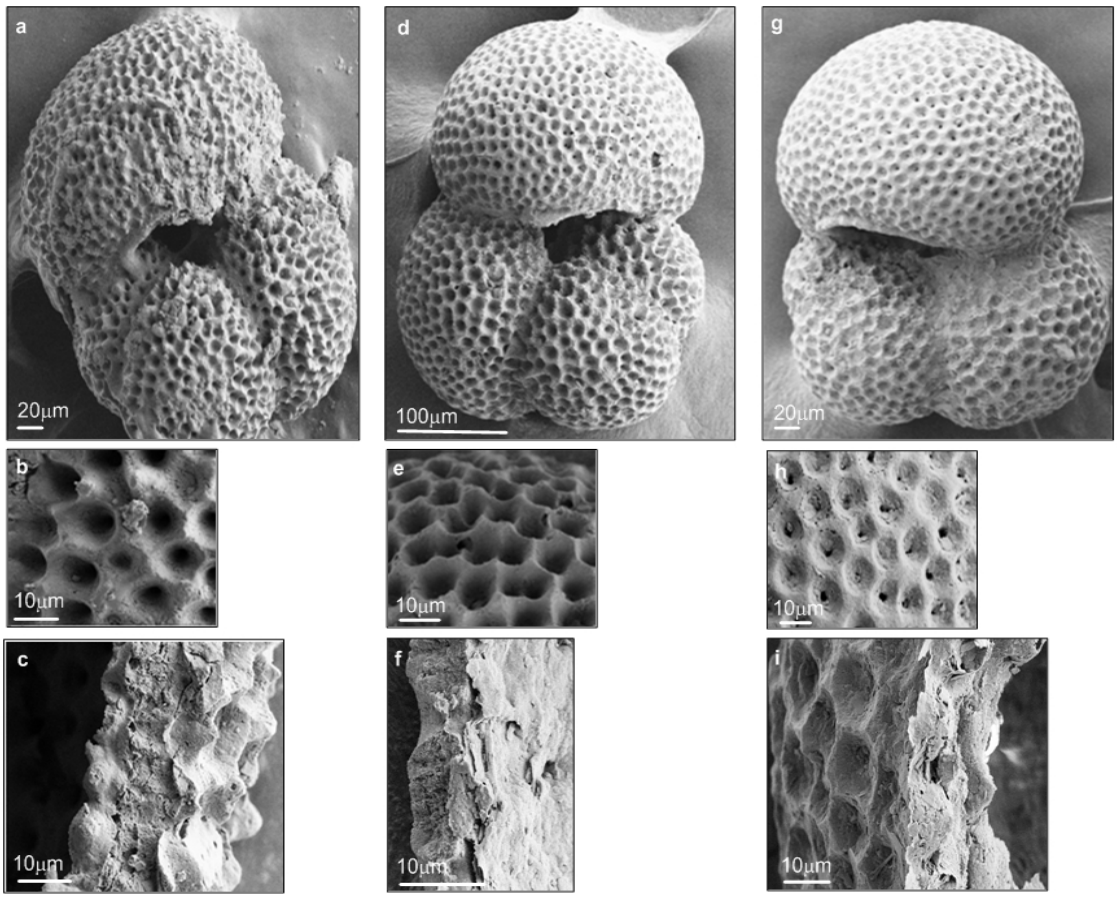

Figure 4.6 SEM images of planktonic foraminifer *S. triangularis*/*roesnaesensis* from ODP 174AX Bass River from core depths (a-c: 1176.3 ft, d-f: 1171.1 ft and g-i: 1169.4 ft) test texture (b, e, h) and cross section of test walls (c, f, i).

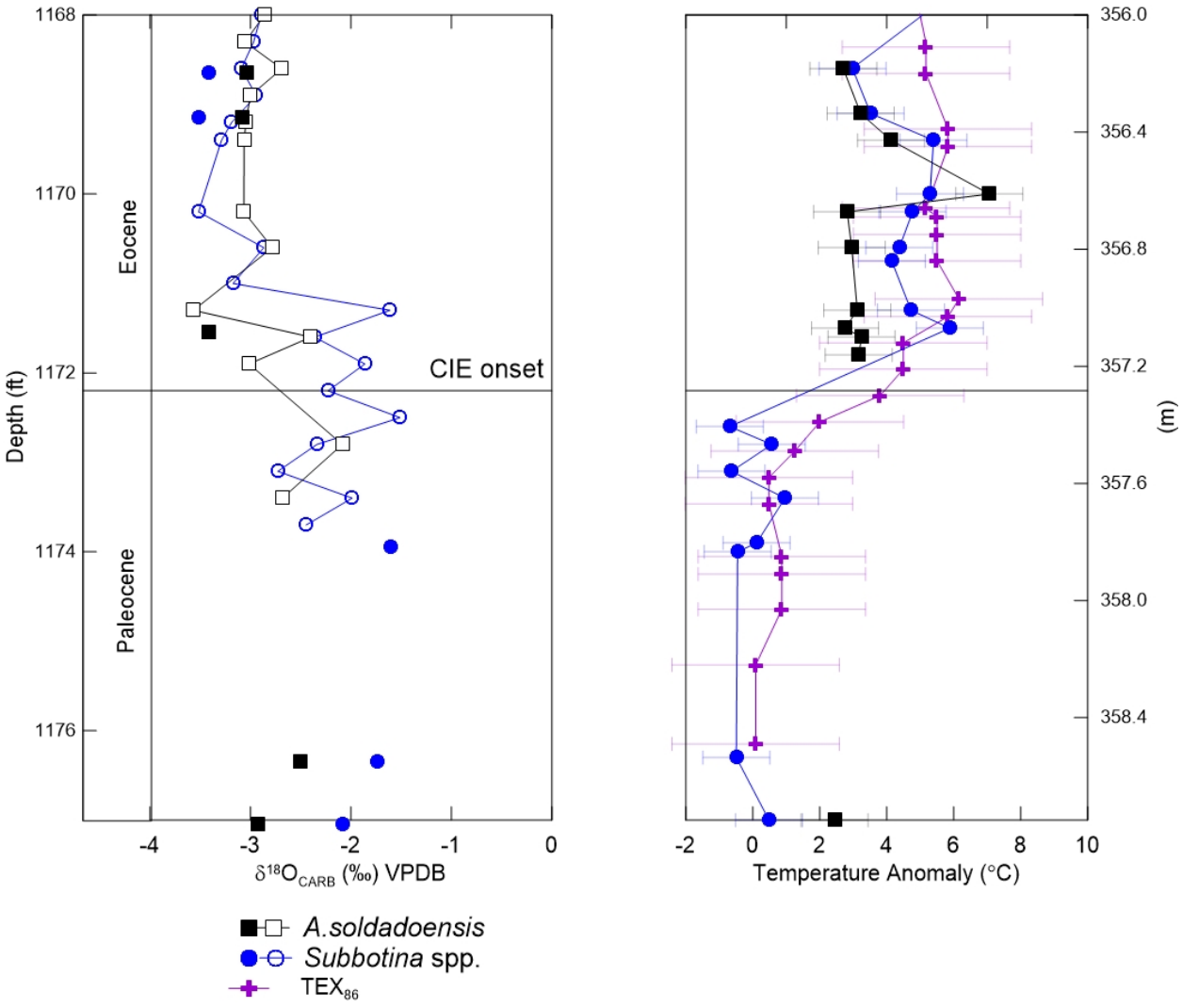

Figure 4.7 Results from Bass River core site. $\delta^{18}O$ data are from this study (solid symbols) and *John et al.*, (2008) open symbols. Foraminifera temperature anomalies are based on Mg/Ca data generated in this study and TEX_{86} estimate is from (*Sluijs et al.*, 2007).

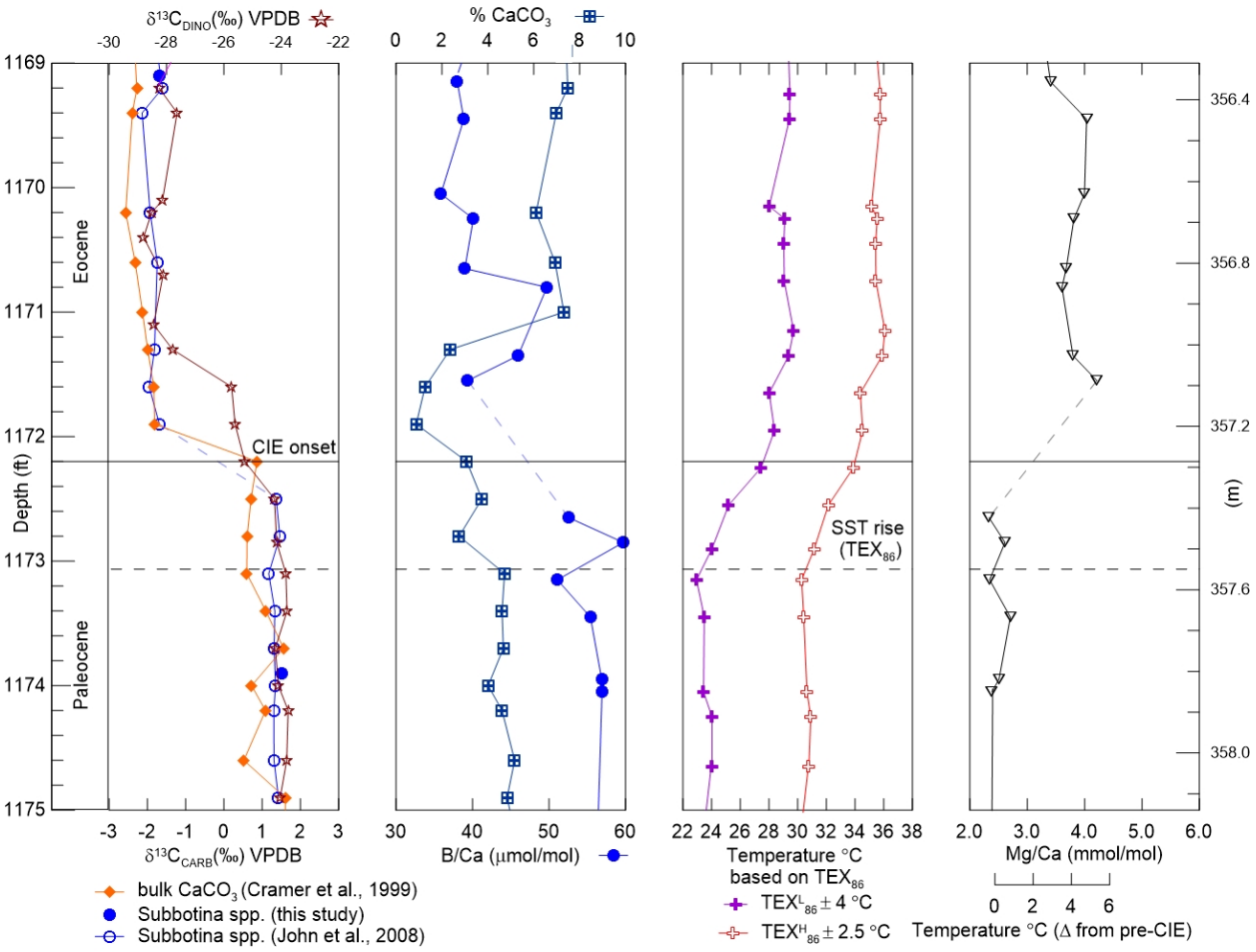

Figure 4.8 Bass River bulk carbonate $\delta^{13}C$ data are from *Cramer et al.*, (1999) and foraminifera $\delta^{13}C$ data for *Subbotina* spp. are from this study (solid symbols) and *John et al.*, (2008) (open symbols). % $CaCO_3$ data are from *John et al.*, (2008). B/Ca and Mg/Ca data are from *Subbotina* spp. generated in this study. Temperature data are based on TEX_{86} estimated using the TEX_{86}^{L} and TEX_{86}^{H} calibrations from (*Kim et al.*, 2010). Solid horizontal line ~1172.2 ft (357.3 m) represents the onset of the CIE and dashed line ~1173.06 ft (357.5 m) represent the onset of surface warming based on TEX_{86} (*Sluijs et al.*, 2007).

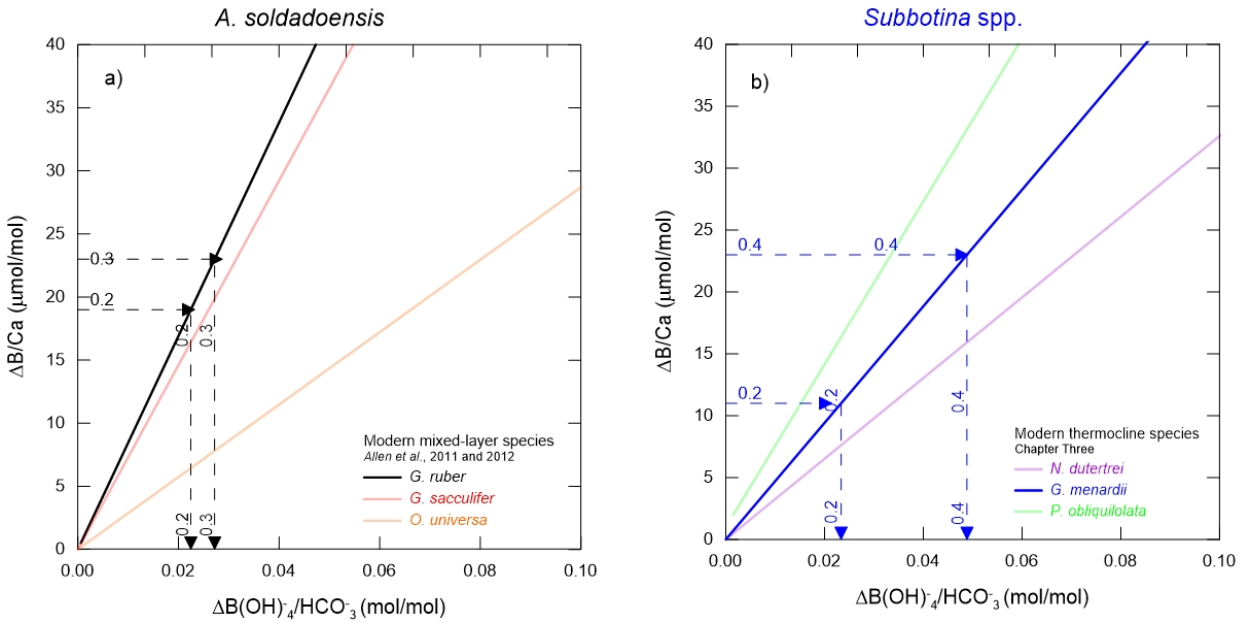

Figure 4.9 Estimate of the magnitude of ocean carbonate chemistry change $[B(OH_4^-)/HCO^-_3]_{SW}$ and pH for *A.soldadoensis* and *Subbotina* spp. B/Ca data from Bass River based on range of modern sensitivities for mixed-layer (*Allen et al.*, 2012; *Allen et al.*, 2011) and thermocline species (Chapter Three).

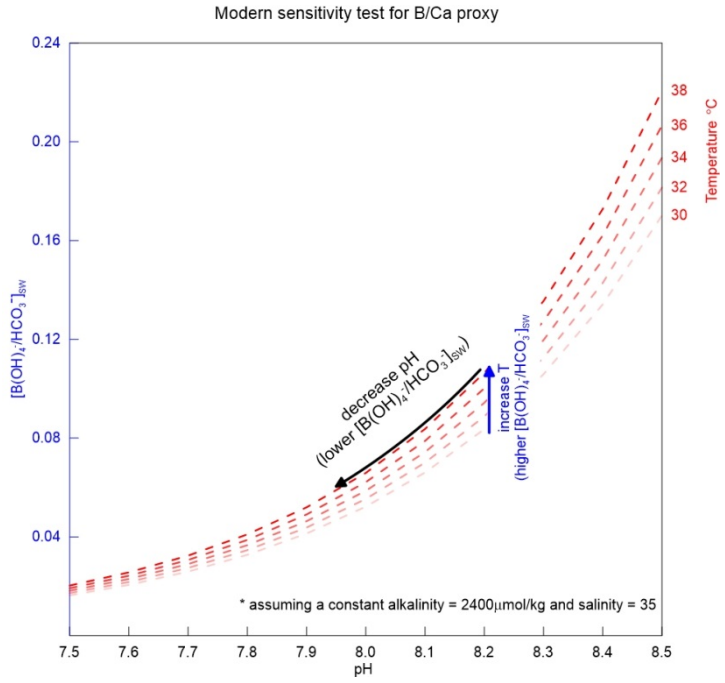

Figure 4.10 Temperature and pH influences on the estimated $[B(OH_4^-)/HCO^-_3]_{SW}$ based on B/Ca anomalies across the P/E boundary at Bass River.

Dissertation Final Remarks

The work in this dissertation contributes to the development of Boron/Calcium (B/Ca) and boron isotopes ($\delta^{11}B$) in planktonic foraminifera as proxies for surface ocean carbonate chemistry and application of B/Ca to reconstruct surface ocean acidification across the Paleocene-Eocene boundary (~55.8 Myr).

In Chapter Two, I utilized the Oceanic Flux Program (OFP) sediment traps (Sargasso Sea) to determine that B/Ca in surface dwelling planktonic foraminifer *Globigerionoides ruber* white is influenced by the presence of symbionts. Variation of B/Ca with test size of *G.ruber* was found to increase in larger foraminifers compared to smaller individuals. It is hypothesized that the internal foraminifer pH is likely modified by the balance between the photosynthetic activity and respiration, which are influenced by seasonal changes in light and temperature.

In Chapter Three, I presented B/Ca calibrations for thermocline and deep dwelling planktonic foraminifera from globally distributed core-top sediments. $\delta^{11}B$ measurements in planktonic foraminifera reveal an isotopic disequilibrium that is suggested to be a result of species vital effects that influence the boron incorporation into calcitic tests.

In Chapter Four, I utilized B/Ca and Magnesium/Calcium (Mg/Ca) from surface and thermocline dwelling planktonic foraminifera to document that sea surface acidification and warming (SST) were coincident with the negative carbon isotope excursion ($\delta^{13}C$) at the Paleocene-Eocene (P/E) boundary. The SST records based on Mg/Ca question the previous observation by *Sluijs* et al., (2007) that sea surface warming preceded the negative carbon isotope excursion ($\delta^{13}C$). In addition, B/Ca records across the P/E boundary from ODP Leg

174AX at the Bass River and Ancora core sites show the first direct evidence for the decline of surface ocean carbonate chemistry.

There remain several questions regarding boron systematics and B/Ca proxy in planktonic foraminifera. A logical study would be to conduct an inorganic calcite laboratory experiment in which the various environmental variables (i.e. $\left[B(OH)_4^-/HCO_3^-\right]_{sw}$, pH, temperature) proposed to influence boron incorporation to be tested under highly controlled conditions without the influence of biological processes on calcite precipitation. In addition culture investigations in which symbiont planktonic foraminifera were grown under various light intensities would be useful to validate the proposed influence of symbiont activity on boron incorporation (Chapter Two). Complimentary sediment trap studies in which pH variability is larger than SST changes, such as an upwelling location (ex. Arabian Sea or Santa Barbara basin) would provide insight on the relative influences of temperature and pH on boron incorporation into planktonic foraminiferal tests. Further core top work that extends the range in $\left[B(OH)_4^-/HCO_3^-\right]_{sw}$ would improve the utility of the core-top B/Ca calibrations of thermocline and deep dwelling planktonic foraminifera (Chapter Three).

A major unknown regarding the application of B/Ca proxy in planktonic foraminifera to the geologic record is the potential influence of dissolution on the preservation of the foraminifer test B/Ca signal. A study using planktonic foraminifera from core-tops along an ocean depth transect (ex. Ontong Java Plateau or Sierre Leone Rise) in which sea surface conditions are similar among sites yet bottom water carbonate saturation state varies can be used to determine the possible influence of test dissolution on B/Ca. Furthermore, the limiting factor in the ability

to determine $\left[B(OH)_4^-/HCO_3^-\right]_{sw}$ and ultimately oceanic pH in the past require the knowledge of past seawater B as their concentration likely changed over the Cenozoic (0-65 Myr).

B/Ca records across the P/E boundary from ODP Leg 174AX at the Bass River and Ancora core sites provide evidence of ocean acidification (Chapter Four). In order to validate that the New Jersey results reflect the global signal of acidification complimentary P/E records should be generated from sections from various ocean settings.

6.0 Appendix 1.1

Trace element ratios from the Oceanic Flux Program

G.ruber white 200-300µm

Sample Mid-Date	Mg/Ca (mmol/mol)	Sr/Ca (mmol/mol)	B/Ca (µmol/mol)
10/13/93	5.01	1.52	129.20
10/27/93	5.20	1.54	109.04
11/10/93	5.11	1.54	117.29
11/23/93	5.08	1.52	117.57
12/9/93	4.91	1.56	105.45
12/22/93	5.12	1.55	102.12
1/5/94	4.16	1.52	108.54
1/18/94	4.18	1.50	104.58
2/2/94	4.03	1.50	96.31
2/16/94	3.78	1.50	108.12
4/1/94	3.96	1.50	91.30
5/16/94	4.06	1.53	110.60
5/31/94	4.12	1.52	109.64
7/21/94	4.02	1.54	123.75
8/5/94	5.01	1.51	115.98
8/21/94	4.83	1.48	120.91
9/5/94	4.79	1.49	112.99
9/21/94	5.12	1.52	108.66
10/5/94	5.24	1.52	114.96
10/18/94	5.42	1.54	109.51
11/1/94	5.03	1.47	118.85
11/17/94	4.52	1.52	96.37
12/4/94	4.71	1.51	98.89
1/8/95	4.47	1.56	93.86
1/27/95	4.49	1.56	101.09
2/11/95	3.84	1.52	94.13
3/30/95	3.41	1.48	101.44
4/12/95	3.53	1.51	93.98
4/25/95	3.53	1.50	96.62
5/9/95	3.70	1.52	94.86
5/25/95	3.78	1.53	123.33
6/10/95	3.77	1.53	116.25
6/25/95	4.08	1.52	118.43
7/10/95	4.41	1.53	135.49
7/27/95	4.49	1.52	137.85
8/11/95	4.90	1.52	134.64
8/26/95	5.25	1.50	134.10
9/11/95	5.10	1.51	133.36
10/11/95	4.81	1.51	116.29
10/25/95	5.01	1.54	112.15
11/17/95	5.16	1.56	112.70

G.ruber white 300-400µm

Sample Mid-Date	Mg/Ca (mmol/mol)	Sr/Ca (mmol/mol)	B/Ca (µmol/mol)
10/27/93	5.19	1.56	123.21
11/10/93	4.97	1.48	134.63
11/23/93	4.91	1.54	140.23
12/9/93	4.44	1.47	138.50
12/22/93	4.86	1.51	113.10
1/5/94	5.29	1.50	114.70
1/18/94	4.87	1.54	113.86
4/1/94	3.46	1.48	114.78
6/24/94	3.65	1.52	144.56
7/21/94	4.60	1.53	135.82
8/5/94	5.05	1.50	134.50
8/21/94	4.98	1.47	135.50
9/5/94	5.06	1.50	133.13
9/21/94	5.62	1.55	139.09
10/18/94	5.77	1.55	135.28
11/1/94	5.27	1.54	130.70
11/17/94	4.39	1.53	122.46
12/4/94	4.53	1.50	117.59
1/27/95	4.27	1.52	112.09
2/11/95	4.34	1.52	104.46
3/30/95	3.44	1.49	116.65
4/12/95	3.46	1.52	110.60
4/25/95	3.61	1.49	111.50
5/25/95	3.69	1.52	148.39
6/10/95	3.58	1.51	147.57
6/25/95	3.94	1.50	147.33
7/27/95	4.29	1.53	152.74
8/11/95	4.63	1.51	153.58
8/26/95	4.93	1.52	143.73
9/11/95	5.07	1.52	158.58
10/25/95	5.08	1.55	120.22
11/7/95	5.19	1.55	109.04

Appendix 1.2

Stable isotopes from the Oceanic Flux Progam

G.ruber white 200-300μm

Sample Mid-Date	$\delta^{13}C$ (‰) PDB	$\delta^{18}O$ (‰) PDB
10/13/93	-0.43	-0.84
10/27/93	-0.31	-0.77
11/10/93	-0.39	-0.81
11/23/93	0.11	-0.85
12/9/93	-0.25	-0.78
12/22/93	-0.31	-0.49
1/18/94	-0.67	-0.31
2/2/94	-0.49	-0.26
4/1/94	-0.64	-0.14
5/16/94	-1.13	-0.34
6/24/94	-0.06	-0.35
8/5/94	-0.36	-0.89
8/21/94	0.02	-1.26
9/5/94	-0.24	-0.97
9/21/94	-0.65	-1.23
10/5/94	-0.08	-1.22
10/18/94	0.17	-1.08
11/17/94	-0.43	-0.69
12/4/94	0.08	-0.74
1/27/95	-0.67	-0.29
2/11/95	-0.68	-0.22
3/30/95	-0.23	-0.13
4/12/95	-0.88	-0.29
4/25/95	-0.45	-0.28
5/25/95	-0.39	-0.05
6/10/95	0.03	-0.30
6/25/95	-0.81	-0.24
7/27/95	-0.37	-0.09
8/11/95	-0.09	-0.75
8/26/95	0.24	-0.76
9/11/95	-0.28	-0.93
10/25/95	0.00	-1.10
11/7/95	-0.17	-0.89

G.ruber white 300-400μm

Sample Mid-Date	$\delta^{13}C$ (‰) PDB	$\delta^{18}O$ (‰) PDB
10/27/93	0.44	-1.39
11/24/93	-0.01	-1.01
12/30/93	0.51	-0.56
7/21/94	0.74	-1.13
8/6/94	0.73	-1.00
8/21/94	0.40	-0.89
10/19/94	0.62	-1.27
11/1/94	0.44	-1.25
11/18/94	0.12	-0.92
12/5/94	0.05	-0.72
1/8/95	0.32	-1.03
1/27/95	-0.09	-0.48
2/12/95	0.07	-0.13
3/31/95	0.10	-0.18
5/25/95	0.18	-0.41
6/10/95	0.05	-0.44
7/28/95	0.83	-0.90
8/12/95	0.27	-0.61
8/27/95	0.69	-0.71
9/11/95	0.37	-1.11

Appendix 2.1

Core top stable isotopes

Species (355-425µm)	Site	$\delta^{13}C$ (‰) PDB	$\delta^{18}O$ (‰) PDB
G.ruber pink	KN178 46	1.23	-1.27
	KN178 1	2.11	-2.01
	DGOM RW 5-3	1.97	-1.81
G.ruber white	KN178 1	1.30	-1.83
	DGOM RW 5-3	1.48	-1.65
	KN195-5 42	0.89	-2.51
	KN195-5 9	1.64	-1.69
	BJ8-03 MC24	1.46	-2.19
G.sacculifer	KN178 46	1.48	-1.25
	KN178 1	2.08	-1.27
	KN195-5 42	1.98	-1.99
	KN195-5 9	2.28	-1.43
	DGOM RW 5-3	1.81	-1.16
	BJ8-03 MC24	1.94	-2.06
G.sacculifer with sac	KN178 46	1.62	-0.98
	KN178 1	2.36	-1.22
	DGOM RW 5-3	2.05	-1.24
	KN195-5 42	1.46	-2.00
	KN195-5 9	1.86	-1.23
	BJ8-03 MC24	1.79	-1.75
G.conglobatus	KN178 46	1.83	0.35
	KN178 1	1.63	-0.01
	DGOM RW 5-3	1.18	-1.83
	DGOM RW 5-3	2.00	-1.94
	KN195-5 42	1.09	-1.40
	KN195-5 9	1.38	-0.55
	BJ8-03 MC24	2.03	-2.35
G.bulloides	KN178 46	-0.42	0.65
	KN178 1	-0.35	0.76
	KN178 1	-0.36	0.91
	RR05-03 12	0.58	1.93
G.siphonifera	KN178 1	1.62	-0.20
	KN178 1	0.82	-0.56
	DGOM RW 5-3	0.88	-0.16
	KN195-5 42	0.99	-0.62
	KN195-5 9	1.40	-0.05
	RR05-03 118	0.59	0.50
	BJ8-03 MC24	1.21	-1.90

Species (355-425µm)	Site	$\delta^{13}C$ (‰) PDB	$\delta^{18}O$ (‰) PDB
P.obliquiloculata	KN178 46	1.03	-0.33
	KN178 1	0.73	0.00
	DGOM RW 5-3	1.01	-0.20
	DGOM RW 5-3	0.86	-0.09
	KN195-5 9	1.21	-0.12
	RR05-03 118	0.97	0.48
	RR05-03 118	-0.12	2.42
	BJ8-03 24	0.67	-2.81
	BJ8-03 24	0.74	-1.48
N.dutertrei	KN178 46	1.50	0.31
	KN178 46	1.07	0.34
	KN178 1	1.58	0.09
	DGOM RW 5-3	1.49	-0.20
	KN195-5 42	1.28	0.03
	KN195-5 9	1.41	0.44
	BJ8-03 24	1.20	-1.64
G.menardii	KN178 46	0.98	0.01
	KN178 1	1.33	-0.06
	DGOM RW 5-3	1.63	-0.25
	KN195-5 42	1.01	-0.65
	KN195-5 9	1.56	0.00
	BJ8-03 24	1.05	-1.58
G.hirsuta	KN178 1	0.70	0.87
	RR05-03 118	1.16	1.39
G.inflata	KN178 46	1.15	1.34
	KN178 1	1.17	1.14
	RR05-03 12	1.25	2.39
	RR05-03 118	0.75	0.54
G.truncatulinoides dextral	KN178 1	1.10	0.73
	KN178 46	1.35	1.61
	RR05-03 118	1.36	0.88
	BJ8-03 24	0.72	0.31
G.truncatulinoides sinistral	KN178 1	1.06	0.79
	RR05-03 118	0.75	1.08
	RR05-03 12	1.29	2.08
	BJ8-03 24	1.06	0.11
G.tumida	KN178 46	1.26	1.72
	KN178 1	1.63	0.21
	KN178 1	2.11	0.00
	BJ8-03 24	1.57	0.69
G.crassaforamis	DGOM RW 5-3	1.06	1.69
	RR05-03 118	0.89	0.84
	BJ8-03 24	0.91	1.12

Appendix 2.2

Foraminifera cleaning $\delta^{11}B$ procedure

Kuo-Fang Huang 7/6/2011 as modified by Tali Babila 9/8/2011

Sample size: 1-4 mg (adjust to have 10-20 ng of B) of foraminiferal carbonates

Crushed foraminifera samples are prepared in a 0.5mL acid-cleaned eppendorf centrifuge tubes.

Reagents used: Tip Rinse (2% HNO3), Milli-Q tip rinse, MilliQ (B-free MilliQ) in squirt bottle, Methanol (two-bottle distilled methanol) in squirt bottle, 6%NaOCl or 0.1M NaOH and hydrogen peroxide (31% ultrapure), 0.0005N ultrapure HNO_3, 1N and concentrated HNO_3 (Ultrapure, SEASTAR), 0.1N ultrapure HNO_3

***Cleaning Procedure**: All cleaning steps should take place in the designated boron only hood. Use the sponge (located under the B-only hood in a plastic box) to clean surface of the hood. Once the surface is cleaned place plastic wrap in the area where samples will be cleaned. Use two sets of gloves. The inside gloves are to protect you and the outside gloves are to prevent contamination of your samples. ONLY wear the outside gloves when in the hood cleaning samples. Prepare a procedural blank with every set of cleaning.*

1. **Removal of fine clays**

a) Set the ultrasonicator temperature to 65°C. Squirt a small amount of Milli-Q into each vial, to cover the foram fragments. Leave the tubes open. Rap the rack to get rid of any air bubbles. If any vials still have bubbles, remove them from the rack, close, and rap on the bench top.

b) Put in ultrasonicator for 2 minutes.

c) Add more Milli-Q water to fill each vial – squirt in water so as to agitate the samples and to have the foram fragments in suspension. Keep the caps open. Rap the rack a couple of times.

d) Let sit for 2 minutes to let the fragments re-settle to the bottom of the vial. Rap the rack 1 or 2 times to knock down any fragments from the side of the vial. Cap vial and rack on bench-top to remove air bubbles. Siphon the water off using a 1000µL Eppendorf pipetter to remove solution (Note: always use acid-cleaned tips and tip rinse (x3 2%HNO_3, x3Milli-Q) before use. Siphon as close to the forams as possible, allowing for maximum solution removal and without sucking up fragments. Expel waster solution into a plastic container clearly identified as waste.

Note: A grayish cloud in the solution is normal and is the clay going into the solution. It should become clearer after each rinsing.

e) Repeat a) through d) for a total of 3 times with Milli-Q.

f) Repeat a) through d) for a total of 2 x using two bottle-distilled methanol, and one final time with Milli-Q, to rinse out the methanol. Note: methanol is less viscous, so be more careful during siphoning; don't go quite to the bottom of the vial.

2. **Oxidizing Step (to remove organic matter)**

Note: If running samples for trace metals use Method 2 as the reagents are cleaner.

Method 1:

Reagents: Sodium hypochlorite 5-10% NaOCl, Tip Rinse (2% HNO3), Milli-Q tip rinse, Milli-Q (B-free Milli-Q) in squirt bottle

a) Add an appropriate volume ~100µL (all samples needs to be immersed!) of 5-10% NaOCl into tubes, leave the vial caps slightly and leave them in the low-B Class-10 flow bench overnight.

b) Next day, use the 1000µL Eppendorf pipetter to siphon off the NaOCl solution.

c) Fill the vials ~2/3 with Milli-Q using the squirt bottle and cap the vials. Carefully, turn the rack upside down so that the foram fragments are moved from the bottom of the vial toward the cap. Place vials in the vortex. Make sure that the vials are secured in the foam vial carousel on the vortex. Start to vortex at a setting of ~5 and quickly to ~8. Repeat several times.

d) Open vials and fill vials/caps with Milli-Q using the squirt bottle. Let the fragments settle for ~2 minutes.

e) Use the 1000µL Eppendorf pipetter to siphon off water from the tube and caps.

f) Repeat c) through e) ten times

Method 2:

Reagents: Hydrogen peroxide H_2O_2 ultrapure, Sodium hydroxide 0.1 N B-free NaOH (use the Amberlite column to clean the NaOH solution prior to using for foram cleaning follow Lemerchand protocol), Milli-Q squirt bottle, 2% HNO_3 Tip Rinse, Milli-Q Tip Rinse

Note: Set-up hot water bath. Use a shallow glass dish filled with enough Milli-Q water to immerse the bottoms of the vials in the sample rack. Set the hotplate temperature to 120°C so that the water bath is ~ 80°C.

a) Add 100 µL of H_2O_2 (do not pipet directly from bottle! Pour small amount into small Teflon beaker) to 30 mL of 0.1 N B-free NaOH in a 50 mL PFA bottle designated for oxidizing solution.

b) Add 250 µL of oxidizing solution to each sample. Cap the samples. Carefully, turn the rack upside down so that the foram fragments are moved from the bottom of the vial toward the cap. This allows for the oxidizing solution to thoroughly mix with the foram fragments.

c) Set the rack into a hot water bath, cover with a watch glass plate (~ 80°C) for 5 minutes, remove and ultrasonicate briefly ~30seconds, rap the rack and make sure that the any air bubbles are removed and then return to hot water bath. After 5 minutes in the water bath, removed, ultrasonicate briefly ~30seconds and then place in the hood.

Note: depending on the amount of organic matter present. The reaction with the oxidizing solution will produce various amounts of bubbles (production of CO_2).

d) Make sure that the bubbles there no air bubbles. Use the 1000µL pipetter to remove the oxidizing solution.

e) Squirt in Milli-Q water (~2/3 full) into the vial and cap. Rap and let settle ~2 minutes. Pipette off solution. Repeat (Total 2 times).

f) Fill tubes halfway with Milli-Q water, cap and set in hot water bath for 5 minutes. Ultrasonicate briefly ~30 seconds, and then pipette off water. Repeat.

g) Fill the tubes half-way with Milli-Q using the squirt bottle, cap the tubes. Carefully, turn the rack upside down so that the foram fragments are moved from the bottom of the vial toward the cap and place in the vortex. Make sure that the vials are secured in the foam vial carousel on the vortex. Start to vortex at a setting of ~5 and quickly to ~8. Repeat several times.

h) Repeat step g) three times.

3. **Sample transfer**

a) In B-only hood, set up and label (same numbers) new, acid-leached vials.

b) Use a small Teflon beaker (rinse x3 with Milli-Q) and fill with Milli-Q water.

c) Use the 1000µL pipetter, set to 250 µL. Use acid-cleaned tips. Tip rinse (x3 2% HNO3, x3 Milli-Q) and rinse once with the Milli-Q water from the Teflon beaker.

d) Open the old tube, suck up 250µL of Milli-Q water from the Teflon beaker and slowly pipette into the side of the old vial with foram fragments. Suck up foram fragments from the old tube and expel into the new vial. Repeat until you are certain all test fragments have been transferred. Pipette off water using the 1000µL pipetter. Tip rinse the pipette tip in between each sample transfer.

4. **Weak acid leach (to remove carbonate overgrowths)**

Note: if samples are small omit this step.

Reagents: Ultrapure Nitric Acid 0.0005 N HNO_3, Milli-Q squirt bottle, 2% Tip Rinse HNO_3, Milli-Q Tip Rinse

a) Add 250 µL of 0.0005 N HNO_3 to each sample, cap and ultrasonicate for ~30 seconds, let settle 2 minute, and pipette solution off.

b) Repeat a) 0-4 times, depending on sample size. Check the sample size each time.

c) Whenever you stop acid-leaching a sample, squirt in Milli-Q water, wait ~2 minutes for forams to settle and pipette off. Cap sample to distinguish it from others that will be leached again, and leave in rack.

d) When all samples have been leached. Rinse with Milli-Q water one last time, pipette off any remaining water. Cap and store samples. The samples can be stored indefinitely at this point.

5. **Dissolution (right before the micro-sublimation)**

a) Add 60 µL of 1N HNO_3 to each sample. For the JCP-1 standard (~3mg dry powder) use 100 µL of 1N HNO_3 to dissolve. Put in ultrasonicator to help dissolve and rap samples to remove bubbles and to insure that the acid is reacting with the carbonate. To check that the samples are dissolved hold samples to the light and observe the bottom of the vial or turn the rack upside and watch for any settling of test fragments.

(If there are still some white powders, add another 5 µL of conc. HNO_3 to the solutions and centrifuge them. At this point, un-dissolvable stuffs are not carbonates!).

b) When samples are completely dissolved, centrifuge for 15 mins at 10,000 rpm. Use the 1mL centrifuge tubes to put in the centrifuge tube holes and then place your samples in them.

c) Remove samples from the centrifuge carefully so that there is minimal disturbance and immediately micro-sublimate.

6. **Micro-sublimation**

a) Label acid-cleaned PFA vials on the v-shaped side so that the label is visible in the hotplate. Set the hotplate to 98°C and place the metal vial holders on the hotplate.

b) Use the hood closest to the hotplate. Place plastic wrap on the bench top.

c) Carefully, hold the sample vial at an angle and pipette 50µL (same volume for JCP-1 and samples) and load sample in the center of the cap of the V-shape PFA vial. Make sure there are no bubbles.

d) Close the vial tightly and place upside-down (upside-is the v-shape bottom and down is the cap side) in the hotplate. Make sure to cover the front of the clean-hotplate shelf and use the plastic vertical bar to tighten.

e) Micro-sublimation should be done the night before analyzing. Allow a minimum of 12 hours and 14 hours at maximum. (This depends on the amount of boron in the samples and the temperature of the hotplate)

Note: A maximum of 30 samples can micro-sublimate at the same time. A single run is a maximum of 10 samples with one JCP-1 standard and one procedural blank.

7. **Final Dilution**

a) Carefully remove the vials from the hotplate. While allowing vials to cool set up labeled 1mL centrifuge vials in the hood.

b) Prepare solutions in the hood by placing down plastic wrap on the area of use.

c) Turn the vial on the side and unscrew cap. Make sure not to let the sublimated solution touch the drop on the cap or fall out of the vial. (Tricky, so be focused)

d) Pipette 350µL of 0.1N HNO3 (950µL of 0. 1N HNO_3 for JCP-1) into the bottom of the sample vial (with the sublimated solution) and turn vial on its side to make sure that any solution adhering to the side is collected into one droplet.

e) Pour the solution into the new acid-cleaned labeled 1mL centrifuge tube. (Note: the final solution might need to be adjusted depending on the flow rate for the day). The JCP-1 in 1000µL is ~70ppb B (assuming ~3mg $CaCO_3$ powder) and needs to be diluted to 20ppb B before running.

f) Finally vortex samples prior to running. Keep samples in a plastic bag in the B-only hood until ready to load on the auto-sampler.

Appendix 2.3

B/Ca and $\delta^{11}B$ core top

Species (355-425µm)	Site	B/Ca (µmol/mol)	$\delta^{11}B$ (‰)	$\delta^{11}B_{B(OH)_4^-}$ (‰)
G.ruber pink	KN178 46	148.21	19.18	19.89
	KN178 1	133.97		
	DGOM RW 5-3	147.17	18.56	17.72
G.ruber white	KN178 46	148.70		
	KN178 1	131.27		
	DGOM RW 5-3	148.61		
	KN195-5 42	155.72	20.93	17.85
	RR05-03 118	137.23	17.92	
	BJ8-03 24	159.82	21.42	20.54
G.sacculifer	KN178 46	97.27		
	KN178 1	84.63	19.18	19.62
	DGOM RW 5-3	93.98	16.72	17.94
	KN195-5 42	99.49	18.68	17.29
	KN195-5 9	100.49	18.40	18.10
	BJ8-03 24	118.80	19.83	18.03
G.sacculifer with sac	KN178 46	101.25		
	KN178 1	92.33	18.92	19.62
	DGOM RW 5-3	91.82	17.18	17.92
	KN195-5 42	93.44	16.03	17.50
	KN195-5 9	96.19	17.42	18.05
	BJ8-03 24	98.01	19.50	17.71
G.conglobatus	KN178 46	80.23		
	KN178 1	86.25		
	DGOM RW 5-3	81.85	17.92	
	KN195-5 42			
	KN195-5 9	86.85		
	BJ8-03 24	97.83	19.43	18.18
G.bulloides	KN178 46	39.68	10.69	
	KN178 1	39.46		
	RR05-03 12	64.91		
G.siphonifera	KN178 46	79.54	15.65	18.35
	KN178 1	89.76		
	DGOM RW 5-3	96.20	15.66	17.73
	KN195-5 42	62.36	16.32	17.85
	KN195-5 9	60.26	14.66	17.35
	RR05-03 118	77.43	17.25	19.71
	BJ8-03 24	69.79	16.31	17.86

Species (355-425µm)	Site	B/Ca (µmol/mol)	$\delta^{11}B$ (‰)	$\delta^{11}B_{B(OH)^-_4}$ (‰)
P.obliquiloculata	KN178 46	75.91		
	KN178 1	76.60	16.08	19.42
	DGOM RW 5-3	68.33	16.47	17.64
	KN195-5 42	62.03		
	KN195-5 9	59.05	14.78	17.64
	RR05-03 118	74.53	16.18	
	BJ8-03 24	54.65	17.19	
N.dutertrei	KN178 46	55.46	15.14	18.43
	KN178 1	61.18	16.69	19.29
	DGOM RW 5-3	53.53	15.11	17.33
	KN195-5 42	50.60	14.49	17.28
	KN195-5 9	51.48	14.99	16.96
	BJ8-03 24	72.04	16.97	17.61
G.menardii	KN178 46	60.11		
	KN178 1	67.27	17.50	19.43
	DGOM RW 5-3	59.65	14.87	17.37
	KN195-5 42	60.06	15.12	17.83
	KN195-5 9	47.90	15.46	17.27
	BJ8-03 24	58.13	16.97	16.98
G.hirsuta	KN178 1	59.63	16.27	17.90
	RR05-03 118	59.16	15.80	18.16
G.inflata	KN178 46	47.90	14.67	17.32
	KN178 1	42.78	15.32	17.80
	RR05-03 12	52.93		
	RR05-03 118	61.50	15.08	19.33
G.truncatulinoides dextral	KN178 1	77.18	16.90	18.00
	RR05-03 118	65.63	15.51	19.01
	BJ8-03 24	60.16		
G.truncatulinoides sinistral	KN178 1	64.64	14.58	17.96
	DGOM RW 5-3	62.25	13.41	
	RR05-03 118	69.15	15.95	18.57
	BJ8-03 24	63.78	11.00	14.83
G.tumida	KN178 46	53.02	14.63	
	KN178 1	59.73	18.04	
	DGOM RW 5-3	53.38	15.17	
	BJ8-03 24	51.71	16.20	16.20
G.crassaforamis	DGOM RW 5-3	52.31		
	RR05-03 118	73.65	16.02	19.04
	BJ8-03 24	64.03	16.03	15.62

Appendix 2.4

B/Ca core top size data

Species	Site	Size (µm)	B/Ca (µmol/mol)
G.ruber white	KN 178 46	250	139.33
	KN 178 46	300	148.70
	KN 178 46	355	147.10
	EN66 30	300	110.17
	EN 66 39	355	116.77
	KN195-5 42	300	140.35
	KN195-5 42	355	155.72
	KN195-5 9	250	134.51
	KN195-5 9	300	136.76
	KN195-5 9	355	137.23
	BJ8-03 20	212	138.23
	BJ8-03 20	250	145.19
	BJ8-03 20	300	166.05
	BJ8-03 20	355	183.68
G.sacculifer	KN178 46	250	98.92
	KN178 46	355	97.27
	KN178 46	300	91.62
	EN 66 30	355	83.76
	EN 66 30	500	77.69
	EN 66 30	600	85.65
	EN 66 39	300	86.20
	EN 66 39	355	89.54
	EN 66 39	425	94.08
	EN 66 39	500	88.45
	KN 195-5 42	250	91.53
	KN 195-5 42	300	98.62
	KN 195-5 42	355	99.49
	KN 195-5 42	425	99.54
	KN195-5 9	250	86.20
	KN195-5 9	300	89.84
	KN195-5 9	355	100.49
	KN195-5 9	425	102.42
G.sacculifer with sac	KN 178 46	355	101.25
	KN 178 46	425	105.77
	KN 195-5 42	250	93.01
	KN 195-5 42	300	97.94
	KN 195-5 42	355	93.44
	KN 195-5 42	425	113.23
	KN195-5 9	250	85.34
	KN195-5 9	300	90.35
	KN195-5 9	355	96.19
	KN195-5 9	425	94.53
	BJ8-03 20	250	99.31
	BJ8-03 20	300	123.66
	BJ8-03 20	355	121.69
	BJ8-03 20	4425	138.90
G.conglobatus	KN178 46	300	90.56
	KN178 46	355	80.23
	KN178 46	425	78.91
	EN66 30	425	75.93
	EN66 30	500	98.06
	EN66 30	600	84.85
	EN66 39	500	90.72
	EN66 39	600	100.95
	KN195-5 42	355	125.27
	KN195-5 42	425	104.52
	KN195-5 9	300	98.45
	KN195-5 9	355	86.85
	KN195-5 9	425	108.06

Species	Site	Size (µm)	B/Ca (µmol/mol)
P.obliquiloculata	KN 178 46	250	72.88
	KN 178 46	300	70.64
	KN 178 46	355	75.91
	KN 178 46	425	69.87
	EN66 30	355	94.03
	EN66 30	500	95.16
	EN66 30	600	129.08
	EN66 39	355	90.28
	EN66 39	425	91.27
	EN66 39	500	84.61
	KN195-5 42	250	68.31
	KN195-5 42	300	65.47
	KN195-5 42	355	62.03
	KN195-5 42	425	61.29
	KN195-5 9	250	70.52
	KN195-5 9	300	58.58
	KN195-5 9	355	59.05
	KN195-5 9	425	57.38
	BJ8-03 20	300	70.92
	BJ8-03 20	355	69.51
	BJ8-03 20	425	76.18
N.dutertrei	KN 178 46	250	69.43
	KN 178 46	300	55.72
	KN 178 46	355	55.46
	KN 178 46	425	53.57
	EN 66 30	300	88.23
	EN 66 30	355	113.61
	EN 66 30	425	103.29
	EN 66 30	500	103.48
	KN195-5 42	250	58.31
	KN195-5 42	300	53.22
	KN195-5 42	355	50.60
	KN195-5 42	425	53.82
	KN195-5 9	250	59.89
	KN195-5 9	300	57.63
	KN195-5 9	355	51.48
	KN195-5 9	425	49.70
	KN195-5 12	355	47.80
	KN195-5 12	425	46.41
G.menardii	KN178 46	300	57.70
	KN178 46	355	60.11
	KN178 46	425	60.66
	EN66 30	500	86.51
	EN66 39	425	98.68
	EN66 39	500	99.96
	KN195-5 42	250	65.39
	KN195-5 42	300	60.12
	KN195-5 42	355	60.06
	KN195-5 42	425	60.83
	KN195-5 9	250	59.19
	KN195-5 9	300	50.53
	KN195-5 9	355	47.90
	KN195-5 9	425	43.95
G.truncatulinoides	KN 178 46	300	65.87
	KN 178 46	355	61.30
	KN 178 46	425	60.10
G.tumida	KN 178 46	355	53.02
	KN 178 46	425	48.42
	EN66 30	355	61.84
	EN66 30	425	64.39
	EN66 30	500	57.14
	EN66 30	600	70.95
	EN66 39	425	69.89
	EN66 39	500	60.19
G.crassaformis	EN66 30	425	82.30
	EN66 30	500	91.16
	EN66 39	355	99.38
	EN66 39	425	90.07
	EN66 39	500	89.36

Appendix 2.5

Core top calibration hydrographic data

Species (355-425µm)	Site	Temperature °C	Salinity	DIC anthro corr (µmol/kg)	Alkalinity (µmol/kg)	$[B(OH)^-_4 /HCO^-_3]$
P.obliquiloculata	KN178 46	20.49	36.04	2015.90	2383.00	0.065
	KN178 1	18.56	35.83	2000.70	2377.00	0.068
	DGOM RW 5-3	20.08	36.36	2071.80	2337.34	0.048
	KN195-5 9	17.05	35.02	2068.00	2292.00	0.046
N.dutertrei	KN178 46	18.42	36.21	2055.40	2381.00	0.057
	KN178 1	18.29	35.88	2008.60	2378.00	0.067
	DGOM RW 5-3	20.38	36.37	2065.22	2335.41	0.046
	KN195-5 42	16.62	35.03	2076.80	2294.00	0.043
	KN195-5 9	15.84	35.03	2105.80	2300.00	0.039
G.menardii	KN178 46	19.17	36.18	2044.20	2384.00	0.059
	KN178 1	18.82	35.76	1999.00	2376.00	0.068
	DGOM RW 5-3	20.65	36.37	2059.02	2333.32	0.046
	KN195-5 42	19.77	34.81	2008.60	2276.00	0.049
	KN195-5 9	16.78	35.02	2075.50	2293.00	0.042
	BJ8-03 24	25.33	34.22	1913.95	2155.90	0.043
G.hirsuta	KN178 1	14.17	35.85	2081.20	2369.00	0.050
	RR05-03 118	11.91	35.05	2096.90	2308.00	0.049
G.inflata	KN178 46	12.77	35.77	2097.50	2354.00	0.044
	KN178 1	12.90	35.73	2084.20	2365.00	0.049
	RR05-03 118	16.54	35.51	2022.20	2316.00	0.064
	RR05-03 12	6.03	34.34	2128.50	2295.00	0.030
G.truncatulinoides dextral	KN178 1	14.97	35.94	2077.60	2372.00	0.051
	KN178 46	11.43	35.58	2108.70	2349.00	0.041
	RR05-03 118	15.28	35.43	2043.00	2314.00	0.060
	BJ8-03 24	13.99	34.55	2112.04	2247.86	0.000
G.truncatulinoides sinistral	KN178 1	14.57	35.89	2079.50	2371.00	0.051
	KN178 46	10.89	35.52	2123.40	2346.00	0.038
	RR05-03 118	13.87	35.28	2065.60	2313.00	0.055
	RR05-03 12	7.43	34.44	2105.90	2295.00	0.034
	BJ8-03 24	14.82	34.56	2093.37	2242.42	0.034
G.crassaforamis	DGOM RW 5-3	11.15	35.38	2191.78	2324.65	0.031
	RR05-03 118	15.61	35.45	2038.50	2315.00	0.060
	BJ8-03 24	11.03	34.48	2171.49	2265.14	0.026

Appendix 3.1

Trace element ratios Bass River

Species	Depth down (ft)	Depth up (ft)	Mg/Ca (mmol/mol)	B/Ca (µmol/mol)	Rejected
A.soldadoensis	1136.2	1136.3	4.63	53.52	
A.soldadoensis	1146	1146.1	2.84	47.83	
A.soldadoensis	1149.1	1149.2	3.02	43.26	
A.soldadoensis	1152	1152.1	4.72	51.18	R
A.soldadoensis	1154	1154.1	5.06	50.27	R
A.soldadoensis	1159	1159.1	7.89	43.88	R
A.soldadoensis	1163	1163.1	4.92	55.87	R
A.soldadoensis	1165	1165.1	3.98	43.04	
A.soldadoensis	1167	1167.1	3.57	38.93	
A.soldadoensis	1167.4	1167.5	10.48	10.14	R
A.soldadoensis	1168.6	1168.7	3.16	37.41	
A.soldadoensis	1169.1	1169.2	3.31	37.02	
A.soldadoensis	1169.4	1169.5	3.60	40.86	
A.soldadoensis	1170	1170.1	4.68	43.24	R
A.soldadoensis	1170.2	1170.3	3.20	40.99	
A.soldadoensis	1170.6	1170.7	3.24	37.63	
A.soldadoensis	1170.75	1170.85	8.68	15.17	R
A.soldadoensis	1170.75	1170.8	8.56	13.68	R
A.soldadoensis	1171.1	1171.2	9.58	14.21	R
A.soldadoensis	1171.1	1171.2	8.41	16.90	R
A.soldadoensis	1171.3	1171.4	3.28	41.16	
A.soldadoensis	1171.5	1171.6	3.18	36.04	
A.soldadoensis	1171.6	1171.7	3.32	42.07	
A.soldadoensis	1171.8	1171.9	3.30	38.52	
A.soldadoensis	1171.9	1172	3.08	45.72	
A.soldadoensis	1173.9	1174	2.50	69.22	
A.soldadoensis	1176.3	1176.4	2.67	65.40	
A.soldadoensis	1177	1177.1	3.09	64.34	
A.soldadoensis	1182.8	1182.9	2.39	59.91	
A.soldadoensis	1183	1183.1	2.59	66.43	

Species	Depth down (ft)	Depth up (ft)	Mg/Ca (mmol/mol)	B/Ca (µmol/mol)	Rejected
S.triangularis	1136.2	1136.3	6.30	21.48	R
S.triangularis	1145	1145.1	3.20	40.50	
S.triangularis	1147	1147.1	3.11	43.00	
S.triangularis	1148.3	1148.4	3.46	42.03	
S.triangularis	1149.1	1149.2	3.53	42.52	
S.triangularis	1152	1152.1	3.93	43.34	
S.triangularis	1154	1154.1	4.04	42.83	
S.triangularis	1157	1157.1	10.64	39.80	R
S.triangularis	1158	1158.1	4.99	37.88	R
S.triangularis	1159	1159.1	5.63	40.70	R
S.triangularis	1161	1161.1	3.32	36.86	
S.triangularis	1163	1163.1	3.39	38.29	
S.triangularis	1165	1165.1	4.66	39.79	R
S.patagonica	1165	1165.1	5.72	38.68	R
S.patagonica	1167	1167.1	4.00	38.42	
S.triangularis	1167	1167.1	4.25	37.14	R
S. roesnaesensis	1167.4	1167.5	4.71	40.09	R
S.patagonica	1168.6	1168.7	3.24	40.48	
S.patagonica	1169.1	1169.2	3.41	38.01	
S.triangularis	1169.4	1169.5	4.03	38.86	
S. roesnaesensis	1170	1170.1	6.45	24.79	R
S. roesnaesensis	1170.2	1170.3	3.81	40.11	
S. roesnaesensis	1170.6	1170.7	3.68	39.00	
S. roesnaesensis	1170.75	1170.85	3.61	49.72	
S.patagonica	1170.75	1170.8	10.50	9.43	R
S. roesnaesensis	1171.1	1171.2	10.41	10.50	R
S.patagonica	1171.1	1171.2	10.93	12.73	R
S. roesnaesensis	1171.3	1171.4	3.80	45.95	
S.patagonica	1171.5	1171.6	4.21	39.38	
S.triangularis	1172.6	1172.7	2.33	52.56	
S. roesnaesensis	1172.8	1172.9	2.61	59.71	
S. roesnaesensis	1173.1	1173.2	2.34	51.08	
S. roesnaesensis	1173.4	1173.5	2.71	55.41	
S.triangularis	1173.9	1174	2.51	56.89	
S. roesnaesensis	1174	1174.1	2.38	56.90	
S.triangularis	1176.3	1176.4	2.37	55.94	
S.triangularis	1177	1177.1	2.59	56.72	
S.triangularis	1178	1178.1	2.55	59.06	
S.triangularis	1179	1179.1	2.68	54.93	
S.triangularis	1180.8	1180.9	2.44	65.83	
S.triangularis	1182.8	1182.9	2.35	58.29	
S.triangularis	1183	1183.1	2.41	57.73	
S.triangularis	1184	1184.1	2.45	54.89	

Species	Depth down (ft)	Depth up (ft)	Mg/Ca (mmol/mol)	B/Ca (µmol/mol)	Rejected
M.aequa	1145	1145.1	3.50	39.79	
M.aequa	1146	1146.1	3.61	46.95	
M.aequa	1147	1147.1	3.95	49.15	
M.aequa	1148.3	1148.4	3.55	41.71	
M.aequa	1149.1	1149.2	3.84	44.35	
M.aequa	1152	1152.1	5.88	48.29	R
M.aequa	1157	1157.1	9.31	44.77	R
M.aequa	1158	1158.1	12.36	34.77	R
M.aequa	1163	1163.1	4.74	43.50	
M.aequa	1163.9	1164	4.25	33.47	
M.aequa	1165	1165.1	6.78	43.69	R
M.acuta	1169.4	1169.5	3.49	40.94	
M.acuta	1170	1170.1	4.12	41.91	
M.acuta	1170.2	1170.3	3.39	44.53	
M.acuta	1170.6	1170.7	4.08	43.16	
M.acuta	1170.75	1170.85	9.66	13.42	R
M.acuta	1170.75	1170.8	9.76	10.59	R
M.velascoensis	1170.75	1170.8	10.26	9.16	R
M.acuta	1171.1	1171.2	9.56	14.16	R
M.velascoensis	1171.1	1171.2	9.26	15.03	R
M.acuta	1171.2	1171.3	9.51	16.28	R
M.acuta	1171.3	1171.4	3.74	45.49	
M.acuta	1171.5	1171.6	3.46	44.93	
M.velascoensis	1171.5	1171.6	3.88	48.66	

Appendix 3.2

Trace Element ratios Ancora

Species	Depth down (ft)	Depth up (ft)	Mg/Ca (mmol/mol)	B/Ca (µmol/mol)	Rejected
A.soldadoensis	525.4	525.5	3.13	79.13	
A.soldadoensis	525.6	525.7	3.13	67.62	
A.soldadoensis	532.2	532.3	2.97	71.34	
A.soldadoensis	533.5	533.6	2.99	57.14	
A.soldadoensis	534.5	534.6	2.89	56.88	
A.soldadoensis	535.4	535.5	2.94	72.57	
A.soldadoensis	535.4	535.5	3.03	50.77	R
A.soldadoensis	536.3	536.4	3.03	77.55	
A.soldadoensis	536.3	536.4	3.12	69.26	
A.soldadoensis	537.5	537.6	3.26	70.84	
A.soldadoensis	537.5	537.6	3.35	79.92	
A.soldadoensis	538	538.1	3.44	62.19	
A.soldadoensis	539.3	539.4	3.35	323.68	R
A.soldadoensis	541.4	541.5	2.91	60.32	
A.soldadoensis	542.8	542.9	3.39	54.62	
A.soldadoensis	542.8	542.9	3.27	49.94	
A.soldadoensis	543.5	543.6	3.50	54.78	
A.soldadoensis	543.9	558.9	2.99	43.15	
A.soldadoensis	544.4	558.9	2.97	41.75	
A.soldadoensis	544.6	558.9	3.78	37.04	
A.soldadoensis	544.9	558.9	3.06	42.89	
A.soldadoensis	545.4	558.9	3.37	38.05	
A.soldadoensis	550.2	558.9	3.25	39.34	
A.soldadoensis	550.7	558.9	3.30	36.15	
A.soldadoensis	551.6	558.9	3.28	37.33	
A.soldadoensis	551.9	558.9	3.94	42.76	
A.soldadoensis	552.3	558.9	3.47	40.07	
A.soldadoensis	552.8	558.9	3.38	42.29	
A.soldadoensis	553.4	558.9	5.92	43.16	R
A.soldadoensis	553.9	558.9	4.64	43.31	
A.soldadoensis	554.1	558.9	4.31	38.65	
A.soldadoensis	555.2	558.9	4.11	39.00	
A.soldadoensis	555.8	558.9	3.55	38.35	
A.soldadoensis	556	556.1	3.00	38.58	
A.soldadoensis	556.4	556.5	3.11	37.12	
A.soldadoensis	556.9	557	3.24	35.92	
A.soldadoensis	557.2	557.3	3.19	37.34	
A.soldadoensis	557.6	557.7	3.32	36.84	
A.soldadoensis	557.9	558	2.96	37.03	
A.soldadoensis	558.1	558.2	2.99	36.71	
A.soldadoensis	558.4	558.5	3.01	38.98	
A.soldadoensis	558.8	558.9	3.09	38.52	
A.soldadoensis	559.7	558.9	3.17	37.53	
A.soldadoensis	559.8	558.9	3.07	38.13	
A.soldadoensis	560	558.9	3.66	38.86	
A.soldadoensis	560.2	558.9	5.56	34.25	R
A.soldadoensis	560.6	558.9	6.38	1.713	R
A.soldadoensis	560.9	558.9	3.12	39.49	
A.soldadoensis	560.9	558.9	3.35	38.00	
A.soldadoensis	561.2	558.9	3.86	37.64	

Species	Depth down (ft)	Depth up (ft)	Mg/Ca (mmol/mol)	B/Ca (µmol/mol)	Rejected
S. roesnaesensis	525.4	525.5	3.08	58.12	R
S. roesnaesensis	525.6	525.7	3.18	37.43	R
S. roesnaesensis	525.6	525.7	3.06	51.06	
S. roesnaesensis	532.2	532.3	2.67	48.84	
S. roesnaesensis	533.5	533.6	2.90	47.06	
S. roesnaesensis	533.5	533.6	2.91	50.44	
S. roesnaesensis	535.4	535.5	2.76	49.47	
S. roesnaesensis	535.4	535.5	2.68	64.67	
S. roesnaesensis	536.3	536.4	2.76	50.95	
S. roesnaesensis	537.5	537.6	3.11	49.11	
S. roesnaesensis	538	538.1	2.79	46.66	
S. roesnaesensis	539.3	539.4	3.27	47.19	
S. roesnaesensis	541.4	541.5	3.01	47.87	
S. roesnaesensis	542.8	542.9	3.01	169.10	R
S. roesnaesensis	542.8	542.9	3.65	52.78	
S. roesnaesensis	543.5	543.6	3.44	50.76	
S.patagonica	543.9	558.9	3.32	40.15	
S.patagonica	544.4	558.9	3.20	234.65	R
S.patagonica	544.6	558.9	4.73	40.14	
S.patagonica	544.9	558.9	3.40	38.39	
S.patagonica	545.4	558.9	3.72	36.96	
S.patagonica	550.2	558.9	3.63	36.60	
S.patagonica	550.7	558.9	3.98	37.35	
S.patagonica	551.6	558.9	3.54	35.83	
S.patagonica	551.9	558.9	3.98	39.08	
S.patagonica	552.3	558.9	3.67	41.08	
S.patagonica	552.8	558.9	3.99	42.34	
S.patagonica	553.9	558.9	10.03	45.31	R
S.patagonica	554.1	558.9	5.30	42.39	
S.patagonica	554.6	558.9	5.41	37.31	
S.patagonica	555.2	558.9	5.47	40.33	
S.patagonica	555.8	558.9	4.65	40.73	
S.patagonica	556	558.9	3.83	37.43	
S.patagonica	556.4	558.9	4.54	39.04	
S.patagonica	556.9	558.9	4.11	39.46	
S.patagonica	557.2	557.3	4.00	48.67	
S.patagonica	557.6	557.7	4.00	36.65	
S.patagonica	557.9	558	6.17	11.74	R
S.patagonica	558.1	558.2	3.91	39.26	
S.patagonica	558.4	558.5	3.79	38.48	
S.patagonica	558.8	558.9	4.00	39.23	
S.patagonica	559.2	558.9	3.71	37.54	
S.patagonica	559.7	558.9	3.31	35.92	
S.patagonica	559.8	558.9	4.72	39.12	
S.patagonica	560	558.9	4.19	38.11	
S.patagonica	560.2	558.9	4.31	27.10	R
S.patagonica	560.9	558.9	3.97	38.39	
S.velascoensis	562.9	558.9	4.12	51.05	
S.triangularis	563.3	558.9	2.56	51.01	

Species	Depth down (ft)	Depth up (ft)	Mg/Ca (mmol/mol)	B/Ca (µmol/mol)	Rejected
M.aequa	525.4	525.5	3.30	75.60	
M.aequa	525.6	525.7	3.69	64.63	
M.aequa	532.2	532.3	3.95	53.87	
M.aequa	535.4	535.5	3.58	64.53	
M.aequa	536.3	536.4	3.54	57.75	
M.aequa	537.5	537.6	3.03	58.95	
M.aequa	537.5	537.6	3.30	57.08	
M.aequa	538	538.1	3.73	59.36	
M.aequa	541.4	541.5	4.79	151.01	R
M.aequa	542.8	542.9	3.59	51.92	
M.aequa	542.8	542.9	3.68	50.57	
M.aequa	543.5	543.6	3.72	54.28	
M.acuta	544.4	544.5	4.24	53.83	
M.acuta	544.9	545	4.60	48.28	
M.acuta	550.2	550.3	4.31	52.51	
M.acuta	550.7	550.8	4.57	48.66	
M.acuta	551.6	551.7	4.18	48.93	
M.acuta	551.9	552	4.63	50.29	
M.acuta	552.8	552.9	5.82	117.83	R
M.acuta	553.9	554	5.66	102.62	R
M.acuta	554.1	554.2	6.39	56.11	
M.acuta	554.6	554.7	5.74	47.11	
M.acuta	555.8	555.9	5.05	74.51	
M.acuta	556	556.1	4.21	52.12	
M.acuta	556.9	557	3.81	56.71	
M.acuta	557.3	557.4	3.83	58.39	
M.acuta	557.6	557.7	3.65	51.82	
M.acuta	557.9	558	3.63	52.04	
M.acuta	558.1	558.2	3.53	174.03	R
M.acuta	558.4	558.5	4.06	67.69	
M.acuta	558.8	558.9	3.95	46.34	
M.acuta	559.2	559.3	4.00	53.56	
M.acuta	559.7	559.8	3.69	49.05	
M.acuta	559.8	559.9	4.16	50.44	
M.acuta	560	560.1	4.01	48.77	
M.acuta	560.2	560.3	3.66	44.35	
M.acuta	560.9	560.3	3.80	120.87	R

Appendix 3.3

Stable isotopes Bass River

Species	Depth down (ft)	Depth up (ft)	$\delta^{13}C$ (‰) PDB	$\delta^{18}O$ (‰) PDB	Rejected
A.soldadoensis	1136.2	1136.3	1.15	-3.97	
A.soldadoensis	1149.1	1149.2	0.45	-2.87	
A.soldadoensis	1161	1161.1	-0.19	-3.16	
A.soldadoensis	1165	1165.1	0.26	-3.14	
A.soldadoensis	1167	1167.1	-0.65	-2.93	
A.soldadoensis	1168.6	1168.7	-0.34	-3.03	
A.soldadoensis	1169.1	1169.2	-0.59	-3.08	
A.soldadoensis	1170.75	1170.85	-2.72	-4.88	R
A.soldadoensis	1171.1	1171.2	-2.12	-5.12	R
A.soldadoensis	1171.5	1171.6	0.01	-3.42	
A.soldadoensis	1176.3	1176.4	3.62	-2.50	
A.soldadoensis	1177	1177.1	2.76	-2.93	
A.soldadoensis	1183	1183.1	4.48	-2.54	

Species	Depth down (ft)	Depth up (ft)	$\delta^{13}C$ (‰) PDB	$\delta^{18}O$ (‰) PDB	Rejected
S.triangularis	1145	1145.1	-0.69	-2.38	
S.triangularis	1147	1147.1	-1.01	-2.42	
S.triangularis	1148.3	1148.4	-0.97	-2.61	
S.triangularis	1149.1	1149.2	-1.08	-2.42	
S.triangularis	1152	1152.1	-1.27	-2.67	
S.triangularis	1154	1154.1	-1.43	-2.88	
S.triangularis	1157	1157.1	-1.40	-2.65	
S.triangularis	1158	1158.1	-1.67	-2.91	
S.triangularis	1159	1159.1	-1.75	-2.79	
S.triangularis	1163	1163.1	-1.53	-2.86	
S.triangularis	1165	1165.1	-1.73	-2.72	
S.patagonica	1165	1165.1	-1.26	-3.18	
S.patagonica	1167	1167.1	-1.69	-3.45	
S.patagonica	1168.6	1168.7	-1.70	-3.41	
S.patagonica	1169.1	1169.2	-1.68	-3.51	
S.patagonica	1170.75	1170.85	-3.83	-5.37	R
S.patagonica	1171.1	1171.2	-3.62	-5.68	R
S.triangularis	1173.9	1174	1.50	-1.60	
S.triangularis	1176.3	1176.4	1.34	-1.74	
S.triangularis	1177	1177.1	1.30	-2.08	
S.triangularis	1182.8	1182.9	1.94	-1.45	
S.triangularis	1183	1183.1	2.16	-2.00	

Species	Depth down (ft)	Depth up (ft)	$\delta^{13}C$ (‰) PDB	$\delta^{18}O$ (‰) PDB	Rejected
M.aequa	1145	1145.1	1.62	-3.12	
M.aequa	1147	1147.1	0.92	-3.20	
M.aequa	1148.3	1148.4	0.86	-3.89	
M.aequa	1157	1157.1	0.68	-3.42	
M.aequa	1158	1158.1	1.45	-3.62	
M.aequa	1161	1161.1	0.44	-3.27	
M.aequa	1163	1163.1	0.46	-3.78	
M.aequa	1165	1165.1	0.36	-3.15	
M.acuta	1170.75	1170.85	-3.06	-5.24	R
M.velascoensis	1170.75	1170.85	-3.09	-5.36	R
M.acuta	1171.1	1171.2	-2.40	-5.49	R
M.velascoensis	1171.1	1171.2	-2.44	-5.33	R

APPENDIX 3.4

STABLE ISOTOPE ANCORA DATA

Species	Depth down (ft)	Depth up (ft)	$\delta^{13}C$ (‰) PDB	$\delta^{18}O$ (‰) PDB
A.soldadoensis	525.6	525.7	3.13	-2.99
A.soldadoensis	534.5	534.6	1.40	-2.39
A.soldadoensis	542.8	542.9	0.94	-2.96
A.soldadoensis	543.5	543.6	0.80	-3.38
A.soldadoensis	543.9	544.0	-0.40	-3.00
A.soldadoensis	544.4	544.5	-0.09	-2.97
A.soldadoensis	544.6	544.7	-0.68	-3.13
A.soldadoensis	544.9	545.0	-0.25	-3.04
A.soldadoensis	545.4	545.5	-0.73	-3.06
A.soldadoensis	550.2	550.3	0.19	-3.34
A.soldadoensis	550.7	550.8	-0.37	-3.10
A.soldadoensis	551.6	551.7	-0.26	-3.44
A.soldadoensis	551.9	552.0	-0.41	-3.50
A.soldadoensis	552.3	552.4	-0.08	-3.50
A.soldadoensis	552.8	552.9	-0.47	-3.26
A.soldadoensis	553.9	554.0	-0.21	-3.18
A.soldadoensis	554.1	554.2	-0.60	-3.24
A.soldadoensis	554.6	554.7	-0.26	-3.36
A.soldadoensis	555.2	555.3	-0.49	-3.21
A.soldadoensis	555.8	555.9	-0.47	-3.04
A.soldadoensis	556.0	556.1	-0.26	-3.04
A.soldadoensis	556.4	556.5	-0.70	-3.08
A.soldadoensis	556.9	557.0	-0.84	-3.21
A.soldadoensis	557.2	557.3	-0.52	-3.17
A.soldadoensis	557.6	557.7	-0.60	-3.30
A.soldadoensis	557.9	558.0	-0.15	-3.28
A.soldadoensis	558.1	558.2	-0.23	-3.40
A.soldadoensis	558.4	558.5	0.20	-3.42
A.soldadoensis	558.8	558.9	-0.34	-3.59
A.soldadoensis	559.2	559.3	-0.19	-3.76
A.soldadoensis	559.7	559.8	-0.20	-3.51
A.soldadoensis	559.8	559.9	-0.21	-3.30
A.soldadoensis	560.0	560.1	-0.04	-3.29
A.soldadoensis	560.2	560.3	-1.18	-3.74
A.soldadoensis	560.9	561.0	-0.43	-3.26
A.soldadoensis	561.2	561.3	-0.15	-2.79

Species	Depth down (ft)	Depth up (ft)	$\delta^{13}C$ (‰) PDB	$\delta^{18}O$ (‰) PDB
S. roesnaesensis	525.6	525.7	0.61	-1.69
S. roesnaesensis	532.2	532.3	0.22	-1.36
S. roesnaesensis	533.5	533.6	0.13	-1.38
S. roesnaesensis	534.5	534.6	-0.13	-1.44
S. roesnaesensis	535.4	535.5	0.12	-1.41
S. roesnaesensis	536.3	536.4	-0.05	-1.26
S. roesnaesensis	537.5	537.6	0.27	-1.91
S. roesnaesensis	538	538.1	0.11	-1.84
S. roesnaesensis	539.3	539.4	0.05	-1.48
S. roesnaesensis	541.4	541.5	-0.09	-1.32
S. roesnaesensis	541.8	541.9	-0.10	-1.95
S. roesnaesensis	542.8	542.9	-0.11	-1.82
S. roesnaesensis	543.5	543.6	-1.46	-2.77
S.patagonica	543.9	544.0	-1.48	-3.35
S.patagonica	544.4	544.5	-1.93	-3.25
S.patagonica	544.6	544.7	-2.05	-3.44
S.patagonica	544.9	545.0	-1.94	-3.05
S.patagonica	545.4	545.5	-1.73	-3.48
S.patagonica	550.2	550.3	-1.62	-3.40
S.patagonica	550.7	550.8	-1.96	-3.54
S.patagonica	551.6	551.7	-1.55	-3.83
S.patagonica	551.9	552.0	-1.71	-3.81
S.patagonica	552.3	552.4	-1.72	-3.65
S.patagonica	552.8	552.9	-1.32	-3.51
S.patagonica	553.9	554.0	-1.46	-3.39
S.patagonica	554.1	554.2	-1.95	-3.66
S.patagonica	554.6	554.7	-2.63	-3.45
S.patagonica	555.2	555.3	-1.76	-3.41
S.patagonica	555.8	555.9	-1.94	-3.57
S.patagonica	557.2	557.3	-1.75	-3.49
S.patagonica	557.6	557.7	-1.74	-3.34
S.patagonica	557.9	558.0	-1.84	-3.64
S.patagonica	558.1	558.2	-1.84	-3.54
S.patagonica	558.4	558.5	-1.72	-3.63
S.patagonica	558.8	558.9	-1.56	-3.50
S.patagonica	559.2	559.3	-2.00	-3.68
S.patagonica	559.7	559.8	-1.95	-3.39
S.patagonica	560.6	560.7	-2.83	-3.44
S.patagonica	560.9	561.0	-2.41	-3.40
S.patagonica	562.9	563.0	1.51	-2.09
S.velascoensis	562.9	563.0	-0.27	-0.99
S.velascoensis	563.2	563.3	1.33	-1.94
S.patagonica	563.3	563.4	0.77	-2.54
S.patagonica	564.2	564.3	1.43	-0.73
S.patagonica	565.2	565.3	1.66	-1.52

Species	Depth down (ft)	Depth up (ft)	$\delta^{13}C$ (‰) PDB	$\delta^{18}O$ (‰) PDB
M.aequa	525.6	525.7	3.43	-2.89
M.aequa	538	538.1	1.60	-2.79
M.aequa	542.8	542.9	1.03	-2.85
M.acuta	550.7	550.8	0.24	-4.12
M.acuta	551.6	551.7	-0.03	-3.83
M.acuta	551.9	552.0	0.00	-3.91
M.acuta	553.9	554.0	-0.13	-3.52
M.acuta	554.1	554.2	0.09	-3.86
M.acuta	554.6	554.7	-0.25	-3.63
M.acuta	558.1	558.2	0.39	-3.80
M.acuta	559.2	559.3	-0.15	-4.18
M.acuta	559.7	559.8	0.08	-3.95
M.acuta	559.8	559.9	-0.04	-3.77